Aus der Hals-, Nasen-, Ohren-Klinik und Poliklinik - Plastische Operationen

der Universitätsmedizin der Johannes Gutenberg-Universität Mainz

„Evaluation of ZnO nanoparticles as an adjuvant therapeutic substance in the radiotherapy of solid tumors using the chorioallantoic membrane assay”

„Evaluation von ZnO-Nanopartikeln als Adjuvans in der Strahlentherapie von soliden Tumoren mittels des Chorioallantoismembran-Assay“

Inauguraldissertation

zur Erlangung des Doktorgrades der

Medizin

der Universitätsmedizin

der Johannes Gutenberg-Universität Mainz

Vorgelegt von

Rachel Caterina Tanner

aus Darmstadt

Mainz, 2025

Wissenschaftlicher Vorstand: Univ.-Prof. Dr. Philipp Drees

1. Gutachter:

2. Gutachter:

Tag der Promotion: 08.09.2025

Table of contents

List of abbreviations

Abbreviation	Meaning
8-OHdG	8-hydroxydeoxyguanosine
AFP	Alpha-fetoprotein
AG	Arbeitsgruppe, meaning working group
Alpha-SMA or α-SMA	Alpha-smooth muscle actin
BrdU	Bromodeoxyuridine
CAM	Chorioallantoic membrane
cAMP	Cyclic adenosine monophosphate
CC3	Cleaved caspase-3
cGMP	Cyclic guanosine monophosphate
CO_2	Carbon dioxide
DAB	Diaminobenzidine
DMEM	Dulbecco's Modified Eagle Serum F-12
DNA	Deoxyribonucleic acid
EDTA	Ethylenediaminetetraacetic acid
EPR effect	Enhanced permeability and retention effect
FBS	Fetal bovine serum
GABA	γ-aminobutyric acid type A
Gy	Gray
HCC	Hepatocellular carcinoma
HE	Hematoxylin-eosin
HET-CAM-Assay	Henn's egg test on chorioallantoic membrane assay
HIF-1α	Hypoxia-inducible factor 1-alpha
HNPCC	Hereditary non-polypoid colon cancer
Huh-7	Human hepatocellular carcinoma cell line 7
IACUC	Institutional Animal Care and Use Committee
IL	Interleukin
keV	Kilo electron Volts
Ki-67	Kiel-67 protein
mRNA	Messenger ribonucleic acid
MV-210	Melanie Viel 210
NMDA	N-methyl-D-aspartate
PBS	Phosphate-buffered saline
PDE	Phosphodiesterase

PEG	Polyethylene glycol
PK	Pan-keratin
PKA	Protein kinase A
P/S	Penicillin and streptomycin
rH	Relative humidity
rpm	Rounds per minute
ROI	Region of interest
ROS	Reactive oxygen species
RONS	Reactive oxygen and nitrogen species
RT	Radiotherapy
TNF-α	Tumor necrosis factor alpha
T/E	Trypsin and EDTA
UV	Ultraviolet
VEGF	Vascular endothelial growth factor
ZnO-NP	Zinc oxide nanoparticles

List of figures

List of tables

1 Introduction

Innovative antineoplastic treatments aim to selectively wield a cytotoxic effect and avert tumor proliferation. As one of the standard treatments against cancer, radiotherapy is used as a predominantly externally applied technique which leads to reduced cell viability within neoplastic tissues. Oftentimes throughout this form of treatment, tumor entities develop radiation resistances whilst normal tissue is unfavorably sensitive to radiation. In order to reduce side effects and enhance treatment success, the radiosensitivity of tumor cells should be restored (1). This may be achieved by applying combination therapies, which means adding other treatment methods such as antineoplastic drugs.

Apart from the possible uses in the fields of diagnostics and imaging in cancer treatment, the use of metallic nanoparticles as anti-tumor agents is a widely researched topic. More specifically, zinc oxide nanoparticles (ZnO-NP) have emerged as promising anti-tumor agents due to their demonstrated cytotoxicity in various human cancer cell lines and their favorable biocompatibility (2). Comparable to the effects of ionizing radiation, the induction of reactive oxygen species (ROS) is a proclaimed mechanism of action, although the exact processes remain uncertain to date. Both released zinc ions and direct cell-nanoparticle interaction contribute to those (3).

This exploratory study investigated the therapeutic potential of ZnO-NP and their combination with radiotherapy. To this end, the well-established Hen’s Egg Test - Chorioallantoic Membrane model (HET-CAM-Assay) was employed. Huh-7 hepatocellular carcinoma cells were transplanted onto the CAM, which is a highly vascularized extraembryonic membrane. The HET-CAM-Assay adheres to the 3R principle (reduce, refine and replace) in experimental design (4). Depending on the division of experimental organisms into study groups, consequences of initial application of ZnO-NP and following radiation were analyzed using immunohistochemical staining methods.

2 Zusammenfassung in deutscher Sprache

Diese Studie untersuchte das antineoplastische Potenzial von Zinkoxid-Nanopartikeln (ZnO-NP) in Kombination mit ionisierender Strahlung sowie deren Einzelwirkungen, wobei das Chorioallantoismembran (CAM)-Modell an soliden Tumoren aus Huh-7-Zellen zum Einsatz kam. Insgesamt wurden 83 CAMs über sechs Versuchsdurchläufe ausgewertet. Die Tumorschnitte wurden mit Hämatoxylin-Eosin sowie Antikörpern gegen Pan-keratin, Ki-67, Cleaved Caspase-3 (CC3) und Alpha-Smooth-Muscle-Actin gefärbt, um Morphologie, Proliferation, Apoptose und Angiogenese zu untersuchen.

Strahlung allein (8 Gy) führte zu einem Anstieg sowohl der Apoptose- als auch der Proliferationsraten sowie zu einer Reduktion der Gefäßstrukturen. Die Monotherapie mit ZnO-NP (13,5 µg intravaskulär) zeigte vergleichbare Trends, jedoch mit geringerer Effektstärke. Auffällig war in beiden Gruppen ein gleichzeitiger Anstieg der CC3- und Ki-67-positiven Zellen, was darauf hindeutet, dass zytotoxische Effekte durch eine Reaktivierung ruhender Zellen in den Zellzyklus begleitet werden könnten. ZnO-NP wurden zuvor als Mittel zur gezielten Eliminierung solcher Zellen nach Strahlentherapie beschrieben und könnten damit zur Überwindung von Radioresistenz und Seneszenz beitragen. Dies wurde in vivo durch den Anstieg CC3-positiver und Rückgang Ki-67-positiver Zellen nach kombinierter Behandlung gestützt.

Die Kombinationstherapie führte zu verstärkter Apoptose und reduzierter Angiogenese, während die Proliferation im Vergleich zur alleinigen Strahlentherapie weiter abnahm. Es wird angenommen, dass ZnO-NP die Wirksamkeit der Strahlentherapie durch Mechanismen wie die Bildung reaktiver Sauerstoff- und Stickstoffspezies (RONS) verstärken, was eine Reduktion der Strahlendosis bei gleichbleibender Tumorzellabtötung ermöglichen könnte. Da die Toxizität von ZnO-NP gegenüber Tumorzellen bereits in anderen Studien in vitro belegt wurde, könnten Anpassungen in Dosis, Applikationszeitpunkt und Strahlungsprotokoll die Therapieeffizienz weiter steigern. Zukünftige Studien sollen diese synergistischen Effekte weiter untersuchen. Zudem könnten gezielte Wirkstoffstrategien und Nanopartikel-Beschichtungen die Tumorspezifität erhöhen. Ihr Einsatz könnte eine vielversprechende Ergänzung im multimodalen Therapiekonzept solider Tumoren darstellen und zur Entwicklung effektiver, zielgerichteter und gewebeschonender Krebsbehandlungen beitragen.

3 Aims

In general, the objective of this experimental work was to evaluate which effects on solid tumors can be observed by the intravascular application of ZnO-NP and combined radiation using the CAM-Assay.

Specifically, cell viability within the tumor areas after treatment with ZnO-NP and radiation was to be evaluated. This was to be achieved by quantifying apoptotic activity through immunohistochemical staining for Cleaved Caspase-3 (CC3), and assessing proliferative potential via expression of Ki-67. Of particular interest was whether ZnO-NP administration could independently induce apoptosis and suppress proliferation in ovo, thereby contributing to tumor regression.

Furthermore, consequences on vascular structures within the tumor area were to be analyzed since these are vital to tumor development and survival. In order for this, the quantity and distribution of vascular structures via alpha-smooth muscle actin (α -SMA) staining was examined. It was of relevance whether a reduction in vascular structures is a consequence of ZnO-NP.

All of these effects of ZnO-NP were to be evaluated as well as whether these exceed the consequences of radiation, specifically when applied as a combination treatment. As a conclusion, for this experimental study it was of interest to evaluate the anti-neoplastic capabilities of ZnO-NP while further providing insight into their potential as a radiosensitizer in tumor treatment.

4 Literature review

In this section, literature sources related to the topics of the thesis and basic scientific knowledge are presented to set a foundation in order to be able to understand the newly gained knowledge from the experimental studies. This spans from topics in oncology and current tumor treatment methods, specifically radiotherapy, to how research is conducted to offer new tumor treatment methods. The underlying mechanisms and proposed common threads of cell damage by radiation and ZnO-NP, namely high concentrations of reactive oxygen species as well as a possible consequence which is apoptosis, the programmed cell death, will be further clarified.

Following this, the HET-CAM-Assay finds special emphasis as the study organism used for the performed experiments. Furthermore, the current state of research on zinc nanoparticles, especially as a possible antineoplastic agent, is scientifically presented, as their application to solid tumors on the HET-CAM-Assay is the intervention to be analyzed in this thesis. In order to comprehend the performed experiments and shown effects afterward, an introduction to the immunohistochemical staining methods as the basis for data analysis is made.

4.1 Tumor medicine

Tumorous diseases pose an ongoing threat to human health even though many new treatment methods have been established during past decades. Cancer is a leading cause of death worldwide, causing approximately 10 million deaths per year or nearly one in six deaths (5). Malignant masses arise through the transformation of normal cells into tumor cells by a multi-stage process, which advances due to a combination of several factors such as genetic and environmental influences. External stimuli called carcinogens can be of physical nature, such as UV light and ionizing radiation, or chemical substances, while biological causes can be infections by certain viruses, bacteria, or parasites. Furthermore, a controllable aspect is the lifestyle with factors like lack of exercise and obesity causing direct and indirect influences as well. Risk factors which are not controllable include a genetic predisposition to tumorous diseases (5, 6).

The genetic composition of every cell incorporates three categories of genes which are distinctive for tumor development: proto-oncogenes, tumor suppressor genes, and DNA repair genes, collectively orchestrating an intricate equilibrium to uphold or restore the physiological milieu of cells and tissues. A short overview will be given for this topic to set a foundation for the understanding of tumorous masses.

Within each cell, a constant metabolism takes place and so-called replication of DNA is needed to prepare the basis for cell division. This activity is intricately regulated and can be visualized as a cycle due to its repetitive actions. Whilst the process is underway, constant checks for correctness take place which usually lead to physiologic cell division or, in the case of an irreparable error: programmed cell death, called

apoptosis. As result of such an early control checkpoint, DNA repair mechanisms undertake the critical role of correcting damaged DNA. Mutations within the genes of the involved molecules themselves may prompt further genetic alterations or structural modifications in chromosomes during events such as duplication, deletion, inversion, insertion, or translocation. Such genetic aberrations hold the potential to allow change of normal cells into tumorous entities or prevent altered cells from being disqualified for further replication (7).

Furthermore, proto-oncogenes, responsible for maintaining normal cell growth and division, assume a pivotal role in upholding cellular homeostasis. In the event of a mutation within these genes, a potential for their heightened activity arises, thereby allowing damaged or aberrant cells to continue their growth unrestricted (8).

In relation, tumor suppressor genes such as the most widely known transcription factor p53, integral to the regulation of cell growth and division, are capable to exert a suppressing influence. A rapid turnover of these molecules takes place within the cell cycle during the system of checks and balances. If mutations compromise the execution of these genes, leading to an overall loss of their suppressing capacity, cells may embark on an uncontrollable path of proliferation (9).

As the aging process unfolds, the efficacy of cellular repair mechanisms diminishes, thereby augmenting the likelihood of unchecked cellular growth, exemplified by the emergence of tumors. The tumor cells may also evade the immune system or alter it in order to survive. The rapid formation of abnormal cells which grow uncontrollably and subsequently invade the organ tissue and neighboring organs as well as spreading and forming satellite tumors is called metastasis. This process occurs when cancer cells break away from the main tumor and enter the body’s bloodstream or lymphatic system (6).

4.2 Tumor treatment

Tumor treatment encompasses a range of therapeutic strategies aimed at modifying or eliminating abnormal cell growth and treating cancerous conditions. Several treatment modalities are employed in clinical practice, often in combination, to enhance

treatment efficacy. The treatment process is designed to either cure the patient from a tumorous disease and reduce the risk of recurrence after an intervention has already taken place or to alleviate tumor-related symptoms in instances where a definitive cure remains elusive. An outline of treatment options will be presented with special emphasis on the process of radiation as it is the same intervention used in the experiments of the performed study.

The basic three tumor treatment methods comprise of surgery, application of systemic pharmaceuticals as in chemo-, immune- or hormone therapy and radiation. Surgical intervention involves the physical removal of a localized solid tumor tissue entirely or partially from the body, minimizing the risk of recurrence. Chemotherapy is used to treat many types of tumors by systemically employing cytotoxic drugs to inhibit or destroy rapidly dividing cells. Since it usually nonspecifically interferes with cell division, it targets both cancerous and some normal cells. It can be applied as intravenous or oral treatment but also locally by injection. It is especially relevant when cancer cells have spread and formed metastases and can be used combining other therapy methods (6).

Furthermore, immunotherapy or targeted therapy methods are newly established therapy methods which are not chemotherapy by definition, but the systemic application method is most often also either intravenous or an oral intake. Immunotherapy modulates the immune system to recognize and reduce cancer cells. It either directly or indirectly enhances the body's natural defenses or introduces synthetic components to target cancerous cells and is particularly relevant for certain types of cancers which evade the body’s immune system (10).

Targeted therapy involves drugs in cancers with identifiable molecular targets which specifically target molecules critical for cancer cell survival by interference with specific pathways or proteins associated with tumor growth. Similarly, hormone therapy works by specifically blocking hormone receptors or reducing hormone production to impede the growth of hormone-sensitive tumors like breast and prostate cancers (11).

Another approach which is primarily necessary in hematologic cancers is stem cell transplantation, which is essentially replacing damaged or destroyed bone marrow with healthy stem cells after high-dose chemotherapy or radiation treatment to eradicate any cancerous blood cells (12).

Commonly used for liver cancer, hyperthermia treatment involves an elevated temperature regionally or systemically which can directly damage cancer cells or make them more sensitive to radiation and certain drugs. It is applied with techniques including external devices like microwave or ultrasound applicators as well as interstitial techniques where heat sources are placed directly into the tumor mass (13).

Another localized treatment is photodynamic therapy which uses a combination of light and a photosensitizing chemical substance to eradicate cancer cells. The process involves three key components including a photosensitizer as a light-sensitive substance which accumulates in cancer cells, absorbs the light applied to the targeted area and produces a form of reactive oxygen species which causes damage to nearby cells. It is most often used to treat surface tumors or cancers in the lining of internal organs. It has the advantage of being a localized treatment with minimal damage to surrounding healthy tissues. However, it may not be suitable for deep-seated tumors or large cancer masses (14).

The definite selection of a specific treatment modality or combination depends on factors such as cancer type, cancer progression, and individual patient characteristics. Multimodal approaches often yield the most ample and effective outcomes in cancer treatment. Ongoing research and advancements continue to refine and expand the array of available tumor treatment methods. This leads to precision medicine involving molecular profiling and genetic analysis to identify specific mutations or alterations offering personalized therapies for better treatment outcomes (15).

4.2.1 Radiotherapy

Radiation treatment, also known as radiotherapy or radiation therapy, is a medical intervention which uses targeted doses of ionizing radiation to treat cancerous diseases and various other medical conditions. As it is the well-established treatment method which was used in the experiments conducted in this thesis, further detail on its characteristics will be given here.

In more than half of all cancer patients, radiotherapy is employed alone or in combination as a treatment modality during the course of the disease. Radiotherapy is

an established technique to eradicate the tumor cells, since ionizing radiation leads to formation of radicals which impair cellular processes on a molecular level, most importantly disrupting the DNA in targeted cells by causing double- and single-strand breaks as well as DNA crosslinks and therefore impairing their ability to continue DNA replication and proliferation. Radiation is effective for localized tumors and often combined with surgery or chemotherapy. The dose of radiation is expressed in grays (Gy), where one gray is equal to the absorption of one joule of radiation energy per kilogram of matter (16-18).

The primary goal of radiation treatment is to damage or destroy parts of the DNA within aberrant cells, preventing their ability to grow and divide. This is typically achieved by γ- or X-rays, which induce typically single or double strand breaks in the cell's genetic material and consequently alter the process of cell-proliferation. This process usually relies on checkpoints but can be aberrant in rapidly dividing cells such as tumor cells. In those cases, an added error in DNA signaling due to ionizing radiation causes uncontrolled cell growth to be terminated by causing apoptosis, autophagy-dependent cell death or necroptosis. Furthermore, the formation of reactive oxygen species (ROS) has been linked to this process as well. As water constitutes the majority of cellular content, ionizing radiation utilized in radiotherapy predominantly induces radiation-mediated hydrolysis of water molecules. This process generates ROS, including hydrogen radicals, hydroxyl radicals, and superoxide radicals, all of which play a critical role in the cellular damage associated with radiotherapy (17, 19).

There are two types of radiation which are mainly used for standard radiotherapy: photon or particle radiation.

Photon beams such as X-rays and γ-rays have a lower mass with a considered low linear energy transfer, therefore carry a low radiation charge and penetrate tissues deeply. X-rays are generated by devices that excite electrons (e.g. cathode ray tubes and linear accelerators, see chapter 5.1.7), while γ-rays originate from the decay of radioactive substances (20).

Particle radiotherapy usually uses highly energized positive ions such as protons or carbon ions. Proton beams have specific absorption profiles in tissue, allowing deposition of maximum effect in deep tissues whilst sparing healthy surrounding tissue. Particle radiation has a higher linear energy transfer than photons with a higher

biological effectiveness. Therefore, these forms of radiations may be more effective for radioresistant cancers (21).

Furthermore, there are different forms of application of radiation therapy: external beam radiation therapy and internal radiation therapy. External beam radiation therapy involves using a machine called a linear accelerator to deliver high-energy radiation to the targeted tissue from the outside. Internal radiation therapy, also known as brachytherapy, involves placing a radioactive source inside the body close to the targeted tissue or organ, often used for prostate or cervical cancer (22).

Moreover, internal radiotherapy with a liquid radiation source is referred to as a systemic therapy because the treatment reaches the tumor via the blood after ingestion or intravenous injection. This is a standard treatment for radioactive iodine therapy in well-differentiated thyroid cancer where due to the physiological process of exclusive iodine-uptake in the thyroid gland, a targeted effect can be achieved (23). Nevertheless, another way of targeted systemic radiotherapy treatment is the labeling of radiopharmaceuticals with an antibody (radioimmunotherapy) or protein (peptide receptor radionuclide therapy) which then targets a specific entity of tumor cells by key and lock principle. Nanoparticles can take on the role as drug delivery vehicles or may serve as sensitizers of external beam radiation (24, 25).

Furthermore, radiotherapy can also be used to alleviate symptoms in a palliative treatment course caused by advanced cancer as for example when osseous metastases are existent, where it may prevent further osteolytic reactions by tumor cells (26).

Before starting radiation treatment, a comprehensive planning process is undertaken which involves imaging studies (such as computed tomography scans or magnetic resonance imaging) to precisely define the target area and spare surrounding normal tissues. Before starting actual treatment, a radiation oncologist determines the appropriate dosage and treatment schedule. This is done on an individual basis, and the treatment plan is tailored to each patient's unique circumstances (27).

The actual radiation treatment is then typically delivered in multiple sessions over several weeks. Each session usually lasts only a few minutes and patients may undergo treatment daily. This is called fractioning and is designed to maximize its

impact on cancerous tissues while minimizing damage to healthy tissues. Another treatment method under investigation is called FLASH radiotherapy which is characterized by the delivery of an exceptionally high dose of radiation at an accelerated rate, typically ranging from 100 to 400 Gy/second. In contrast to conventional radiation therapy, flash therapy aims to administer a concentrated dose within a fraction of a second, leading to reduced damage of surrounding healthy tissue. Although the radiobiological mechanisms underlying the efficacy of flash radiation therapy are still under investigation, ongoing clinical trials are assessing its safety and effectiveness in human patients. Technical challenges, including the development of specialized equipment capable of delivering such high doses rapidly, accompany the exploration of this innovative radiation therapy technique (27, 28).

In contrast to the other basic treatment options of surgical resection and chemotherapy, external beam radiotherapy is non-invasive. Additionally, it is mostly a local intervention, which is carefully planned after performing imaging procedures such as computed tomography of the region of interest, thereby ideally minimizing damage to healthy tissue and confining side effects by careful planning radiation according to anatomical structures. Common temporary side effects may include fatigue, skin changes, nausea, and other symptoms depending on the treatment area. In rare cases, radiation therapy can cause long-term side effects such as damage to multiple organs. Also, strict safety measures such as shielding and monitoring devices are mandatory to protect healthcare providers and ensure the safe administration in minimizing exposure to radiation (29, 30).

After completing radiation therapy, patients undergo follow-up appointments to monitor their progress. Imaging studies and other tests can be conducted to assess treatment effectiveness. Nevertheless, the efficacy of radiotherapy in achieving treatment outcomes and its potential for cure are frequently impeded by genetically and/or environmentally mediated mechanisms of tumor radioresistance and radiotoxicity of non-cancerous surrounding tissue (1, 30).

4.2.2 Radiation resistance

The sensitivity of tumor cells to radiation is not uniform, and some show signs of radioresistance, leading to reduced treatment effectiveness and recurrences. This can be due to several factors. In general, tumor cells commonly have different types of genetic mutations which affect DNA repair mechanisms, apoptosis, and cell cycle regulation which can let them continue proliferation even after exposure to radiation and following damage to DNA (6, 31).

The tumor microenvironment can also contribute to radioresistance. It is characteristic for tumor entities that low levels of oxygen exist within the tissue. This arises from an imbalance between the elevated oxygen demand of rapidly growing and proliferating cancer cells and an inadequate oxygen supply. This insufficiency is primarily attributed to irregular blood flow, a disorganized and dysfunctional tumor microvasculature as well as potentially reduced oxygen transport. Since the cytotoxic effects of radiation relies on oxygen to produce ROS, low levels of oxygen max decrease DNA damage and thus resistance to radiotherapy-induced cell killing may occur (32, 33).

Furthermore, hypoxic conditions can reduce the effectiveness of radiation therapy by upregulation of hypoxia-inducible factor 1 (HIF-1α) and following release of additional angiogenic growth factors such as VEGF which in turn may lead to angiogenesis within the tumor (34, 35). Consequently, tumor vessels initiated by oxidative stress induced by ionizing radiation may give way to survival of tumor cells after radiation.

Moreover, it has been postulated that after radiation, cancer cells may survive by different escape pathways. Firstly, there may be a specific subpopulation of cancer stem cells which have the ability to self-renew and give rise to more differentiated cancer cells. These stem cells are thought to be more resistant to radiation, contributing to treatment failure. Furthermore, a selection of tumor cells may enter a dormant state and even though the immediate regrowth via already mentioned mechanism doesn’t emerge, an activation of dormant tumor cells with reoccurrence is not excluded (36). These cancer stem cells and senescent cells have been the focus of recent research to investigate recurrence of tumors after radiotherapy (37, 38).

Furthermore, complex molecular processes may lead to cell survival after an intervention with either repair mechanisms salvaging the proliferation process of

malignant cells or abnormal and reduced control of proliferation processes so as they may continue unchecked (39, 40). Understanding the molecular and cellular mechanisms underlying radioresistance is crucial for developing more effective and targeted cancer treatments. Efforts to achieve this can be based on the principles of enhancing the radiosensitivity of tumor tissue as well as radioresistance of healthy tissue and potentially blocking radiation resistance mechanisms specifically in tumor cells (41).

Moreover, strategies to enhance the effectiveness of radiation therapy including the development of radiosensitizers and the investigation of combination therapies which target multiple pathways are underway. Radiosensitizers, which are primarily metal-based nanoparticles enhance radiotherapy efficacy through the photoelectric effect. Incoming radiation ejects an orbital electron of the high-Z atom, which is replaced by higher-energy electrons, releasing energy which amplifies therapeutic outcomes (19). Attempts at overcoming radioresistance have been made by adding radiosensitizers such as metalloid semiconductors generating radicals upon absorption of visible light as in photodynamic therapy (14, 42-44). Furthermore, metalloid substances could be used to convey local hyperthermic effects or cause enhanced generation of ROS by stimulation after local accumulation by magnetic forces (25, 45).

More personalized approaches which may consider the specific characteristics of each tumor, including its genetic profile and microenvironment, may also be explored in the future to improve treatment outcomes.

4.2.3 ROS

The effects of radiation can be further described on a cellular and molecular level, especially mentioning the process of the formation of ROS. The high-energy rays cause ionization of atoms and molecules of the tissues. As water is the main component of cells, the ionization of the H_2O molecule into hydrogen (H^+) and hydroxyl (HO^-) radicals paves the way for further molecular reactions. These consist of numerous redox reactions within all sections of the cells, such as most decisively DNA double strand breaks, which eventually lead to cell death (46, 47). This so-called

overflow of redox-active substances is called “oxidative stress” and will be further elucidated upon.

Other ROS and also nitrogen-based reactive species (RNS) such as superoxide (O_2^-), singlet oxygen ($^1O_2$), hyperoxide anions (O_2^{2-}), hydrogen peroxide (H_2O_2), ozone (O_3) as well as nitric oxide (NO^-), nitrogen dioxide (NO_2), ammonia (NO_3), nitrous oxide (N_2O) and nitrous tetroxide (N_2O_4) are reactive components which are naturally produced during cellular metabolism and influence the balance of the cellular redox system at all times via temporarily and locally increased concentrations. Especially during mitochondrial respiration, when oxygen is reduced to water, a manifold of radicals can be produced as byproducts - to mention the most important process of ever-ongoing cellular metabolism. This can cause numerous changes in biological tissues mediated by changes in the liquid cell environment and is directly linked to their concentration (48, 49).

Whilst predominantly perceived as byproducts of cellular metabolism implicated in the pathogenesis of numerous diseases as well as the aging process, a vital role of Reactive oxygen and Nitrogen Species (RONS) in cell signaling cascades has been acknowledged widely. This includes physiological processes such as the immune system's defense mechanism, impulse transmission in nerve cells, blood coagulation cascades, regulation of vascular tone, inflammation, and angiogenesis (50).

While low concentrations of RONS are necessary for the functioning of signaling cascades, cells experiencing so-called “oxidative stress” due to high concentrations of RONS may undergo cell cycle arrest and ultimately apoptosis. This concept of oxidative stress arises from an imbalance between oxidative and antioxidative species within the cell. It is a detrimental condition which can negatively impact cellular structures such as membranes, lipids, proteins, lipoproteins, and DNA by oxidation and conformational changes with following partial or total reduced function. When this occurs, processes are activated within the cell and depending on the extent of the damage and the repair possibilities, cell cycle arrest, senescence, apoptosis, or necroptosis take place. Illustrating this, a crucial marker for DNA double-strand breaks is phosphorylated histone γ-H2AX, which has been found to be elevated corresponding to the rise of ROS (34, 46, 48, 51).

However, intracellular defense mechanisms and structures exist to prevent this. Redox pairs such as superoxide dismutase, glutathione, and catalase are reducing partners that deescalate the oxidative overflow. Nevertheless, the capacities of these antioxidative enzymes can be exceeded (50).

Furthermore, base excision repair can also compensate for damage which has already occurred to a certain extent in the DNA. A frequently described oxidative damage to DNA is the formation of 8-hydroxydeoxyguanosine (8-OHdG), which may lead to alterations in epigenetic information and could play a role in the pathogenesis of carcinomas (52).

It has been postulated that malignant cells, due to their elevated and partially aberrant metabolism, inherently possess a higher baseline concentration of intracellular RONS compared to a physiological environment in cells. For example, it has been shown that malignant cells exhibit higher expression of aquaporins in their cell membrane which offer a transport mechanism of ROS to intracellular space (53). Furthermore, the oxidation of phospholipids by ROS in a region of the phospholipid bilayer can lead to enhanced diffusion through the cell membrane. Therefore, pores could form in the membrane through which ROS diffuse into the cell interior. In these processes, cholesterol plays a crucial role in the stability and order of lipids in the membrane as it is the most abundant lipid in the cell membrane, therefore determining its stability and fluidity. A lower concentration of cholesterol in tumor cell membranes is known, and following this, a diverse overall architecture of the phospholipid bilayer presents itself. This may explain a faster intracellular rise of RONS in tumor cells (46). Furthermore, it potentially renders malignant cells more susceptible to escalating concentrations of reactive species and ensuing oxidative stress therefore leading to cell cycle arrest, apoptosis, and necrosis (34, 54).

4.2.4 Cell death

Further explaining the above-mentioned processes of cell death, especially apoptosis, is necessary to understand antineoplastic efforts and results of the performed experiments.

Apoptosis, also known as programmed cell death, is a highly regulated and orchestrated process which plays a crucial role in various physiological and pathological conditions. It is a fundamental mechanism for maintaining tissue homeostasis, eliminating damaged or unwanted cells, and shaping embryonic development (6).The apoptotic process involves a series of molecular events that ultimately lead to the controlled and orderly dismantling of a cell without inducing any response from the immune system. It is characterized by distinct morphological changes, including cell shrinkage, chromatin condensation, nuclear fragmentation, and the formation of apoptotic bodies. Apoptosis is executed by two main pathways: the intrinsic (mitochondrial) pathway and the extrinsic (death receptor-mediated) pathway.

For the intrinsic pathway, signals from cellular stress or damage to DNA and mitochondria lead via stabilization of the p53 concentration to the activation of pro-apoptotic proteins such as bax and the inhibition of pro-survival proteins such as bcl-2, resulting in the permeabilization of the mitochondrial outer membrane. This, in turn, leads to the release of cytochrome c and other pro-apoptotic factors into the cytoplasm. Cytochrome C activates caspases, a family of protease enzymes which orchestrate the dismantling of cellular components (6, 48, 55).

The extrinsic pathway is triggered by external signals, typically involving death receptors on the cell surface. Binding of specific ligands to these receptors activates caspases directly, initiating the apoptotic cascade. Both pathways converge on the activation of caspases, which execute the cleavage of key cellular substrates, leading to the characteristic changes observed during apoptosis (6, 55, 56).

While apoptosis represents a tightly regulated form of programmed cell death essential for maintaining cellular homeostasis, other mechanisms of cell death, such as necrosis and autophagy, exhibit distinct characteristics and responses to cellular stress or injury. For better understanding, these processes will be explained in short as well. Necrosis is an unregulated form of cell death that occurs when cells experience traumatic damage beyond their capacity for repair. Unlike apoptosis, necrosis is characterized by the uncontrolled rupture of the cellular membrane, which subsequently triggers an immune response. Autophagy, on the other hand, is initiated in response to cellular starvation and involves the degradation of intracellular components. This process may be reversible, allowing cells to resume proliferation

under favorable conditions, or it can culminate in autophagy-associated cell death. A special kind of cell death leading to mechanisms similar to autophagy is ferroptosis. It is a regulated cell death which occurs when the balance of redox homeostasis in a cell is disturbed, particularly due to the accumulation of iron and the overproduction of reactive oxygen species (ROS). The predominant form of cell death depends on the specific cell type and the nature of the injury. Notably, there is significant cross-talk among the various types of cell death at multiple levels (56, 57).

In summary, cell death may be a tightly regulated process, and its dysregulation can contribute to various diseases, including cancer, autoimmune disorders, and neurodegenerative conditions. Understanding the molecular mechanisms underlying apoptosis is decisive for developing therapeutic strategies targeting cell survival and death pathways in different pathological contexts (58).

4.3 Tumor research

In order to establish a new therapeutic method for tumorous diseases and before clinical application on humans can take place, it must first undergo a year-long development process of testing and evaluation. Oncological research is generally performed by initial laboratory research on *in vitro* cell cultures and secondly *in vivo* animal models before the tertiary step of tests with humans can take place (59). It is of utmost interest to follow this specific process and meanwhile upholding basic ethical principles of research. The different stages of the research process will be presented in the following sections, finally leading to the introduction of the HET-CAM-Assay in chapter 4.4.

4.3.1 *In vitro* tumor models

In order to begin the research process, most often cell culture models are used. These allow basic mechanisms of a therapeutic substance or mechanism to be investigated on the altered cells at low cost with simple handling. The *in vitro* cultivation of malignant cell lines stands as an indispensable model in oncological research, playing a pivotal role in unraveling fundamental biophysiological and biomolecular mechanisms

characteristic to the cultured cells. Predominantly, established cell lines from diverse tumor entities such as the first immortal human cell line, called HeLa cells, ensuring unlimited growth potential, constitute the primary tools for these investigations (60).

4.3.1.1 Two-dimensional cell cultures

The conventional and still prevalent method of cell culture involves the adherent 2-dimensional (2D) growth in containers such as Petri dishes or cell culture flasks, immersed in a nutrient-rich medium. In this model, cells form a monolayer on the plastic surface, allowing them uniform access to nutrients, oxygen, and growth factors within the medium which covers them (61). Nevertheless, an optimal condition of nutrient supply and the constrained two-dimensional growth paradigm significantly deviates from the complex growth patterns observed in *in vivo* tumor tissue such as crucial cell-cell and cell-extracellular matrix (ECM) interactions (62).

4.3.1.2 Three-dimensional tumor cell cultures

Therefore, in recent years, three-dimensional (3D) *in vitro* cell culture models have emerged as valuable tools in biomedical research, aiming to realize an approximation to the complex cellular microenvironment found *in vivo*, fostering improved representation of cell-cell and cell-matrix interactions. Among the various 3D culture systems, so-called spheroids, self-assembled spherical structures comprised of aggregated cells, have gained prominence (63). These 3D *in vitro* models offer several advantages over their 2D counterparts by providing a spatial arrangement which mimics tissue architecture. Spheroids facilitate the study of cell behavior, signaling pathways, and drug responses in a manner more reflective of *in vivo* conditions. Additionally, the establishment of concentration gradients enhances nutrient and oxygen diffusion, contributing to the more realistic physiological milieu (64, 65).

It has become clear that beginning in cell culture models, three-dimensional tumor models *in vitro* and models of solid tumors *in vivo* are superior in adaptation of the findings of model systems to clinically growing solid tumors. Three-dimensional (3D) cell cultures introduce a more physiologically appropriate environment, wherein cells

either grow within an ECM-like matrix such as Matrigel® serving as a scaffold (62) or are cultivated in a dynamic suspension and can then be transferred to animal models.

Solid tumors grow three-dimensionally usually infiltrating or displacing surrounding tissue. They consist of mutated tumorous cells and the stroma surrounding them, containing acellular components such as the ECM, as well as cells such as fibroblasts, endothelial cells and cells of the immune system. Tumor cells and tumor stroma are in constant interaction and influence the tumor microenvironment, which largely determines the characteristics of a solid tumor (6).

A hallmark of this development can be perceived when the mass of tumorous cells exceeds a certain size and diffusion, which usually takes place 150-200 µm from a vessel into the tissue, is no longer sufficient to supply the tumor with nutrients and oxygen (66). Then the induction of tumor angiogenesis becomes essential for further growth. To ensure this, tumor cells release angiogenic growth factors, notably Vascular Endothelial Growth Factor (VEGF), exerting a paracrine influence on neighboring vessels and stimulating the sprouting of new capillaries. Nevertheless, the intricately orchestrated parallel development of tissues and blood vessels characteristic of physiological conditions becomes unbalanced within the tumor milieu. As tumor cells typically exhibit accelerated growth compared to the induced blood vessels, regions within the tissue emerge where adequate supply through diffusion is compromised. Moreover, the newformed vessels within tumors often deviate in structure and organization from their physiological counterparts. Variances in properties such as vessel diameter, branching pattern and vessel density contribute significantly, resulting in irregular blood flow. Elevated vascular permeability, coupled with the absence of functional lymphatic vessels precipitates in an escalation of interstitial pressure within the tumor tissue (67, 68). This phenomenon can hinder the diffusion of substances, including chemotherapeutic agents, into the tumor tissue, potentially also accelerating their removal from the site (69-71). Additionally, the undersupplied and hypoxic areas, marked by poor perfusion, accumulate metabolic byproducts such as lactate and carbonic acid, prompting a decline in extracellular fluid pH value (72-74).

Tumor cells respond to the aberrant tumor microenvironment, characterized by diminished perfusion, oxygen and nutrient deprivation, acidosis, and heightened interstitial pressure through alterations in gene expression and protein biosynthesis.

Such adaptive changes wield a profound impact on the malignant progression and metastatic potential of these cells, consequently also influencing their responsiveness to therapeutic interventions. A reduced expression of vascular endothelial growth factor (VEGF) for example may in turn decelerate tumor angiogenesis and impede the continued proliferation of tumor cells (73).

Being able to successfully simulate the specific properties of solid tumors in model systems represents an important step towards the transferability of findings from tumor models to clinical tumors.

4.3.2 *In vivo* tumor models

Even more close to clinical reality, an *in vivo* model such as an animal model reproduces the growth of a tumor and its reaction to a therapy than *in vitro* models. The most common *in vivo* tumor models are mouse models, in which mice serve as a model organism. For oncological research, they may be genetically engineered or exposed to oncogenic stimuli in order to provoke tumor development. Furthermore, tumor cells from other organisms may be transplanted as so-called “xenografts”. By utilization of animals, studies of human diseases can be performed to gain a deeper understanding of the disease process, all while minimizing the ethical and safety risks associated with human experimentation. However, due to more complex experimental conditions, they may be time-consuming as well as cost-intensive and are subject to high ethical and bureaucratic hurdles (61).

The translation of experimental findings from animal models still represents a barrier which is not easily surmountable. This is due to numerous reasons and inherent differences between animal and human biology. Some reasons why animal models may not be directly applicable to clinical outcomes include differences in metabolism, immune response, and organ function as well as genetic variations between species.

Many diseases manifest differently in animals compared to humans, particularly complex diseases with multifactorial origins such as tumorous diseases. Therefore, animal models may not fully replicate the intricacies of human diseases, leading to variations in treatment responses. The pharmacokinetics and pharmacodynamics of

drugs may differ significantly between species resulting in differences in drug efficacy, toxicity, and side effects. Certain animal models may develop unique pathophysiological responses or artifacts not reflective of human conditions and possible immunological responses in animals may not accurately represent human immune reactions, affecting the evaluation of vaccines, immunotherapies, and infectious diseases as well as tumor research. Differences in metabolic pathways and regulatory systems between species may affect the relevance of animal study results for human application in the field of drug development and testing. Similarly, small sample sizes in animal studies may not capture the heterogeneity observed in human populations which then furthermore include differences in age, gender, and genetic diversity (61).

While animal models remain invaluable for certain types of research and preclinical testing, researchers must exercise caution when extrapolating results to human clinical contexts, recognizing the limitations and potential discrepancies between animal and human biology. Integrating diverse approaches, including *in vitro* studies and human-based research as well as the use of new cell culture methods can enhance the robustness of translational findings.

4.3.3 Animal Testing and the 3R principle

As already stated, *in vivo* models are an essential tool in oncological research for the development and testing of new therapeutics, as well as for the understanding of molecular and cell biological processes of tumorigenesis. Nevertheless, every study on animals must undergo a strict ethical and moral evaluation and critically scrutinize the necessity of suffering being caused to the animals.

As early as 1959, Russel and Burch called for the implementation of the 3Rs concept as a framework for experimental scientific work. The goal of the 3R Principle is to avoid animal experiments altogether (Replacement), to limit the number of animals (Reduction) and their suffering (Refinement) in tests to an absolute minimum (75).

This concept of replacing, reduction and refinement of animal experiments was also elaborated and legally recognized in 2010 in the European Union guidelines on the protection of animals used for scientific purposes (76). The provisions of the European

directive and hence also the 3R Principle were implemented in German law in 2013 in the form of the amended Animal Protection Act and the Animal Protection Act for Test Animals (77).

In more specific terms this means that every scientist planning an animal experiment and applying for approval from the competent authorities must answer the following questions as part of the approval process:

- Are there other methods or strategies not entailing the use of animals?
- Is the number of used test animals reduced to an absolute minimum?
- Is animal suffering kept to the very lowest level possible?

The 3R Principle and its recognition can ultimately pursue the final goal of replacing animal experiments completely, as soon as this is scientifically feasible.

4.4 The Hen's Egg Test - Chorioallantoic Membrane Assay

A special case within the realms of *in vivo* animal testing is portrayed by the Hen's Egg Test with Chorioallantoic Membrane Assay (HET-CAM-Assay). How exactly it differs from other standard animal test models and why it is not necessary classified as one will be explained in detail within this chapter.

Chicken eggs have been used as model systems for scientific studies since the late 19th century particularly for toxicological and teratological investigations (78, 79). In 1985, in search of alternative methods to the ethically questionable Draize Rabbit Eye Test, Luepke further developed the then established Henn's Egg Test (HET) into the HET-CAM test for toxicological investigations: New substances could be tested by applying them onto the CAM and then examining them for irritations such as hyperemia or bleeding (80). The well perfused and easily accessible CAM allows a manifold of experimental settings which range from investigations in wound healing, tissue transplantation, biomaterial sciences, angiogenesis and ultimately the growth and development of tumors (4). The Hen's Egg Test - Chorioallantoic Membrane assay (HET-CAM-Assay) is an enhancement of the chick-development model in the sense that a direct access to the experimental organism is ensured by removal of the egg

shell so that a direct view of the chorioallantoic membrane (CAM) as well as the embryo is possible (81). Furthermore, toxicological analyses can be performed by analysis of organ damage and ultimately death of the embryo. Further information and explanation as to why it is a suitable experimental organism for this thesis in accordance with above-mentioned requirements for animal testing will be specified later on.

The base of the experimental setup in the HET-CAM-Assay is the egg: A self-contained entity, the egg provides all the necessary substances for development, except for oxygen, which diffuses from the external environment. It further comprises the eggshell, inner and outer shell membranes, an air sac, yolk, and albumen (egg white). The eggshell is primarily composed of calcium and protects the embryo as well as delivers calcium for bone mineralization, meeting an increased calcium demand in the last 11 days of development. The inner and outer shell membranes are closely connected, except in the air sac region, which is situated at the blunt end and plays a role in respiration of the developing embryo during incubation. The egg yolk primarily comprises lipids and proteins, synthesized by the hen in its liver and primarily functions in nutrient supply and blood formation. The albumen contains mainly proteins, including lysozymes, and is encased by the eggshell and its membranes. At the beginning of the incubation period, the developing embryo resembles a small cytoplasmic accumulation, resting on the yolk, giving rise to the blastoderm (82-84).

Simultaneously, four extraembryonic membranes form in the egg: yolk sac, amnion, chorion, and allantois, all of which play essential roles in supporting embryonic development. The yolk sac membrane, beginning development quite early, encloses the egg yolk by day five. It consists of a poorly vascularized area, vitellina, and a highly vascularized area, vasculosa. Serving nutrient absorption from the yolk, the yolk sac membrane connects to the embryo through the yolk stalk. Additionally, it plays a role in gas exchange and early blood formation. The amnion provides a protective environment for the embryo, filled with amniotic fluid. The allantois, developing last, serves as a urine storage organ and aids respiratory function through the CAM (83, 84). The described membranes and their position within the egg during chick development is depicted in Figure 1.

The CAM forms from the fusion of the allantois and chorion on day 6 of development, creating three cellular layers: ectoderm (chorion), mesoderm (chorion/allantois), and

entoderm (allantois) (85). It is essentially the equivalent of a placenta for the chick embryo and ultimately comprises a vascular network connected to the embryonic circulation (86). The CAM offers the organic surface for the metabolic exchange of oxygen and carbon dioxide (84). For this purpose, a high vascularization is necessary, which undergoes three phases in its development: capillary sprout penetration, tissue column formation, and intracapillary network development (85). This vascular network also aids calcium supply, ensuring proper bone development whereas the CAM additionally serves as a repository for waste products, such as urea and uric acid (83).

After oviposition, developmental stages unfold within 21 days of incubation, with optimal temperatures ranging between 37 °C and 39 °C. Germ layer formation (gastrulation) and basic body shape with following organogenesis and development of species-specific features, further growth, and maturation of the embryo take place within the incubation period until hatching on day 21 (82).

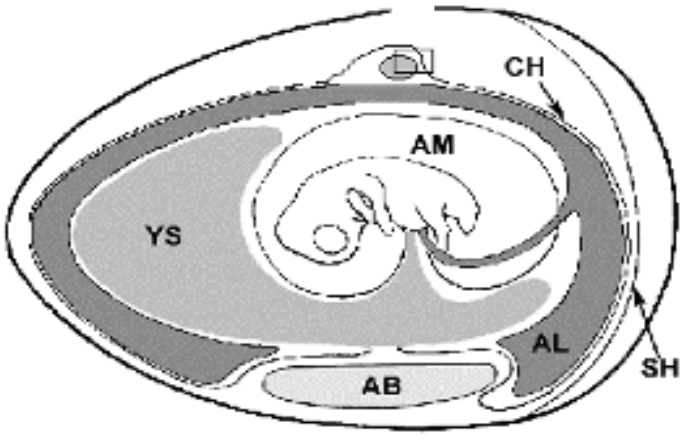

Figure 1: The HET-CAM-Assay, modified after EUGENIN, J. 2005 (87), CH=chorion, AL=allantois, AM=amnion, SH=shell membrane, AB=albumin, YS=yolk sac

4.4.1 CAM-Assay *ex ovo* and *in ovo*

The CAM assay can be conducted using either an *ex ovo* or *in ovo* method with the main difference being the amount of eggshell to be removed.

In the *ex ovo* method, the embryo and its extraembryonic membranes are transferred to another vessel, such as a Petri dish, by breaking and removing the entirety of the

eggshell on day 3 or 4 of incubation. This is illustrated in Figure 2.The further development of the embryo and CAM can be observed without impairment of the field of view. The main advantage, in addition to better visibility of the CAM, is an overall accessibility to the CAM. However, the transfer of the embryo and the CAM may lead to an increased mortality rate (88).

In contrast to this, the *in ovo* method is much closer to the physiological conditions in the egg by only partial removal of the eggshell after drainage of a certain amount of albumen. Only a small part of the CAM is visible and can be treated, but the setup of the *in ovo* method is both closer to natural conditions during the egg breeding process and the mortality rate of the embryos is lower compared to the *ex ovo* method (81). Therefore, the *in ovo* method was chosen for the experiments conducted in this thesis and will be explained in detail in the Methodology chapter.

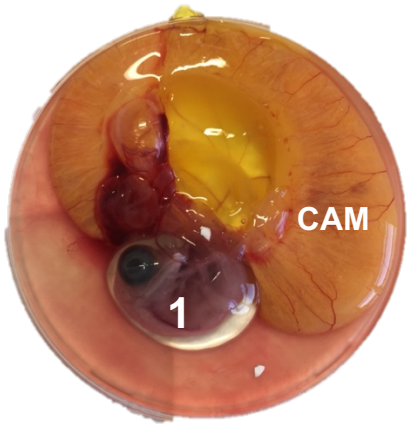

Figure 2: The HET-CAM-Assay *ex ovo* method showing a chicken embryo (1) and surrounding CAM in a petri dish on day 14 of its development, picture taken in the laboratory at the University of Mainz Medical School

4.4.2 Assessment of the HET-CAM-Assay as a model organism

The goal of every research project aiming at the implementation of new therapeutic options is to establish an evidence-based groundwork with clear results, whilst also examining potential harm. Animal models are ultimately the most adequate

experimental models at this stage, before studies can be performed on healthy humans and patients.

The HET-CAM-Assay can be seen as a link between *in vitro* experiments on cell cultures and complex *in vivo* models. In fact, it is considered an embryonic test and not an animal test until day 17 of its development after fertilization, which means there is no obligation to petition to the ethics committee (89). The CAM as an extraembryonic membrane is not innervated and the nervous system of the chicken embryo is only incompletely developed up to day 14 of incubation, which makes the experiments on the CAM ethically justifiable. Xenogeneic tissues and tumors can proliferate on the chorioallantoic membrane (CAM) due to the absence of immune rejection as well as the rich vascular network that supplies essential oxygen and nutrients (90).

Moreover, the solid tumors which were used in this study can be monitored on the CAM at all times during the experiment. This model is amenable to a range of analytical techniques, such as imaging techniques like *in vivo* microscopy or ultrasonography, enabling detailed examination of tumor behavior and tissue interactions. After termination of the experiment, immunohistochemical analyses can be performed of the tissues of interest which will be reviewed in the following chapters (91). The embryo itself is not directly analyzed in the performed tests during this study, but other experiments concerning the effect of nanoparticles have included the analysis of the embryo itself and its organs as well (92).

Overall, the HET-CAM-Assay holds new possibilities to avoid unnecessary experimentation on animals, which is very much in line with the ethical 3 R principle which form the basis of ethical research on animals. The combination of these factors and the straightforward procedure enables the CAM assay to achieve a high quantitative outcome, resulting in improved standardization and reproducibility. In summary, the HET-CAM-Assay is in itself a simple, cost-efficient and well-maintainable research organism with manageable ethical conflict and a genuine alternative to experiments using the mouse model (4).

4.4.3 Application of pharmaceuticals in the HET-CAM-Assay

In order to test substances and pharmaceuticals by using the HET-CAM-Assay , administration of the drugs to be tested can be applied locally to the CAM tissue or injected into the embryonic tissue, albumen or blood vessel system whereas an oral uptake of the drugs to the embryo is not possible (4). A systemic application via intravascular injection of ZnO-NP was performed in the experiments which will be described further on in detail.

Drugs dripped onto the CAM can enter the systemic circulation after absorption and influence the development of the embryo. The activity or toxicity of a drug on the CAM as well as xenogeneic tumors on the CAM and on the development of the embryo can be tested. The toxicity of the tested drug can be assessed by organ analysis, the death of the embryo or a negative effect on the CAM such as irritation (4, 80).

4.4.4 HET-CAM-Assay in oncology

Since the early 20th century, the CAM has been utilized for studies on tumor growth and angiogenesis, establishing the CAM as an experimental system for exploring tumor biology. Rous and Murphy have pioneered in this field by inoculation of chicken sarcoma and moreover the first xenogeneic tumor on the CAM which was originally retrieved from rat and mouse species (93, 94). By transferring tumors onto the CAM, it is possible to investigate the morphological aspects of the tumor tissue, interaction with blood vessels in the CAM when tumor cells penetrate the chorion epithelium and grow into the well-vascularized mesenchymal connective tissue of the CAM within two to five days. Furthermore, metastatic invasion and possible dissemination to the embryo can be monitored as well (90, 95).

All of this is possible due to the lack of an fully functional immune response from the chick embryo itself, since T-cells cannot be detected up until day 11 and B-cells from day 12 of incubation. An unspecific inflammatory reaction was partially described from day 15, and the chicken embryo is considered fully immunocompetent from day 18 of incubation (96, 97). Therefore, the growth of tumor cells originating from different species can be evaluated using the HET-CAM-Assay. Ribatti gives an overview of

most commonly used tumor cell lines which can be administered onto the CAM (90, 95).

Furthermore, the HET-CAM-Assay enables the observation of the supply system through blood vessels and therefore the development of methods and substances which are intended for use as anticancer agents (98). Angiogenesis and metastasis development can be closely monitored within the HET-CAM-Assay model organism by pure visual accessibility to the study organism and further imaging techniques (91). In the HET-CAM-Assay, tumor cells stimulate neo-angiogenesis by secreting angiogenic factors such as VEGF, leading to sprouting of vessels from the surrounding CAM vessels into the tumor tissue (99). It was demonstrated that tumors without sufficient blood supply in the CAM did not exceed a diameter of approximately 1 mm. The so-called vascular phase begins after xenografts have been set on the CAM for 72 h and instigate rapid growth (100). Either via spontaneous cell migration or purposely injected tumor cells, metastases in the lung, liver, and brain of the chicken embryo can then be formed (101). An increased mRNA expression of metastasis-associated genes and VEGF was measured within the CAM tissue as early as six hours after injection of the cells. Up to eighty percent of malignant cells survived within the capillary system and migrated within 1-3 days into peripheral tissue (102). The important process of extravasation could be investigated in more detail by the microscopic observation of fluorescently labeled malignant cells within the vasculatory system of the CAM. A detailed description of studies on tumor cells as well as the process of metastasis and angiogenesis carried out on the HET-CAM-Assay can be found in the publications of Ribatti (95) and Deryugina (103).

On a side note, data collected from experiments on tumor biology and treatment methods performed with the CAM assay present input for mathematical models and algorithms to simulate tumor dynamics. Similar to new molecular structures of antibiotics generated by multi-scale computational studies on the base of existing physicochemical mechanisms, it is fathomable that the data collected from the CAM assay with a rapid turnover may pose important data to generate new methods for antineoplastic therapies. This is a new experimental study form also called *in silico* which offers new opportunities well in line with the 3R principle. By integrating a three-dimensional study organism, *in vivo* data may advance tumor simulations due to more realistic representation of tumor behavior and vasculature. Pre-clinical evaluation of

the susceptibility of the tumors to possible anti-neoplastic agents could also be investigated using this model (104-106).

4.4.5 Huh-7 tumor cell line and the HET-CAM-Assay

In order to consolidate the chapters on oncological research, an overview of the experimental setup will be given. The experiments for this thesis were conducted by using the Human Hepatocellular Carcinoma (Huh-7) cell line. This was first established in Japan by cultivation of well differentiated cells of a human hepatocyte derived cellular carcinoma in 1982 (107). It is a well-examined and widely used immortal cell line of epithelial-like tumorigenic cells.

After forming a solid three-dimensional tumor using a basement membrane matrix called Matrigel® (62), the tumors were then placed onto the CAM in the chicken egg using the *in ovo* method, essentially combining above-mentioned stages of tumor research models. Further details will be described in this and the following chapter as well as the Material and Methodology part.

The inoculation of a xenograft derived from Huh-7 cells in Matrigel® and the subsequent successful growth of a solid tumor in the CAM of a HET-CAM-Assay have been previously documented and are well-established (108). Furthermore, the induction of apoptosis through reactive oxygen and nitrogen species (RONS) by ZnO and ZnO-NP in Huh-7 cells in a conventional cell culture has also been investigated (3).

4.5 Zinc

The initial intervention administered to the HET-CAM model organisms involved the application of ZnO-NP. To expound upon the significance of zinc and zinc oxide within the realm of oncology, particularly in its nanoparticulate form within oncology, comprehensive details will be provided in the following chapters. These details will include fundamental insights into zinc as an element, toxicity mechanisms, and hypotheses concerning the effects of ZnO-NP.

Zinc is an essential trace element which is involved in endogenous metabolism and abundant in all body tissues, as a compound with oxygen to form zinc oxide (ZnO) but predominantly dissolved in its ionic form Zn^{2+}. Ranging after iron, zinc is the second most common metal found within the human body and is located mostly in the musculoskeletal system where it is present intracellularly and associated to membranes (109). Zinc assumes a pivotal role in numerous essential physiological processes, including cellular proliferation, differentiation, and metabolic homeostasis. This is underscored by the binding potential of zinc to up to 3,000 proteins and approximately 10% of the human genome encoding zinc-binding proteins, reflecting zinc's diverse involvement in bodily functions, including its central role in synthesis of (deoxy)ribonucleic acids, signaling pathways, apoptosis, and enzymatic activities. Zinc can for example serve as a cofactor for catalytic activities such as in carbonic anhydrase converting carbon dioxide into bicarbonate or carboxypeptidase cleaving peptides (110, 111). Another important function of zinc-dependent proteins are transcription factors with zinc-finger domains, typically involved in DNA repair, migration, transcriptional regulation, and signal transduction (112, 113).

The human zinc homeostasis is finely regulated and responds sensitively to fluctuations. The gastrointestinal tract plays a central role in zinc homeostasis, as it serves as a key route for zinc absorption and release. In contrast, renal excretion remains consistently low and contributes minimally to regulation (114).

Humans require a daily intake of between 12 and 15 mg of zinc, obtained through dietary sources. Although a reliable method for determining individual zinc status is lacking, it is known that approximately 2 g of zinc are physiologically present in the human body, primarily in the form of zinc oxide. In plasma/serum, the concentration is in the range of 12-16 µM, primarily bound to albumin. Intracellularly, the majority of zinc ions are bound to zinc-binding proteins, and the concentration of free or loosely bound zinc ions is in the picomolar range (115).

Intracellularly, the regulation of the cytosolic zinc ion concentration involves two main mechanisms: stable states, where zinc-binding proteins act as buffers, and non-steady states, where more complex mechanisms, such as transporters, come into play. This regulation, termed the muffling reaction, includes the influence of calcium channels and zinc transporters on zinc redistribution between cellular compartments. For

instance, when a cell encounters an influx of zinc ions, muffling reactions will moderate the subsequent increase in cytosolic zinc ion concentration. These reactions aim to ultimately return the cytosolic zinc ion concentration to its initial level by either transporting zinc ions into subcellular storage or discharging them from the cell to prevent high zinc concentrations and formation of zinc complexes (116-118).

Zinc is present in enzymes such as superoxide dismutase, acts as a protein stabilizer, and can function as a signaling molecule or second messenger. Using the example of zinc-dependent and ubiquitously occurring phosphodiesterase, it becomes evident how the influence on individual components of signal transduction can be interconnected. The phosphodiesterase (PDE), which cleaves the second messengers cyclic adenosine monophosphate (cAMP) and cyclic guanosine monophosphate (cGMP), is stimulated by low zinc ion concentrations, while high concentrations can inhibit PDE (116).

There is evidence suggesting that zinc, similar to calcium, can also function as a signaling molecule since intracellular signaling cascades are influenced by the zinc concentration and it has been found that zinc can be secreted by neurons. Consequently, zinc is discussed in the role of a neurotransmitter, modulating the release of N-methyl-D-aspartate (NMDA) and γ-aminobutyric acid type A (GABA) (116).

Additionally, under the influence of hydrogen peroxide (H_2O_2), zinc can shift the ratio of mitochondrial antiapoptotic Bcl-2-like and proapoptotic Bax-like membrane proteins to an antiapoptotic balance. Low zinc concentrations can favor apoptosis in cells through caspases since their allosteric inhibition by zinc binding is then reduced (119, 120).

Various studies have demonstrated that zinc deficiency is associated with increased oxidative stress. However, excessively high zinc concentrations may also lead to high amounts and activity of ROS. Under physiological conditions, zinc is not redox-active but it acts as an indirect antioxidant. Even though zinc ions themselves are redox-inert, zinc is termed pro-antioxidative. In physiological conditions, zinc acts as an indirect antioxidant, protecting enzyme thiol groups, scavenging radicals through metallothionein, and inhibiting ROS sources like Nicotinamide Adenine Dinucleotide Phosphate Oxidase (121). Additionally, zinc competes with iron and copper for

bindings, which are redox-active metals, thereby impeding ROS generation and neutralizing superoxide ions (115, 122, 123).

Zinc flux and homeostatic zinc signals also collectively regulate the optimal functioning of both innate and adaptive immunity. In this context, zinc emerges as a crucial guardian of the immune system, given that the optimal performance of virtually all immune cells is intricately dependent on adequate zinc levels. There are indications that zinc influences cytokine production. Zinc affects several key cellular signaling cascades relevant to the immune system, including Mitogen-activated protein kinases, caspases, and transcription factors (123). The so-called "zinc waves", which are calcium-dependent zinc fluxes spanning minutes, are suspected to promote the production of interleukin 6 (IL-6), tumor necrosis factor alpha (TNF-α) (116, 124). Additionally, stimulation of the immunoglobulin E receptor on mast cells results in the release of intracellular zinc ions from the endoplasmic reticulum, independent of external entry into the cell (125).

It has been shown that several functions of the immune system were diminished in cases of zinc deficiency. T-helper cells, macrophages, neutrophilic granulocytes, cytotoxic T cells, and natural killer cells all experience restricted functionality, resulting in an overall reduction of peripheral T-cells. Due to the diversity of its purposes, it is acknowledged that both excessive and insufficient zinc concentrations can be harmful and their impact on immune responses is an area of active investigation. Consequently, zinc may hold the potential of offering a beneficial influence on the well-being of patients grappling with immune-related disorders or immune-related neoplastic disorders (126, 127).

As previously mentioned, zinc exerts its influence on the response to oxidative stress through a multitude of indirect mechanisms. Zinc deficiency predisposes individuals to heightened oxidative stress and consequent development of degenerative diseases (115). However, categorizing zinc solely as an antioxidant fails to capture its nuanced role. Depending on its concentration, zinc demonstrates a spectrum of effects, ranging from anti- to pro-apoptotic, anti- to pro-inflammatory, and exhibiting both cytoprotective and cytotoxic properties.

4.6 Nanoparticles

The forthcoming sections of this chapter will offer the introduction to the broader concept of nanoparticles and, more specifically, the exploration of ZnO-NP with further outlook on the context of their potential applications in antineoplastic therapies as is aimed to explore further during the performed studies.

The European Commission defines nanomaterials as materials that occur naturally or are manufactured through natural processes, containing particles where at least 50 percent of them fall within the nanoscale range from 1 nm to 100 nm (128). Materials which fall into the contemporary definition of nanoparticles were already employed 4,500 years ago for stabilizing ceramics (129). However, the first scientific description of nanoparticles occurred in 1857 by Michael Faraday (130). In present times, nanoparticles have become integral components of various everyday substances and industrial products, including particulate matter, aerosols in both consumer goods and the environment, nutrition, packaging materials, cosmetics, and pharmaceuticals (131, 132). Nanoparticles manifest in various shapes, including spheres, discs, hemispheres, cones, and rods, and can be either hollow, solid, or porous. This diverse array allows for the meticulous selection of nanoparticles based on interactivity, binding capacity, and transportability. The individual nanoparticles can form agglomerates when loosely assembled and aggregates when they firmly interconnect or fuse (133).

A distinctive characteristic of nanoparticles is their large surface area relative to size and volume. This heightened surface area implies a manifold of physical, chemical, and biological properties such as a greater proportion of atoms on the particle surface, feasibly rendering nanoparticles more reactive than conventional larger molecules (134). The augmented surface area is also responsible for the improved water solubility and bioavailability commonly associated with nanoparticles. Furthermore, the extensive surface area allows for engineered nanoparticles with a variety of surface features, enabling for example precise drug targeting. Nanoparticles utilized in current nanodrug formulations encompass various shapes such as lipid- or polymer-based carriers. Furthermore, they may consist of metals or metal oxides, other inorganic materials, and proteins (25, 135, 136).

4.6.1 Nanoparticles in medical and pharmaceutical fields of use

The pharmacological potential of nanomaterial medications therefore constitutes a highly intriguing and promising field of research, as nanoparticles exhibit specific and diverse properties. Their possible properties, particularly defined by their pharmacokinetics, encompass enhanced efficacy, reduced toxicity, and improved drug targeting. Existing drugs are frequently conjugated with nanoparticles to modify their pharmacokinetic and/or pharmacodynamic attributes, resulting in notable enhancements in therapeutic outcome (137, 138). The small size of nanoparticles contributes to improved solubility, enabling the reevaluation of poorly soluble bulk drugs. This, in turn, facilitates the transformation of insoluble or poorly soluble drugs into aqueous suspensions, eliminating the necessity for toxic organic solvents. Additionally, their diminutive size imparts increased bioavailability and extended half-life. Particles smaller than 200 nm demonstrate a prolonged half-life compared to larger counterparts, irrespective of surface modifications (139).

As already stated, another promising application of nanoparticles is in drug delivery. An essential proposed advantage of nanoparticles over conventional preparations in drug transport for tumor therapy is the assumed Enhanced Permeability and Retention Effect (EPR effect). This effect is made possible by the growth of immature vessels in tumor tissue, characterized by low endothelial-endothelial interaction and a reduced number of pericytes, resulting in endothelial spacing on the order of 100 nm or more. In contrast, normal vessels have an endothelial cell spacing of 6.5-7.5 nm. Consequently, nanoparticles accumulate more readily in tumors, aided by impaired lymphatic drainage, aberrant interstitial pressure of tissues, and consequent diminished venous drainage, inhibiting particle removal by the immune system (25, 140, 141).

To ensure and enhance this “passive targeting”, various nanoparticle forms are employed to optimize the properties of nanoparticles, including liposomes, albumin-bound nanoparticles, polymer nanoparticles, dendrimer nanoparticles, ligand-bound nanoparticles, and metallic nanoparticles. An example would be the conjugation of nanoparticles with macromolecules such as polyethylene glycol (PEG), forming a protective coating around the particles to prevent premature degradation (142).

The application of nanoparticles in medicine is already established and further researched on in the following fields: drug delivery, cancer control, diabetes treatment, and bioimaging. In addition to this they may possess antibacterial, antimicrobial, anti-inflammatory, and wound-healing properties (143, 144). In the field of imaging techniques, nanoparticles present a compelling prospect for optimizing and/or substituting conventional contrast agents. Experiments have demonstrated that nanoparticles yield significantly superior resolution outcomes compared to conventional contrast agents in magnetic resonance imaging and contrast-enhanced sonography (145). Furthermore, as was already made clear, the ongoing efforts to use antineoplastic potential of metallic nanoparticles in the clinical setting is an area of high interest. The therapeutic application of gold nanoparticles against prostate cancer has already been established while nanoparticles of various other elements are being researched on (146, 147). Moreover, the use of nanoparticles in the therapy of non-solid cancers such as leukemia has gained interest and may be perceived as a new therapeutic strategy with systemic application (148). This experimental study in the preclinical phase will contribute to the effort in further elucidating the potential of ZnO-NP as possible therapeutic anti-neoplastic agents in the future.

4.6.2 ZnO-NP

ZnO as a manufactured inorganic compound forms the base for the nanoparticulate form of ZnO-NP. ZnO is classified as a "GRAS" (generally recognized as safe) substance by the US Food and Drug Administration (FDA), whereas ZnO-NP have not yet officially been categorized (2). An overview of ZnO will be made before further elucidating physical and chemical basics of ZnO-NP to understand their biochemical behavior and special potential.

Zinc oxide (ZnO) exists naturally as the coarse-grained mineral zincite and is technically derived through the oxidation of zinc or zinc vapor with atmospheric oxygen, commonly known as zinc white. Alternatively, it can be obtained through the calcination of various precursors like zinc hydroxide, zinc carbonate, or zinc nitrate. ZnO manifests as colorless, hexagonal crystals or a white, non-flammable loose powder, exhibiting a reversible color change from white to lemon-yellow upon heating and cooling. Its density is measured at 5.61 g/cm³, and it undergoes vaporization at 1300 °C,

sublimating at 1800 °C without forming a liquid melt. It is widely used in various branches of industry ranging from rubber manufacturing to pharmaceutical and cosmetics as well as electrotechnology and photocatalysis (132).

ZnO-NP also find diverse applications across various industries, showcasing their versatility and utility. Since ZnO-NP exhibit both UV-A/UV-B protection and transparency and possess antibacterial and fungistatic effects, they are used in textiles, clear coatings in the wood and furniture industry, as well as in transparent plastics and plastic films (plastic lenses). These exhibit high transparency (>90% transmission) in the visible spectral range and UV opacity (<10% transmission) for wavelengths below 360 nm. In the realm of cosmetics, these nanoparticles are therefore prominently featured in products like sunscreens and lotions, leveraging their capacity to effectively absorb ultraviolet (UV) radiation for enhanced skin protection. The food industry incorporates ZnO-NP as an additive in items such as breakfast cereals, underscoring their multifunctional role. Beyond cosmetics and the food sector, ZnO-NP play a pivotal role in the manufacturing processes of rubber and cigarette filters. Their incorporation in these products demonstrates their functional attributes in enhancing performance and meeting specific industry requirements. In the field of ceramics, ZnO-NP serve as valuable additives, contributing to the overall composition and properties of ceramic materials. Furthermore, these nanoparticles play a crucial role in the realm of paints, where they are employed as coating agents, imparting specific characteristics to various paint formulations. In summary, the widespread utilization of ZnO-NP across industries highlights their adaptability and significance in fulfilling distinct functional roles (132, 133, 149).

On a side note, as zinc and zinc oxide are known to exhibit antibacterial properties (used in zinc ointments), consequently, inhibition of the growth of various bacterial species by ZnO-NP has been observed (150). This is put to use in wound healing preparations (149). The growth inhibition was intensified under (UV) light exposure and was more pronounced with smaller particles than larger ones (151, 152).

It is furthermore characteristic that ZnO-NP exhibit a positive charge and are highly soluble in water. They display a high tendency to agglomerate and are prone to dissolution, meaning that, in addition to the actual particles, aqueous solutions also contain dissolved zinc ions. The zeta potential of ZnO-NP refers to the electric charge

of a moving particle in a medium such as water or another buffer. Particles with a zeta potential of -10 mV to +10 mV are considered neutral, while particles with a zeta potential of +/-30 mV are strongly charged (153). The greater the zeta potential deviates from neutral values the higher the colloidal stability, which in turn describes the resistance of nanoparticles to aggregate, agglomerate or sediment. This is crucial when nanoparticles enter biological systems; for example, the zeta potential is an essential factor in overcoming mostly negatively charged cell membranes (154). Abdelmonem et al. demonstrated that ZnO nanoparticles with a positive zeta potential are better absorbed by cells, making it a potential advantage for cell uptake and intracellular effects (155). Passive diffusion and endocytosis are also discussed as uptake mechanisms. Condello et al. demonstrated that individual particles and aggregates smaller than 100 nm tend to enter the cell through passive diffusion and accumulate in the cytoplasm, endosomes, lysosomes, mitochondria, as well as in the cell nucleus. In contrast, agglomerates of various sizes predominantly enter cells through endocytosis. The solubility behavior of ZnO-NP can also be influenced by surface coatings (154, 156).

4.6.2.1 Toxicity of ZnO and ZnO-NP

It is of utmost interest to further understand interactions and consequences of ZnO-NP entering a biological system, especially when considering a pharmaceutical application of ZnO-NP. Primarily, the human body is able to maintain a well-regulated zinc homeostasis, as it is involved in the regulation of many crucial biological processes. If administered in excessively high doses or when located inappropriately, it can, however, have a toxic effect and lead to cell death, following Paracelsus' principle (92).

Further exploring the toxicity of ZnO, a lethal dose 50%, LD_{50}, for ZnO is 240 mg/kg was measured as intraperitoneal application in rats and when oral application took place, the dose was 7950 mg/kg (92). Translating this to ZnO-NP, relatively high toxicity levels for cells from various tissues and organisms have been demonstrated in *in vitro* studies. The ZnO-NP exhibit a steep dose-response curve, meaning that the toxic effect sharply increases beyond a certain concentration. For most cell types, this concentration ranges from 10-20 µg/ml (3, 157). Details of the toxicity mechanisms will be proposed further along.

The exposition of the human body to ZnO(-NP) takes place in several ways such as by skin contact, oral intake, or inhalation. As an example, metal fume fever, also known as "brass founders' ague" or "zinc fever," is a self-limiting inflammatory response caused by the inhalation of metal fumes containing zinc oxide or other metal oxides. It commonly occurs in individuals exposed to the fumes generated during the welding, cutting, or heating of metals such as zinc, brass, or galvanized steel. Similarly, administration of fine or nanoscale zinc oxide particles into the lungs of mice or rats induces a temporary pulmonary inflammation. Interestingly, both the intensity and course of this reaction were similar for fine ZnO and nanoscale ZnO (57, 158, 159).

As they are commonly used in cosmetics, the dermal uptake of ZnO-NP remains an important question. The size of zinc oxide particles used in sunscreens ranges from 20 to 60 nm. However, the very small ZnO nanoparticles are additionally coated with silicon or aluminium oxide before being added to sunscreens. They then aggregate into clusters of 200-500 nm which usually do not penetrate healthy skin and thus presumably pose no health risks to consumers (123, 160). *In vitro* studies have shown genotoxic effects when direct uptake of ZnO-NP by skin cells occurred (161).

In order to clarify these genotoxic and cytotoxic effects, various toxicity mechanism of ZnO-NP have been suggested (162). In order to understand toxicity mechanisms further, the dissolution of ZnO nanoparticles and their pathways into the cell remain subjects of ongoing research. It has been postulated that the electronic properties or solubility of the particles, rather than their size, are decisive for their cellular effects: within the aqueous milieu of the human organism, ZnO-NP partially or completely dissolve, releasing zinc ions. Many studies attribute harmful effects to the release of ions from the nanoparticles. However, the dissolution process is not uniformly efficient for different ZnO-NP and is also dependent on the precise composition of the aqueous solution. Therefore, the cells' uptake of either zinc oxide particles or dissolved zinc ions appears to be contingent upon the stability of the nanoparticles in the respective environment. Factors such as ambient temperature and pH value can furthermore influence agglomeration and ion release. When pH value is low and many hydrogen ions H^+ are within the aqueous solution, they transfer on the surface of ZnO-NP, preparing a positive surface load which is more prone to attraction to negatively charged cells (163, 164).

In addition to this, the site of dissociation also seems to have an impact. While dissociation of the nanoparticles outside the cell led to reduced cell toxicity *in vitro*, intracellular dissociation resulted in more severe damage *in vitro* (163). This could be explained by the formation of precipitates of zinc in the cell culture medium and/or formation of a protein corona around the ZnO-NP, making them unavailable for intracellular uptake and direct interaction (165, 166). Literature encompasses studies which describe the direct uptake of ZnO-NP by cells via endocytosis, further establishing that cell surface and NP coating influence uptake and cell interaction correspondingly (161, 167). Especially within the cellular uptake structures of the endo-lysosomal system it has been shown that the characteristic low pH values within lead to dissolution and high concentration of zinc ions (42, 164, 168-171).

Remarkably, it has become clear that not only dissolution of ZnO-NP leading to free zinc ions causes toxicity, but also that nanoparticle-specific reactions are significant, although exact mechanisms are further to be elucidated (172). Their reactivity is increased since nanoparticles are small in size, and therefore have more surface area relative to their volume. This effect may increase interaction with the environment and lead to enhancement of reactions such as catalysis, dissolution, and biological activity. In addition to this, defects in the lattice structure of ZnO nanoparticles have been identified, contributing significantly to increased reactivity, which is then associated with an increased generation of reactive oxygen species (ROS) in ZnO-NP compared to larger ZnO microparticles. Interestingly, this effect was observed even when excluding or reducing UV light to rule out UV-induced ROS formation (152). *In vitro*, zinc oxide nanoparticles also induced an enhanced production of inflammation markers in human endothelial cells, possibly linked to a rise in ROS (173).

In summary, released zinc ions and consequently newly formed reactive oxygen radicals are of heightened interest when talking about toxicity mechanisms of ZnO-NP.

4.6.2.2 ZnO-NP and ROS

To further understand the effects of ZnO nanoparticles on biological systems, it is necessary to understand associated ROS formation and the following complex cascade of possible consequences. This will be further elucidated in this chapter.

Zinc oxides are semiconductors with a wide band gap of 3.37 eV. They absorb a wide range of the solar spectrum and can thus engage in photocatalysis, enhancing chemical reactions due to energy by light in the presence of the catalyst, in this case ZnO-NP. It can be prompted when the ZnO-NP absorb photons with a higher energy than their band gap and react with surrounding molecules. Oxygen from the environment can react via the conduction band electrons to form superoxide radicals and water can react to form hydroxyl radicals, protonated superoxide radicals or hydrogen peroxide, notably all ROS. These are either attached to the nanoparticles or exist as free entities in aqueous solutions (25, 150).

It was found on the one hand that these reactions may take place without biological matter present (163). Moreover, it was also shown that ROS could be generated directly via interactions of ZnO-NP with the biological cell environment or via interaction with the mitochondria, meaning intracellular reactions (150, 174).

Additionally, to differentiate between damage caused by ZnO nanoparticles due to ROS and damage caused by increased zinc ions and direct nanoparticle interaction, Shen et al. demonstrated that ZnO nanoparticles increased zinc ion concentration and ROS, but under the influence of antioxidants such as vitamin E or vitamin C, ROS levels decreased while cell toxicity remained constant (170). Although ROS undoubtedly play a major role in toxicity of ZnO-NP, this further suggests that ZnO-NP toxicity goes beyond generation of ROS and consequences.

Furthermore, it is well observed that the generation of ROS in cellular systems is not only attributed to surface effects but also depends on the concentration of released zinc ions, which is specific for these metallic nanoparticles (163). Pinpointing the exact mechanism underlying the intracellular elevation of ROS is exceptionally challenging, as the visualization of ZnO-NP, zinc ions, and ROS within the living cells is highly intricate (162).

The formation of ROS also takes place due to the disruption of the iron homeostasis by ZnO-NP, since iron is a highly redox-active element. Certain results suggested defects in the mitochondrial iron transport after application of ZnO-NP. This then led to iron overload, rise of ROS, lipid peroxidation and depletion of anti-oxidative buffer systems, ultimately causing ferroptosis. Both ZnO-NP and zinc ions contribute to this (172).

Whilst the rise in ROS is frequently associated with mitochondrial damage, it is yet to be determined whether this damage is either an initiating factor or a downstream effect – or both. Zinc appears to physiologically inhibit complex III of the electron transport chain in the mitochondria during mitochondrial respiration. Furthermore, it inhibits the α-ketoglutarate dehydrogenase complex and the citrate cycle, all part of aerobic glycolysis (49). Likewise, studies have shown that ZnO-NP can influence the cellular respiration of cancer cells (175). Damage to mitochondria with upsurge of cytochrome c and therefore induced intrinsic mitochondria signaling pathway of apoptosis have been identified (164).

As a result of high zinc ion concentration, O_2 consumption is reduced, the mitochondrial membrane potential decreases and ROS creation increases further by reactions with free electrons. The antioxidative defense mechanisms such as glutathione can buffer ROS, but eventually become scarce, which leads to depletion of the capacity of the cellular antioxidant defense system. Cellular damage caused by ROS includes lipid peroxidation, DNA damage, or protein denaturation and therefore impairment of function of most important cellular players as already described in chapter 4.2.3 (176, 177). Furthermore, the zinc homeostasis is disrupted.

Genotoxic effects can occur by direct interaction of ZnO-NP with the DNA, or as an indirect effect of the induction of oxidative stress as mentioned above. It is known that zinc ions can interact with the DNA in the form of several binding mechanisms, which presumably have a regulatory function *in vitro* and *in vivo* (178-180). Similarly, ZnO-NP have been detected to interact with DNA molecules directly, although only measured *in vitro* (181). A presumed mechanism of action is the intercalation in DNA molecules. This is especially decisive when ionizing radiation is applied and high production of ROS takes place, since their effect on DNA can be enhanced by present ZnO-NP (182). The DNA damage which was measured after application of ZnO-NP consisted of single- and double-strand breaks in the DNA with chromosomal breaks, similar to effects due to ionizing radiation. These were measured by comet assay or specific staining methods over elevated nucleobase derivative 8-OHdG, which are present after to oxidative reactions with DNA molecules have taken place. These experiments were mostly abiotic experiments although special emphasis must be set on Zijno et al. since they performed cellular models (51, 183-186). Furthermore, ROS-dependent impairment of DNA repair mechanisms leads to mutagenic potential and

cell cycle arrest (187). Although these investigations have been made, a wide and exact portrayal of genotoxic mechanisms of action remains elusive, especially when a distinction of direct ZnO-NP action and indirect ROS action is to be made.

Further examining the role of mitochondrial damage as a toxicity mechanism, it has become clear that mitochondrial dysfunction can be the consequence of a rise of ROS in the cell as well as a consequence of direct nanoparticle interaction with the mitochondria. It is well established that ZnO-NP influence mitochondrial function negatively (188-190). The failure of mitochondrial activity may also be due to an exhaustion of anti-oxidative cell systems in the form of enzymes such as catalase and superoxide dismutase since it was shown that ZnO-NP inhibit these directly (191).

These mechanisms of toxicity lead to mitochondrial disruption and apoptosis (via intrinsic pathway), measured via revealed upregulation of Bax and downregulation of Bcl-2 in cancer cells. Downstream, caspases are the enzyme family which execute the apoptotic effects (192, 193). Furthermore, it has been concluded that this is a p53-dependent process, as high ROS lead to cell death via p53 whereas it has to be noted that mild ROS causes p53 to stimulate antioxidant genes (172). This is also relevant in the already mentioned process of ferroptosis, a cell death characterized by accumulation of iron after mitochondrial dysfunction (148, 172). Additionally, necrosis in combination with apoptosis has also been observed when examining the cellular reactions after application of ZnO-NP (119, 174, 194).

Notably, the production of reactive oxygen species may also partially be a result from cytotoxic effects of the ZnO-NP themselves rather than serving solely as the initial trigger of cell death. During cell death induction, ROS may be released during processes such as (mitochondrial) membrane disruption (170). The exact cellular effects of ZnO nanoparticles, whether caused by direct interaction, free zinc ions or generated ROS consequently, continue to be the subject of current research.

4.6.2.3 ZnO-NP as an anti-tumor agent

After consideration of the above stated toxicity mechanisms, the question of how one might be further able to use it in the efforts of antineoplastic research was posed as it

is a major subject of current research to find new therapeutic methods against cancer. The effects of ZnO-NP on solid tumors have been a subject of research with the perspective that ZnO-NP might have beneficial effects in cancer treatment and might also enhance other therapy mechanisms. However, they also raise concerns about possible risks, such as toxicity or unintended side effects. It is important to note that findings vary based on factors such as nanoparticle characteristics, dose, and specific tumor types(157). As with all therapeutic options in oncology, it is of utmost interest to specifically target the cancerous tissue and reduce side effects on other tissues (149, 195).

Several research projects have been aimed at gaining insight into nanoparticles' effects on tissues, each examining specific cells. For instance, Taccola et al. showed an increased uptake of ZnO-NP in healthy mesenchymal cells compared to healthy osteocytes and therefore suspect a fundamentally increased toxicity of zinc oxide-containing nanoparticles towards highly proliferating cells, regardless of their malignancy (157). In 2008, Hanley et al. showed that ZnO nanoparticles exhibited increased toxicity towards neoplastic cells in a direct comparison between healthy and neoplastic T cells (196). Other *in vitro* experiments demonstrated more pronounced damage to tumor cells compared to healthy cells by ZnO nanoparticles even beyond immune cells (54, 120, 197, 198).

A definite set of mechanisms to explain tumor-specific toxicity cannot be specified yet while many concepts have been researched on. One possible explanation for a tumor-selective toxicity of ZnO-NP could be the increased metabolic proliferation rate of tumor cells (157, 196). The heightened metabolic activity leads to increased anaerobic glycolysis with a lack of oxygen and nutrients within the tumor micromilieu (199, 200). The low pH value within the tumor microenvironment may then add to increased cytotoxicity as the degree of dissociation of ZnO nanoparticles depends on the pH value, with lower pH values leading to a higher dissociation degree and thus increased free zinc ion concentration (201, 202).

As the concentration of free zinc ions plays a crucial role in ROS formation with above-mentioned cytotoxic effects, it was shown that extracellular release of zinc ions from ZnO-NP leads to higher toxicity (163). This presents another argument for ZnO

nanoparticles in cancer therapy, as tumors create an acidic environment with decreased pH values due to.

Furthermore, tumor cell-specific vulnerability to suffer from oxidative stress, high phagocytotic activity as well as absence of functional DNA repair mechanisms was proposed (203, 204). A direct antiproliferative effect can be attributed to the following effects on a molecular basis: Induction of apoptosis through cell cycle arrest by continual damage of DNA mostly consisting of double strand breaks and by predominantly creation of reactive oxygen species (ROS) causing so-called “oxidative stress”. The accumulation of these effects and lacking control mechanisms in malignant cells prevents proliferation of tumor cells, thus a stagnation in growth and spread of tumor mass (54).

Moreover, tumor cells exhibit a high concentration of anionic phospholipids and lactate acid on their outer membranes and thus have a measurable negative membrane potential (205, 206). The interaction of tumor cells with positively charged ZnO-NP is driven by electrostatic interaction, which promotes cellular uptake via phagocytosis and cytotoxicity of ZnO-NP (203).

In addition to this, ZnO-NP have demonstrated anti-angiogenic properties, inhibiting the formation of new blood vessels which tumors generally need for growth and the process of metastasis (207-209). As was further already stated, ZnO-NP may influence the immune response, affecting the tumor microenvironment. Certain studies suggest immunomodulatory effects of ZnO-NP which could impact tumor progression (124).

The influence of the shape and size of zinc oxide particles on their toxic effects is still unclear. It is to be further evaluated and considered that the size of ZnO-NP appears to influence their biological effects as well. Presumably, smaller particles may have higher cytotoxicity and penetrate tissues more effectively, potentially impacting their therapeutic potential and safety (25, 124, 210).

But not only the ZnO-NP themselves have direct effects, they can also be used as a vehicle for other substances. Their biocompatibility and tunable surface make them suitable for drug delivery. In order to obtain a targeted effect and avert non-specific interaction, the specificity of ZnO-NP to cancer cells could be enhanced by adding molecules to their surface such as individual receptors, minimizing off-target effects,

and improving their efficacy in solid tumor treatment. Furthermore, coating ZnO-NP with gold or aluminium as well as silica-coating has significantly reduced their toxicity for non-malignant cells (136, 142, 211, 212).

In summary, the different properties and combination possibilities of ZnO-NP are offering the prospect of tumor-specific zinc release or a combined zinc-drug release. In addition to these characteristics, numerous combination possibilities arise and promise to further improve overall targeting as well as tumor-specific toxicity (213).

Following this thought, a combination of ZnO nanoparticles with conventional cancer therapies is conceivable, as already demonstrated in the combination of ZnO nanoparticles with daunorubicin/doxorubicin (210, 214, 215) and other standard chemotherapeutics (216) to enhance toxicity of ZnO-NP as well as UV-radiation or visible light in the sense of photodynamic therapy (210, 216-219). Previous studies have also demonstrated that ionizing radiation can enhance the antimicrobial activity of ZnO-NPs, further suggesting that their antineoplastic efficacy could also be potentiated when combined with radiation (220, 221). It is feasible that the applied radiation could enhance the cytotoxic effect of ZnO-NP by generation of even more ROS and thus induced cell death via apoptosis, as has been evaluated by promising studies (182, 222). However, a comprehensive evaluation of ZnO-NPs as radiosensitizers for cancer treatment remains lacking, highlighting the need for detailed research in this area.

Currently, metalloid nanoparticle-based antineoplastic research is mainly in fundamental stages, with experiments being mostly limited to *in vitro* and *in vivo* models. However, the developments in this area of research are accelerating by the year. Since successful experiments have been conducted on different cell lines, the future promises a broad application potential for zinc oxide-containing nanoparticles in cancer treatment. This thesis aims to advance the state of knowledge and evaluate the combination of ZnO-NP and the established antineoplastic process of radiation. A thorough understanding of their mechanisms of action, dose-response relationships, and potential safety concerns is crucial. It is a declared goal of the development of tumor therapies to maximize efficacy and minimize adverse effects.

5 Material and methodology

The following tables of the used material and presentation of the methodology will allow a detailed insight into how experiments were conducted using standard cell culture techniques as well as the HET-CAM-Assay and how the results were obtained.

5.1 Material

The below-mentioned materials were used to conduct the experiments. Chemical agents, expendable material, and devices are listed with manufacturer information.

5.1.1 Chemical agents

Table 1: List of the used chemical agents

Chemical agent	**Manufacturer**
Albumin Fraction V	AppliChem, Darmstadt, Germany
Ampuwa® sterile water for injection (Ph.Eur.)	Fresenius Kabi AG Bad Homburg, Germany
Antifungal Spray, GermDecon Spray	Sereva Electrophoresis GmbH, Heidelberg, Germany
Autoclaved distilled water	Freshly produced with Autoclave, Tuttnauer Systec 5050 ELVC
Avidin solution	Life technologies, Carlsbad, US
Diaminobenzidine (DAB) + Chromogen	Dako, Glostrup, Denmark
Diaminobenzidine (DAB) + Substrate Buffer	Dako, Glostrup, Denmark
Dulbecco's Modified Eagle Serum F-12 (DMEM)	Gibco Life Technologies, Carlsbad, US
Eukitt® Entellan	Sigma Aldrich, Taufkirchen, Bayern
Fetal bovine serum (FBS)	VWR International GmbH, Darmstadt, Germany
Formaldehyde 4%	VWR International GmbH, Darmstadt, Germany
Goat Serum (Normal)	Dako, Glostrup, Denmark
Hydrogen peroxide 30%	Carlroth, Karlsruhe, Germany
Isopropylalkohol	Hedinger, Stuttgart, Germany

Matrigel® Matrix	Corning, Kaiserslautern, Germany
Methanol	Honeywell, Ludwigshafen, Germany
Penicillin/Streptomycin (P/S)	Sigma Aldrich, St. Louis, US
Phosphate buffered Saline (PBS)	Gibco Life Technologies, Carlsbad, US
ROTI®Plast	Carlroth, Karlsruhe, Germany
Streptavidin/Horse Radish Peroxidase	Dako, Glostrup, Denmark
Terralin® liquid	Schülke & Mayr GmbH, Norderstedt, Germany
Trypan blue	Sigma Aldrich, St. Louis, US
Trypsin EDTA (T/E)	Sigma Aldrich, St. Louis, US

Table 2: List of the prepared solutions

Solution	**Components and stock solutions**
Cell culture medium	DMEM + 5% FBS + 2% P/S
Cell culture detaching solution	1% T/E in PBS

Table 3: List of the used antibodies

Antibody	**Manufacturer**
Monoclonal Mouse antibody **alpha - Smooth Muscle Actin (alpha-SMA)** Clone 1A4	Sigma Aldrich, Taufkirchen, Bayern
Monoclonal Mouse antibody **Ki-67 Antigen Clone MIB-1**	Dako, Glostrup, Denmark
Monoclonal Mouse antibody **Pan-Keratin (PK) C11**	Cell Signaling Technology, Cambridge, UK
Polyclonal Goat **Anti-mouse** Immunglobulins/Biotinylated	Dako, Glostrup, Denmark
Polyclonal Goat **Anti-rabbit** Immunglobulins/Biotinylated	Dako, Glostrup, Denmark
Polyclonal Rabbit Antibody **Cleaved Caspase-3 (CC3) Asp175**	Cell Signaling Technology, Cambridge, UK

5.1.2 Expendable material

Table 4: List of the used expendable material

Material	Manufacturer
Adhesive tape	Tesa SE, Norderstedt, Germany
Cell culture flask Cellstar® 75 cm^2	Greiner Bio-One International GmbH, Frickenhausen, Germany
Cell culture flask Cellstar® 175 cm^2	Greiner Bio-One International GmbH, Frickenhausen, Germany
Centrifuge tubes 50 ml, 20 ml, 10 ml	Greiner Bio-One International GmbH, Frickenhausen, Germany
Coverslip 50 mm	Carl Roth GmbH + Co. KG, Karlsruhe, Germany
Filter for embedding cassettes, TISSUE-TEK 2	Vogel GmbH & Co. KG, Giessen, Germany
Folded filter, diameter 150mm	Schleicher & Schuell GmbH, Dassel, Germany
Hydrophobic Dako Pen	Dako, Glostrup, Denmark
Injection needle 21 G, BD Microlance 3	Becton, Dickinson and Company, Franklin Lakes, US
Injection needle 25 G, Hypodermic-needle	Becton, Dickinson and Company, Franklin Lakes, US
Injection needle 30 G, BD Microlance 3	Becton, Dickinson and Company, Franklin Lakes, US
Microscopic slides, 76 x 26 mm	Diagonal GmbH & Co. KG, Münster, Germany
Microscopic slides Superfrost Plus	Gerhard Menzel B.V.& Co. KG, Braunschweig, Germany
Parafilm® Bemis	Hecht Pharma, Bremervörde, Germany
Petri dish Cellstar® 6 well	Greiner Bio-One International GmbH, Frickenhausen, Germany
Petri dish Cellstar® 145 cm^2	Greiner Bio-One International GmbH, Frickenhausen, Germany
Pipet, Serological 5 ml	Greiner Bio-One International GmbH, Frickenhausen, Germany

Pipet, Serological 10 ml	Greiner Bio-One International GmbH, Frickenhausen, Germany
Pipet, Serological 25 ml	Greiner Bio-One International GmbH, Frickenhausen, Germany
Precision Wipes®, Kimtech Science	Kimberly-Clark Europe Limited/Professional Sector, Reigate, UK
Scalpel, single-use size 11 AESCULAP	B. Braun AG, Melsungen, Germany
Silver nitrate 50% tips	Rösch & Handel BANO Healthcare GmbH, St. Anton/Arlberg, Germany
Surface disinfection spray, terralin liquid	Schülke & Mayr GmbH, Norderstedt, Germany
Syringe 1 ml Injekt®-F	B. Braun AG, Melsungen, Germany
Syringe 10 ml Discardit™	Becton, Dickinson and Company, Franklin Lakes, US
Tape Micropore™	3M, Neuss, Germany
Tips for Eppendorf™Pipets	Eppendorf AG, Hamburg, Germany
Tissue embedding sponge	Kartell, Noviglio, Italy
Tissue embedding cassette	Katell Spa, Noviglio, italy
Tubes 1,5 ml	Eppendorf AG, Hamburg, Germany
Tubes Safe-Lock 5 ml	Eppendorf AG, Hamburg, Germany

5.1.3 Devices

Table 5: List of the used devices

Device name	**Manufacturer**
Autoclave Tuttnauer Systec 5050 ELVC	Systec GmbH, Linden, Germany
Biological safety workbench class II HERA flow	Heraeus GmbH, Hanau, Germany
Cell incubator HERACell 150i CO2	VWR International GmbH, Darmstadt, Germany
Centrifuge Multifuge 1L-R	Heraeus GmbH, Hanau, Germany
Drying oven	Heraeus GmbH, Hanau, Germany
Egg Incubator Type 3000 – D	Brutmaschinen-Janeschwitz GmbH, Hammelburg, Germany
Heated Paraffin Embedding Module Leica EG1140 C + H	Leica, Wetzlar, Germany

Microscope camera Nikon DS-Fi1	Nikon Corporation, Tokyo, Japan
Microscope Nikon Eclipse TE2000-U	Nikon Corporation, Tokyo, Japan
Microscope TMS-F	Nikon Corporation, Tokyo, Japan
Neubauer counting chamber 0,1 mm depth	BRAND GmbH, Wertheim, Germany
Pipet boy acu (automatic pipet)	INTEGRA Biosciences, Biebertal, Germany
Pipets Eppendorf Research® plus	Eppendorf AG, Hamburg, Germany
Paraffin Stretching bath MH8517	Carlroth, Karlsruhe, Germany
Precision scale, Kern ABT120-5DM	Kern & Sohn GmbH, Balingen, Germany
Rotary Microtome 2165	Leica, Wetzlar, Germany
Software NIS-Elements D 5.11.00	Nikon Corporation, Tokyo, Japan
Spatula 18/10 Stainless steel, 150x7 mm	Bochem Instrumente GmbH, Weilburg, Germany
Surgical scissors	Fine Science Tools, Heidelberg, Germany
Ultrasonic bath EMMI-40HC Sonicator	EMAG, Mörfelden-Walldorf, Germany
Vortex Device VV3	VWR, Radnor, Pennsylvania, US
X-ray machine D3000 Controller	Gulmay Medical, Krefeld, Germany
X-ray machine D3150	Gulmay Medical, Krefeld, Germany

5.1.4 Cell line

The Huh-7 cell line was established in 1982 by harvesting cells from a human hepatocellular carcinoma, a primary malignancy of the liver, of a 57-year old patient in Japan (107). The cells have been extensively utilized in biomedical research, particularly in studies related to liver physiology, cancer biology, and therapeutic development. It is commonly used in research for pharmacological studies and experiments dealing with virus-related diseases such as hepatitis C since it is a well-suited replication system which allows the *in vitro* production of infectious virus particles, specifically those of the Hepatitis C virus (223, 224).

Previous studies and experiments in the laboratory of the AG have established this cell line. It has proven itself by an overall good success rate of transfer from the typical two-dimensional monolayer culture into the three-dimensional solid tumor and subsequently an adequate tumor growth on the CAM. The Huh-7 cells used in this experimental setting were checked for contamination with mycoplasma frequently and

subculturing was performed until passage 30 at most. The cells exhibit epithelial morphology and grow adherently, as is showcased in Figure 3Figure 3Figure 3Figure 3, with a doubling time of 1,5 to 2 days. The cells were originally provided by the research group Lynch Syndrome HNPCC at the University of Frankfurt Medical School.

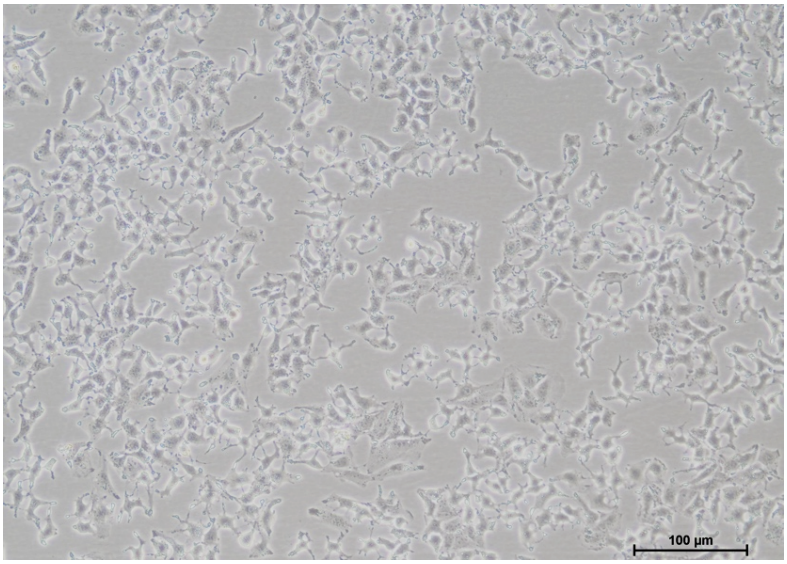

Figure 3: Huh-7 cells under the microscope with a 100x magnification.

5.1.5 Hen's eggs

The hen's eggs of the breed White Leghorn which were used for the HET-CAM model were delivered by the company LSL Rhein-Main GmbH, Dieburg, Germany and were eggs sold for breeding purposes. The eggs were usually delivered one day before the experimental set up began and stored in a cool and dry space until this point of time.

5.1.6 Nanoparticles

The nanoparticles used in these experiments were produced by Dr. rer. nat. Melanie Viel of the AG Tremel at the Department of Inorganic Chemistry of the Johannes Gutenberg University of Mainz. The synthetization was performed according to Cheng et al. (225). The nanoparticles were at all times stored in a cool and dry storage space.

The analysis of the zeta potential of the used nanoparticles from batch number 210 (MV210) resulted in a mean value of +22,4 mV while the size was determined at

10,73 nm ± 0,3 nm. This measurement was performed with the Zetasizer nano ZS (Malvern Instruments Ltd., Malvern, UK). A representative image of the ZnO-NP is shown below in Figure 4.

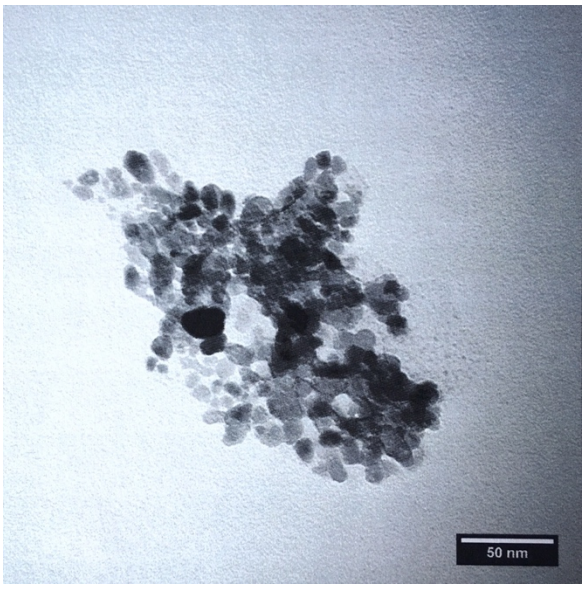

Figure 4: A representative transmission electron microscopy image of ZnO-NP, obtained by Melanie Viel of the University of Mainz.

5.1.7 Radiation device

The Gulmay Medical X-ray machine D3150 is a superficial X-ray therapy system which is put to clinical use for treatment of various cutaneous carcinoma types and eczema as well as an analyzation method for materials and objects in the industrial use of radiography.

The low-energy X-rays with a range of 10-100 keV penetrate the specimen up to a depth of 4 ± 1 mm.

5.2 Methodology

5.2.1 Timeline of the experimental setting

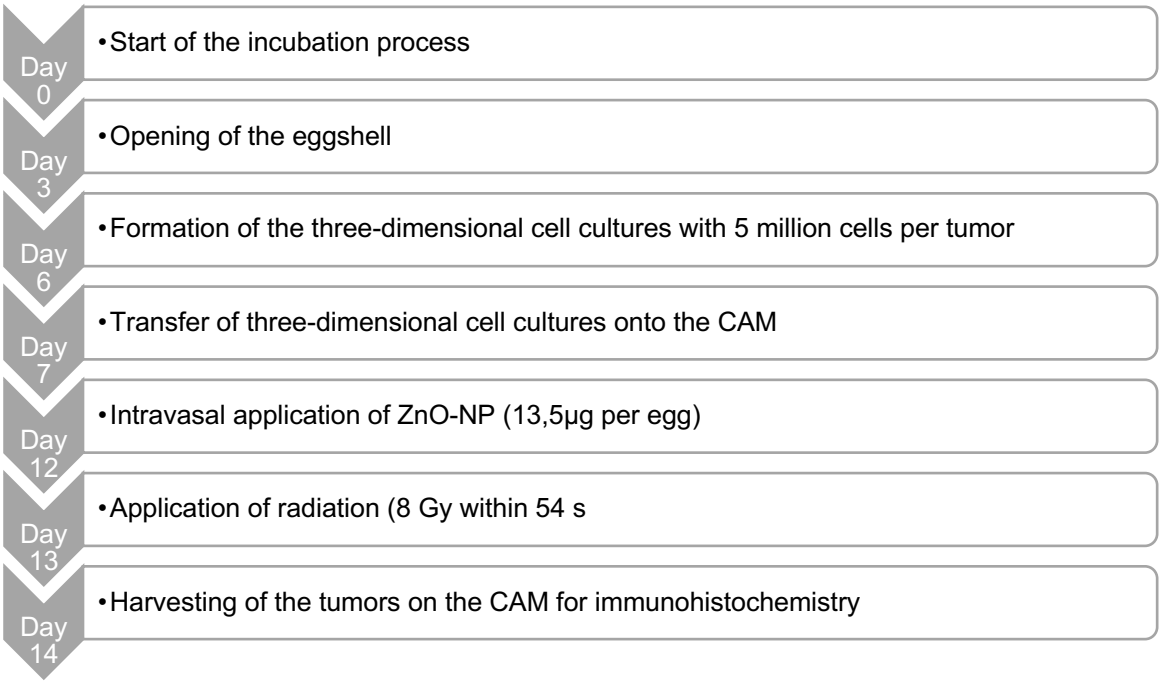

Figure 5: Timeline of the experimental setting of the HET-CAM-Assay.

The timeline which is shown above in Figure 5 Figure 5gives an overview to portray at which point of time every step of the experimental process was performed in relation to the others. It embraces the temporal guidelines of the HET-CAM-Assay.

5.2.2 Cell culture handling

The Human Hepatocellular Carcinoma Cells (Huh-7) were cultivated with DMEM as a medium which contained water, amino acids, vitamins, glucose as an energy source and electrolytes as well as a bicarbonate buffer system to which 5% fetal bovine serum (FBS) and 2% Penicillin/Streptomycin (P/S) were added.

The cells were incubated at 37°C and 5,1% CO_2. A quick and thorough examination of the cell culture in each cell culture flask was performed every second day using a light microscope to check for cell size, viability, uniformity, confluence, and possible contamination.

The culturing of the cells was performed on a clean workbench with laminar air flow which ensured a contamination-free cultivation of cells. A Trypsin/EDTA solution (T/E) was prepared by diluting it to attain a 1% solution and then stored at 4 °C as well as the prepared cell culture medium.

After discarding the old medium, a quick lavage with Phosphate Buffered Saline (PBS) was performed which was then disposed of as well. Applying a simple solution of 4 ml Trypsin EDTA (T/E) and incubating this for approximately 4 min detached the cells from the cell culture flask. Adding 10 ml new cell culture medium stopped the proteolytic effect of T/E so that the cells could be harvested into a 50 ml tube. This was centrifuged at 1500 rpm for 5 min. to separate the cells from the liquids.

After discarding the supernatant, the cell pellet could be mixed with cell culture medium again, where the volume was separated into at least two new cell culture flasks with a volume of 25 ml cell culture medium each in order to allow the cells to multiply. This was performed every two to three days.

5.2.3 Formation of three-dimensional cell cultures

In order to form a solid tumor, three-dimensional cell cultures using Matrigel® as a substrate material were created. Since each egg would need a solid tumor and there were at least 15 eggs within each study group as a minimum at this point of the experiment, it was planned to form at least 60 solid tumors.

Every tumor was to consist of 5 million cells. To ensure this, the number of cells in each cell culture flask had to be calculated using the Neubauer counting chamber. The cells were harvested from the cell culture flasks as mentioned above. The cells of six cell culture flasks or petri dishes were combined and resuspended with cell culture medium in a 50 ml tube.

Taking 20 µl of the suspension of each tube and mixing it with 20 µl Trypan blue produced a 1:2 dilution which was put into the Neubauer counting chamber. Then followed the counting of all cells within the four main squares of the chamber leaving out the dead cells stained blue by the trypan blue.

The number of cells calculated at this point could be further evaluated using the following formula:

$$\frac{N \times 2 \times 10.000 \quad \times 50ml}{5.000.000} = n$$

N = total number of cells counted within the four main squares of the counting chamber
n = amount of solid tumors which could be created from the number of cells [ml]
10.000 is a constant variable of the Neubauer counting chamber

The cells which were at this point suspended in 50 ml medium would now be centrifuged and resuspended in the exact amount of millilitres of medium corresponding to the number of tumors (n) which could be formed, resulting in 5 million cells per 1 ml. The cell culture was divided in the sense that 1 ml of the cell suspension was put into one 1,5 ml Eppendorf tube. After placing this in the centrifuge for 8 min. at 1500 rpm, the supernatant was removed. The cell pellets were then diluted in 20 µl ice-cold Matrigel® and three-dimensional cell cultures were formed on 6-well plates with a maximum of 4 cell cultures per well. The cell substrate Matrigel® was stored on ice to keep it liquid throughout the whole process. Its components offer the Huh-7 cells an adequate substrate to form a three-dimensional solid tumor *in ovo.*
Incubation of the prepared Matrigel® cell cultures in the incubator for 30 min solidified them. To store them overnight, 2,5 ml of cell culture medium were added for each well and then incubated at 37 °C in the cell incubator again.

5.2.4 Chorioallantoic Membrane Assay (HET-CAM-Assay)

5.2.4.1 Preparation and incubation of the eggs

The eggs were checked for damage upon arrival and the eggshell was cleaned thoroughly with autoclaved distilled water and precision wipes. The incubators were prepared by cleaning with antifungal spray at least 24 hours before the new incubation process and insertion of water reservoirs filled with autoclaved distilled water directly before insertion of the eggs into the incubator. The temperature was set to 38°C and an approximate humidity of 45% (displayed as 45rH). This was monitored by the

incubator and more water was added if needed. Now the eggs could be set into the incubators in a horizontal position. This marked day 0 of the experiment.

After three days of rest, so that the developing embryo could position itself within the egg, the opening of the eggshell was performed. To make this possible, 6 ml of the egg white, the albumin, was removed beforehand by inserting a 10 ml syringe with a 21 G needle at the blunt end of the egg. The hole was then closed by adhesive tape to prevent further leakage of albumin from the egg.

Subsequent to the lowered level of albumin in the egg, the CAM was also lowered in such a manner that cutting an oval hole in the upwards facing side of the eggshell using surgical scissors was possible without damaging the CAM. This was further supported by adding Micropore® tape on the eggshell to prevent parts of the eggshell from contaminating the CAM. A layer of transparent Parafilm® closed the opening of the egg back up while guaranteeing gaseous exchange and protection from evaporation. This mimics the original eggshell with the added advantage of being see-through. At this point, the developing embryo could be seen as a beating heart within a vascular structure which will later form the CAM.

Check-ups for vitality of the developing embryos and morphology of the CAM as well as checks for contamination and water levels of the incubators were mandatory from now on. This was performed at least every two days. The embryo and CAM within the egg which could be observed during this time are shown in Figure 6.

Figure 6: CAM assay with developing chick embryo on day 6

The experimental set-up continued with the transfer of the three-dimensional cell cultures onto the CAM on day 7 which were produced as described in chapter 5.2.3. This was performed by cutting into the CAM close to a vessel with a scalpel size 11 and then adding the solid tumors with a spatula on top of this. A layer of 20 µl cooled Matrigel® was added with a pipette to enhance the probability of adequate growth of the tumors. The eggs were then closed again with Parafilm® and put back in the incubators.

A resting phase for five days without movement of the eggs and daily checks for viability of the embryos was necessary to further ensure tumor growth on the CAM.

On day 12, before the next intervention, the eggs were sorted into four groups which had the defined treatment specifications as listed in Table 6 below.

Table 6: Definition of treatment groups

Group number	ZnO-NP (yes/no)	Radiation (yes/no)
1	no	no
2	yes	no
3	no	yes
4	yes	yes

5.2.4.2 Application of ZnO-NP

The ZnO-NP were stored in Eppendorf tubes at 8°C as a powdery substance, which then had to be prepared accordingly in order to obtain a suspension for intravascular injection. From the weight of the ZnO-NP it was calculated how much Ampuwa® sterile water had to be added to acquire a 10 mg/ml stock suspension which was then vortexed and treated in an ultrasonic bath at 37 kHz for 5 min (226).

Further dilution was performed to acquire a 450 µg/ml suspension which was then diluted 1:2 once more. Of this resulting suspension a volume of 60 µl, which is equivalent to 13,5 µg ZnO-NP, was injected intravasally into each egg after careful homogenization by sonification.

On day 12 the intravascular injection of ZnO-NP for groups 2 and 4 or injection of water in the control groups with a volume of each 60 µl per egg was performed. After removal of the Parafilm® cover, a 30 G cannula with an Injekt®-F syringe was then used to inject the ZnO-NP suspension or Ampuwa® for the control group into a vessel of the chick embryo.

To stop leakage from the vessels in form of a bleeding after injection, silver nitrate sticks were used to cauterize vessels after injection. The view of the AM at this point of time during the experimental setup is portrayed in Figure 7. Parafilm® was once more added to close the eggs and they were put back into place within the incubators.

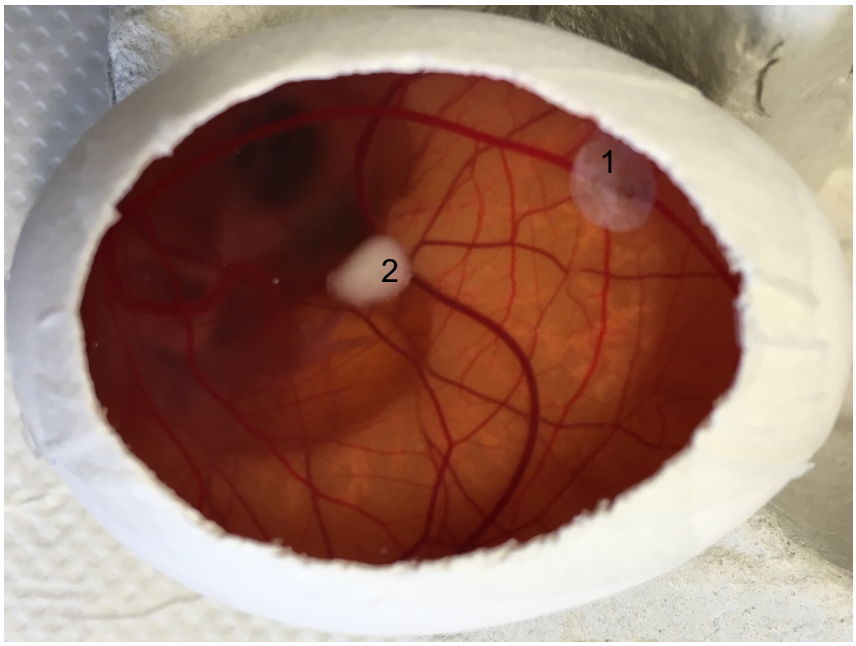

Figure 7: CAM assay with developing chick embryo on day 12, solid tumor (2) and injection site (1)

5.2.4.3 Radiation

On day 13 of the CAM assay and 24 hours after injection of ZnO-NP, radiation was applied with attached Parafilm® on the eggs to reduce changes in temperature, humidity, and the general environment of the CAM as much as possible as well as the prevention of contamination. The eggs were stored in polystyrene containers for the transport. The control group was also transported and set into the X-ray machine to mimic the stress by movement and temperature changes equivalently.

The applied dose with the Gulmay Medical X-ray machine was 8 Gy which was achieved by operating the machine at 80 kV and 30 mA for 54 s (0,9 min) with a 2 cm tube and filter number 4.

5.2.4.4 Harvesting of the tumors

After another 24 hours following the last intervention, on day 14, the experimental study cycle was finalized by harvesting of the tumors. This was achieved by cutting the egg open vertically along the lateral poles while lying in a petri dish. The CAM spread out superficially on the contents of the egg. The chick embryo was sacrificed by cutting the neck. The tumor was then harvested by cutting the CAM around it with a diameter of around 1 cm. This resulting specimen was collected by a spatula and cleaned as well as stretched out in distilled and autoclaved water. Then it was transferred onto a filter paper and put in an embedding cassette together with a sponge which were then stored in formaldehyde 4% for two days.

5.2.5 Immunohistochemical staining

The method of immunohistochemistry was chosen for tissue analyses in order to obtain assessable results from the experiments of this study. This chapter will give basic knowledge to understand the immunohistochemical stainings of the CAM specimen containing the solid tumors. They were chosen to evaluate the overall architecture, proliferation, and apoptosis rate as well as vascularization of the tumorous tissue.

Completing the experiment after collection of the specimen, a bath in distilled water and then an ascending alcohol series (70/80/90% isopropanol) was performed.

Afterwards, the specimens were embedded in paraffin, which allowed to cut them in slices of 4 µm thickness. The paraffin then had to be removed again to allow the following staining methods. These were performed by , medical technical assistant of the AG in the laboratory of the Department of Otorhinolaryngology, Head- and Neck Surgery of the University of Mainz Medical School's Hospital. The exact protocols can be found in detail in another piece of literature of the working group (91, 92).

The basis for the examination of the solid Huh-7 tumors was made possible by a hematoxylin-eosin (HE) staining. The pan-cytokeratin staining specified the amounts of the solid tumor further in a brown color. As described in the available literature, the following immunohistochemical staining methods were used for further analyses. Antibodies marking Ki-67 allowed to examine the rate of cell proliferation, whereas the quantification of apoptotic cells was made possible by the staining with antibodies marking Cleaved Caspase-3 (CC3). For the evaluation of vascularization, an antibody against alpha – Smooth Muscle Actin (alpha-SMA) was used. For Pan-Keratin (PK) the concentration of 1:500 was used (227), for Cleaved-Caspase 3 (CC3) 1:50 (228), Ki-67 1:150 (229) and for alpha - Smooth Muscle Actin (alpha-SMA) 1:1500 (230).

5.2.5.1 Hematoxylin and eosin staining

The Hematoxylin and eosin staining method (HE) is a widely employed histological technique which uses two contrasting dyes to visualize both cellular and tissue morphology, which is essential in differentiating structures. It enables the assessment of tissue architecture, cellular organization, and the overall presence of abnormalities which is routinely used for the diagnosis and classification of tumors, inflammatory conditions, and various structural changes in disease. Standardized protocols are essential for consistent and reproducible HE staining results (231).

Hematoxylin is a natural dye and acts as a basic or nuclear stain, binding to acidic components in the cell, such as DNA and RNA, marking it a blue or purple color and facilitating the visualization of nuclear morphology and density. Eosin is an acidic dye that binds to alkaline components in cells, including cytoplasmic proteins, showing them as pink or red hues in a contrast to above-mentioned hematoxylin. Cellular

components can be distinguished and therefore epithelial cells, connective tissue and blood cells can be easily differentiated (232).

5.2.5.2 Pan-keratin

Keratins, also called cytokeratins, are intermediate filament proteins found primarily in epithelial cells providing structural support as part of the cytoskeleton and maintaining structural integrity and mechanical resilience of epithelial tissues. Pan-keratin (PK) is a term used to describe a collection of numerous isoforms of intracellular keratin which assemble into filaments and form heterodimers of an acidic keratin and a basic keratin part (233). Keratin isoforms exhibit tissue- and differentiation-specific profiles, marking an important role in histopathology, allowing for the detection and characterization of epithelial cells in tissues (234). Their application is particularly valuable in cancer diagnosis, aiding in the accurate identification and classification of tumors based on their origin and differentiating them to other neoplasms (235). Likewise, as a tumor of epithelial origin, the hepatocellular carcinoma cell line Huh-7 is positive for a specific set of keratins (107).

The pan-keratin (PK) mouse antibody used in this study detects a various number of keratin filaments, namely keratin 4,5,6,8,10,13 and 18 simultaneously, providing a comprehensive evaluation of epithelial cells (227). Therefore, the detection and characterization of tumor cells within a microscopic tissue sample is ensured. The assessment of cytokeratin expression profiles can also be used to aid in subclassifying malignant masses and determining their likely tissue of origin by considering each isoform since a tissue-specific and differentiation dependent expression can be observed. The interpretation should always consider factors such as antibody specificity, potential cross-reactivity, and the heterogeneity of cytokeratin expression in different tissues (236, 237).

5.2.5.3 Cleaved Caspase-3

Cleaved Caspase-3 (CC3) serves as a valuable diagnostic and prognostic marker in various pathological conditions, including cancer. Its characterization provides

valuable insights into the regulation of apoptosis and its relevance in various physiological and pathological contexts. Its presence indicates ongoing apoptotic processes and can be correlated with disease severity and treatment responses (238). In cancer research, the assessment of CC3 levels may provide insights into the effectiveness of anti-cancer therapies.

Cleaved caspase-3, also known as active caspase-3, is a crucial component of the caspase family of cysteine proteases and plays a central role in the execution phase of apoptosis, which is critical for tissue homeostasis, development, and the elimination of damaged cells. Activation of caspase-3 requires proteolytic processing of its inactive proenzyme at an aspartic acid residue into two activated fragments and the generation of an active heterotetramer, therefore being referred to as “cleaved caspase-3”. It plays a main role in both the intrinsic and extrinsic pathways as one of the most important triggers of apoptosis, serving as a downstream effector caspase which is either wholly or partially responsible for the proteolytic cleavage of numerous key proteins, such as the nuclear enzyme poly ADP-ribose polymerase (PARP-1) (58, 238, 239).

Immunohistochemistry and Western blotting are common techniques for detecting CC3 by using specific cleaved caspase-3 antibodies which detect the endogenous levels of the large fragment of activated caspase-3 resulting from cleavage adjacent to aspartate 175 (238). This enables the visualization and quantification of activated caspase-3 in tissue samples or cell lysates. While cleaved caspase-3 is a widely accepted and reliable marker for apoptosis, its interpretation should also consider factors such as the specificity of antibodies used, potential non-apoptotic functions, and the dynamic nature of apoptotic processes.

5.2.5.4 Ki-67

Ki-67 is a valuable marker for assessing cellular proliferation, particularly in the context of cancer research and clinical applications in cancer diagnostics and prognostics. Its expression patterns provide crucial information about the status of cellular division and therefore tissue vitality, aiding in the understanding of various physiological and pathological processes (240).

The Ki-67 antigen is a large non-histone nuclear protein (345, 395 kDa) which is expressed during active phases of the cell cycle due to Ki-67s function of maintaining structural integrity of chromosomes. It is absent in resting (quiescent) cells. Thus, this antibody can be used to mark actively proliferating cells within normal and tumorous tissue (241).

It is clinically used in addition to grading systems for breast cancer and neuroendocrine tumors. After immunohistochemical staining and further microscopic observation, the number of mitotic cells with positive Ki-67 staining within the aberrant tissue is counted and expressed as a percentage. This labeling index is graded with grades ranging from 1 to 3, where an index of more than 20% results in grade 3 which marks a high proliferation rate. This in turn correlates with poor differentiation of the tumorous tissue as well as a higher probability of tumor growth along with further spreading (240, 242). Although it has to be noted that there are various staining methods and scoring criteria with individual cutoff values. In breast cancer for example, Ki-67 expression is used to classify tumors into different molecular subtypes and guide decisions about treatment strategies since it is considered a potential predictive marker for the response to certain therapeutic methods. Tumors with high Ki-67 expression may respond better to treatments targeting rapidly dividing cells such as chemotherapy and radiotherapy (243).

Furthermore, Ki67 expression is used to study cell proliferation in various contexts in developmental biology, neuroscience, and regenerative medicine with the possibility of investigating cell turnover in tissues under diverse conditions (241).

5.2.5.5 Alpha-smooth muscle actin

Alpha-smooth muscle actin (α-SMA) is a protein which plays a significant role in cellular structure and function, particularly in the context of smooth muscle cells. It is a member of the actin protein family, which are essential components of the cytoskeleton. The primary function of α-SMA is to participate in the contractile machinery of smooth muscle cells which are commonly found in organs such as the gastrointestinal tract, blood vessels, and airways. When actin filaments are activated, these cells contract and a myriad of cellular processes including locomotion, secretion, cytoplasmic

streaming, phagocytosis, and cytokinesis can be initiated, leading to the regulation of various physiological processes such as regulation of the blood vessel diameter and the movement of substances through hollow organs (244).

α-SMA is also involved in the process of myofibroblast differentiation. Myofibroblasts are cells with characteristics of both fibroblasts and smooth muscle cells, and their presence is often associated with tissue repair by cell contraction as well as fibrosis by abnormal accumulation of extracellular matrix components. α-SMA is frequently used as a biomarker in pathology to identify the activation of myofibroblasts and the presence of smooth muscle cells in tissues (245).

The monoclonal antibody used in this study is specific for the isoform α-SMA (mouse IgG2a isotype) and derived from a hybridoma generated by fusion of mouse myeloma cells and splenocytes from an immunized mouse. It reacts specifically with α-SMA in immunoblotting and indirect immunofluorescence labeling of formalin-fixed, paraffin-embedded, or frozen tissue sections resulting in the possible identification of smooth muscle cells and myofibroblasts (230). Furthermore, it is a marker of pericytes, which are vascular mural cells embedded within the basement membrane of microvessels. These cells play a crucial role in angiogenesis, as well as in maintaining the morphology and stability of blood vessels (246). Therefore, it is possible to use it as a marker for (newly) developed vessels as it was done in this experimental study.

5.2.6 Guidelines for data analysis

The specimens were analyzed using an inverted microscope and the software NIS-Elements D 5.11.00 (Nikon) as well as ImageJ-win64. Different objectives were used to reach magnification settings of 40-times, 100-times, or 200-times. The images were then fused to display the entire specimen by using the ImageJ software with a “Stitching” plugin (247) and saving the data in tiff format.

First of all, the tumors were evaluated with the HE staining for adequate display of both the CAM and the tumor. The PK staining specified the borders of the solid tumor further. It was evaluated whether the tumor had grown into the CAM tissue and only such specimens were used for the following analyses. The PK staining offered the

base for the calculation of the tumor area, which was performed digitally by the ImageJ software.

For the quantification of apoptosis within the solid tumors, the antibody marking cleaved caspase-3 (CC3) was used. The total number of CC3-positive cells relative to the size of the tumor (in μm^2) which was calculated with the NIS Elements software was then acquired and is displayed in the graphs of the result section.

As an indicator for proliferating cells, the immunohistochemical staining method for antigen Ki-67 was analyzed. First defining at least 5 and up to 10 regions of interest (ROIs) in the PK staining (100x magnification with a 250x250 pixels size of the ROIs) and then choosing the same ROIs within the Ki-67 staining led to calculating the mean with standard deviation of Ki-67-positive cells within the solid tumor as well as portrayal of the relative amount of Ki-67-positive cells comparing it to Ki-67 negative tumor cells within the ROIs.

The alpha-SMA staining was used to show the vascularization of the solid tumor and surrounding CAM tissue. An assessment of the vascularization of the tumor area was performed by count of alpha-SMA-positive structures resembling microvessels relative to the size of the tumor (in μm^2), which was defined by the above-mentioned positive area of the PK staining.

5.2.7 Statistical analyses

The statistical analyses were conducted with the software GraphPad Prism version 6.01 for Windows. “N” describes the number of study subjects (CAMs) analyzed. The middle values of the data set within each group of each experimental run were calculated and shown in the graphs, see section 4. The data was checked for Gaussian distribution by the Shapiro-Wilk test. A one-way analysis of variance (ANOVA) by performing Tukey's multiple comparisons test was used to check for statistical significance (p-value <0,05) for comparison of results between different treatment groups.

6 Results

A total of six experimental study cycles as described above and a quantity of 83 CAMs were included in the statistical analyses with a minimum of 17 CAMs per group in total to heighten reliability and validity of the results. Further detail can be found in the Attachments section.

6.1 HE staining

As described above, the HE staining is a standard technique to portray tissue samples and analyze their basic architecture. It was initially important to gain an overview of the sample of the CAM by following the cellular architecture. The CAM was oriented with the chorion as a multi-layered epithelium on the superior edge and single-layered allantois below as showcased in Figure 8. After being set onto the CAM, the tumor (marked by +) grew from the chorion into the mesothelial area, ultimately reaching the allantois. This is portrayed in the following pictures as a growth from top of the specimen downward.

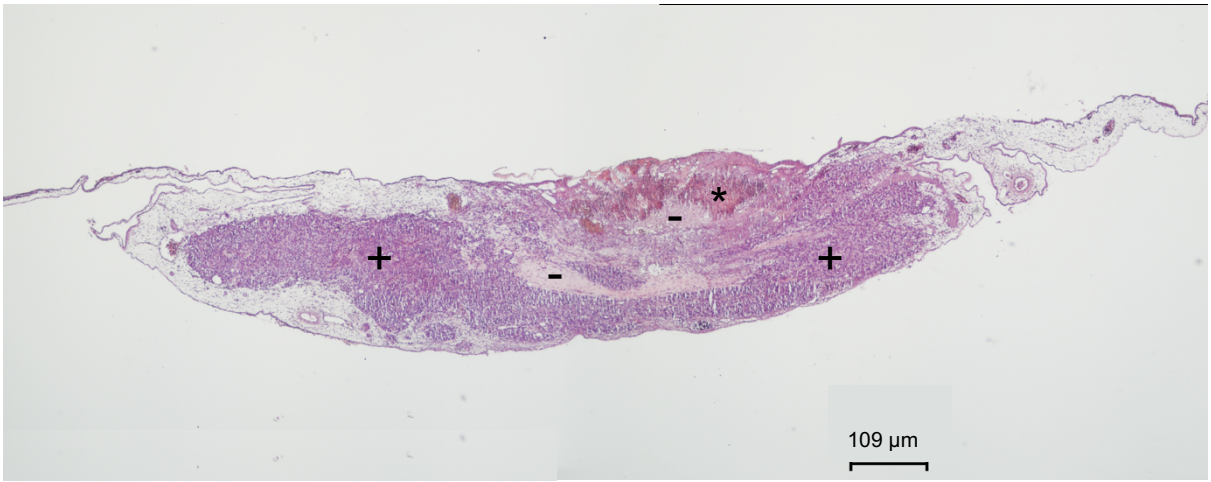

*Figure 8: Hematoxylin-eosin staining of CAM 68_20 as a representative specimen. Cell nuclei are marked by a purple color and red hues mark alkaline structures. The presumed tumor mass shows dense cellular architecture (marked by +). A mass of aberrant cellular architecture can be seen in the top part of the specimen (marked by *) and an area with reduced presence of cell nuclei (shown by -) are to be distinguished. (With 40-times magnification pictures fused into one picture as mentioned in the Guidelines for data analysis of the Methodology section.)*

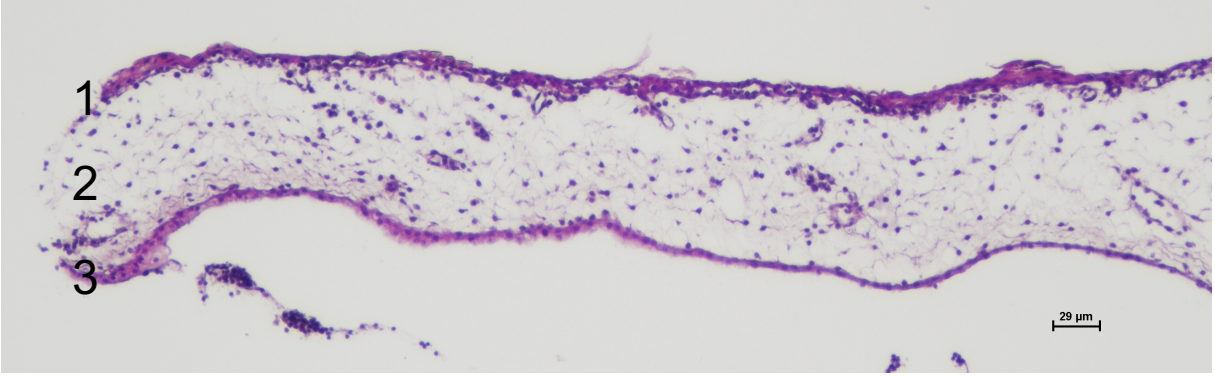

Figure 9: Hematoxylin-eosin staining of CAM 158_19 as a representative specimen (with 200-times magnification) portraying the chorion (1), mesenchymal connective tissue (2) and allantoic membrane (3).

It was of utmost interest to ascertain whether the solid tumors had successfully grown into the CAM tissue. This is due to the fact that the vascular network of the CAM could be reached and tumor cell survival was more probable since nutrients and oxygen were supplied, as it is necessary during oncogenesis (see chapter 4.1). This was used as the basis to select CAMs for the acquisition of data as tissue specimens which did not fulfil this criteria were ruled out from data analysis (see chapter 6.3).

It was furthermore evident that not all parts of the tissue specimens were homogenous in their appearance. At the top part of some samples a clearly aberrant tissue area could be observed, which is shown in Figure 8 by the mark of an asterisk (*). The HE staining allows us to see that tissue morphology differs from other parts which resemble tumor tissue (marked by +) by reduced density of cell nuclei (purple color) and more alkaline structures such as cytoplasmic proteins (red hues).

Another area within the tissue samples which showed irregular architecture was defined by very low presence of cell nuclei and homogenous red hues (marked by -). Due to the homogenous extracellular area it was presumed to be mostly made of Matrigel®, as it is a basement membrane matrix made of alkaline proteins (62).

6.2 Pan-keratin staining

The PK staining delivered the base to calculate tumor size and to set the regions of interest (ROIs) within the tumorous tissue. The following sample is in the same orientation as determined by HE staining with selective staining of epithelial-origin cells which are in fact the Huh-7 tumor cells.

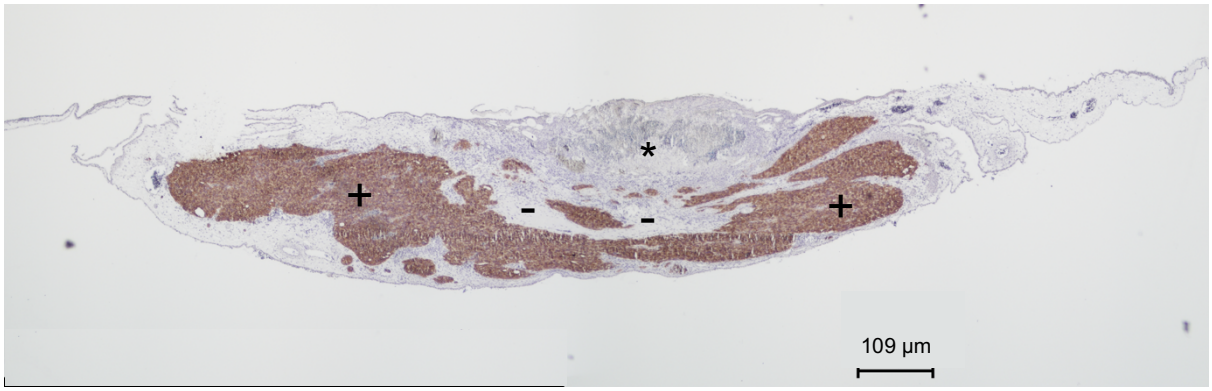

Figure 10: Pan-keratin staining of the CAM 68_20 as a representative specimen showing the tumor tissue in a brown color (marked by +) and cell nuclei in purple. A clearly aberrant cellular mass shows no brown color (*) and an area with reduced cell count is also pan-keratin negative (shown by -). (Fused version of single pictures of a 40-times magnification each, fused into one picture as mentioned in the Guidelines for data analysis of the Methodology section.)

The overall architecture of the tumor tissue (marked by + and in brown color) as seen in the PK staining is shown by CAM 68_20 as an exemplary specimen in Figure 10. The architecture of the tumorous tissue is marked by a large mass and several other areas of tissue stained in brown, which are sometimes not directly connected to the larger parts. This is most probably due to the two-dimensional nature of the microscopic images. All areas are surrounded by tissue which are of CAM origin. If this was not the case, CAMs were ruled out from data analysis (see chapter 6.3).

An area of interest which was already identified in the HE staining is marked by an asterisk (*) in Figure 8. While in the HE stainings it was unclear whether it was tumorous tissue, the PK staining shows clear results. The area does not show a brown color, which identifies it to be of non-epithelial origin. Furthermore, it can be observed that cell nuclei are present (purple color) in a high density. Overall, the tissue morphology does not resemble the rest of the tissue of non-epithelial origin within the microscopic image. It might nevertheless be of CAM origin or, in fact, tumorous tissue

which has lost cell-specific gene expression and therefore might be inactive or dead cells.

As was already perceived in the HE staining, an area of in the middle of the specimen could be distinguished (marked by -), which furthermore wasn't colored by the PK staining. This matches with the above-mentioned hypothesis that it is mostly Matrigel®, not tumorous tissue, and supported it further.

In order to calculate the tumor size, which was relevant for the data acquisition of CC3- and alpha-SMA-positive-structures, a digital function of the ImageJ software was used and manually controlled. In order to set the regions of interest (ROIs) within the tumorous tissue, which were relevant for the data acquisition of Ki-67-positive structures, ten random areas (with a size of 250 pixels and 250 pixels) were set within the PK-positive area. In the case that the tumor area was too small for all ten ROIs, a minimum of five ROIs was set (see Guidelines for data analysis).

6.3 Selection of CAMs for analyses

Overall, the HE and PK staining samples were compared for each specimen and the tumorous tissue was determined by matching above-mentioned observations. This was successfully done by manual means and evaluated carefully. Some Cam specimens were unfit for further analyses because of inadequately low tumor size, no detectable tumor cells (e.g. PK-negative), and no tumor growth into the CAM. A more detailed list of the CAM specimens can be found in the Attachments section (Table 7). A specific accumulation of CAMs which were unfit for data acquisition in a certain experimental group was not evident after discerning samples due to above-mentioned reasons.

6.4 CC3 staining

Cleaved caspase-3 staining showcases cells during the process of apoptosis which was of great interest to evaluate the amount of apoptotic cells within the tumor region. The depiction of CC3-positive cells in a brown color due to the antibody-mediated

staining method is shown in the following figures. In Figure 11, it has to be noted that the superior part of the tumorous mass with a very intense brown color (marked by *) were not positive in the PK staining (see Figure 10) and also presented itself as a mass without clear cellular organization in the HE staining (see Figure 8). Therefore, it was ruled as non-viable tissue which has undergone apoptotic processes. It might have been of tumorous origin. Furthermore, it could be presumed that due its position on the top of the tumorous tissue (marked by +) and distance from CAM tissue, a supply with nutrients and oxygen was unsuccessful, which led to its death.

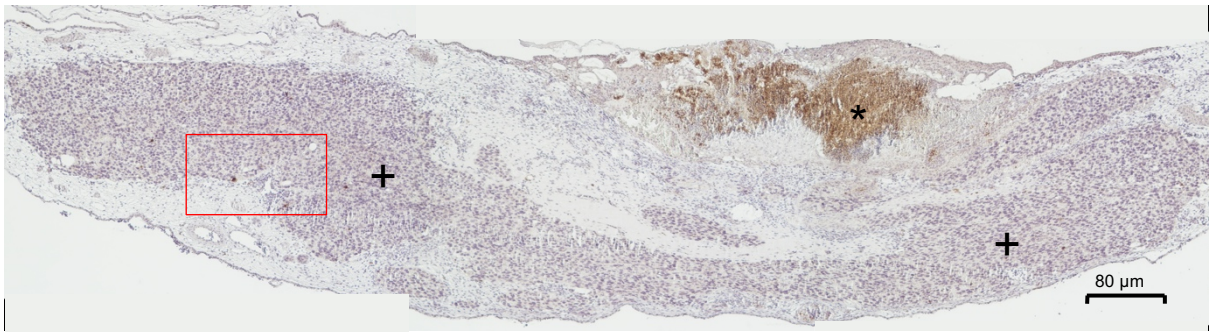

*Figure 11: CC3 staining of CAM 68_20 as a representative specimen showing the tumorous tissue (marked by +) as a fusion of single pictures of a 100-times magnification with marked focus (with red frame) on area shown in detail below. A clearly aberrant tissue area with an intense CC3-positive staining is to be found on the superior part of the specimen (marked by *). (Fused into one picture as mentioned in the Guidelines for data analysis of the Methodology section)*

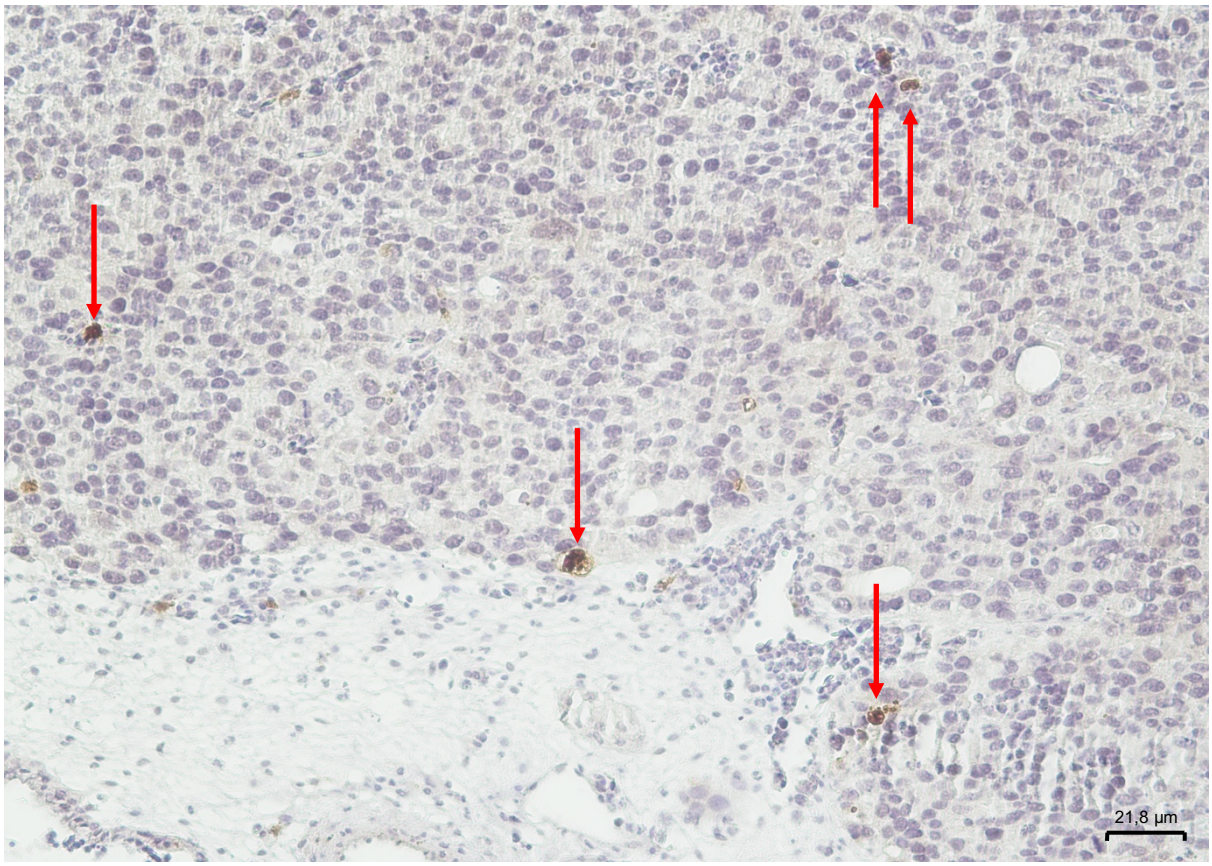

Figure 12: Detailed CC3 staining of CAM 68_20 as a representative specimen showing tumorous tissue with CC3-positive cells (marked by red arrows) in 200-times magnification.

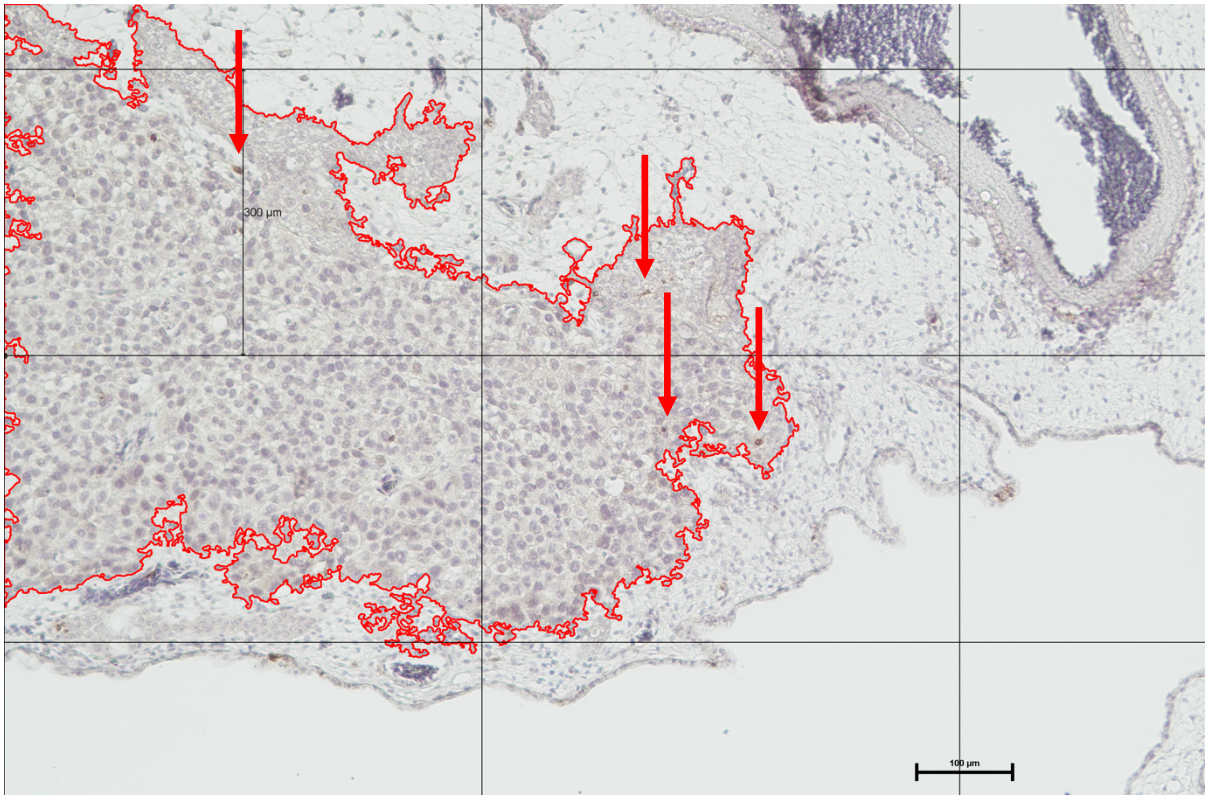

Figure 13: Detailed CC3 staining of CAM 396_19 as a representative specimen showing tumorous tissue with marked CC3-positive cells (red arrows) in 100-times magnification showcasing the pan-keratin positive tumor area with red margins.

After counting CC3-positive cells within the entire PK-positive tumor area of each specimen, the middle values of all CC3-positive cells of each experimental round were calculated so that six values per group were used to construct the following graph.

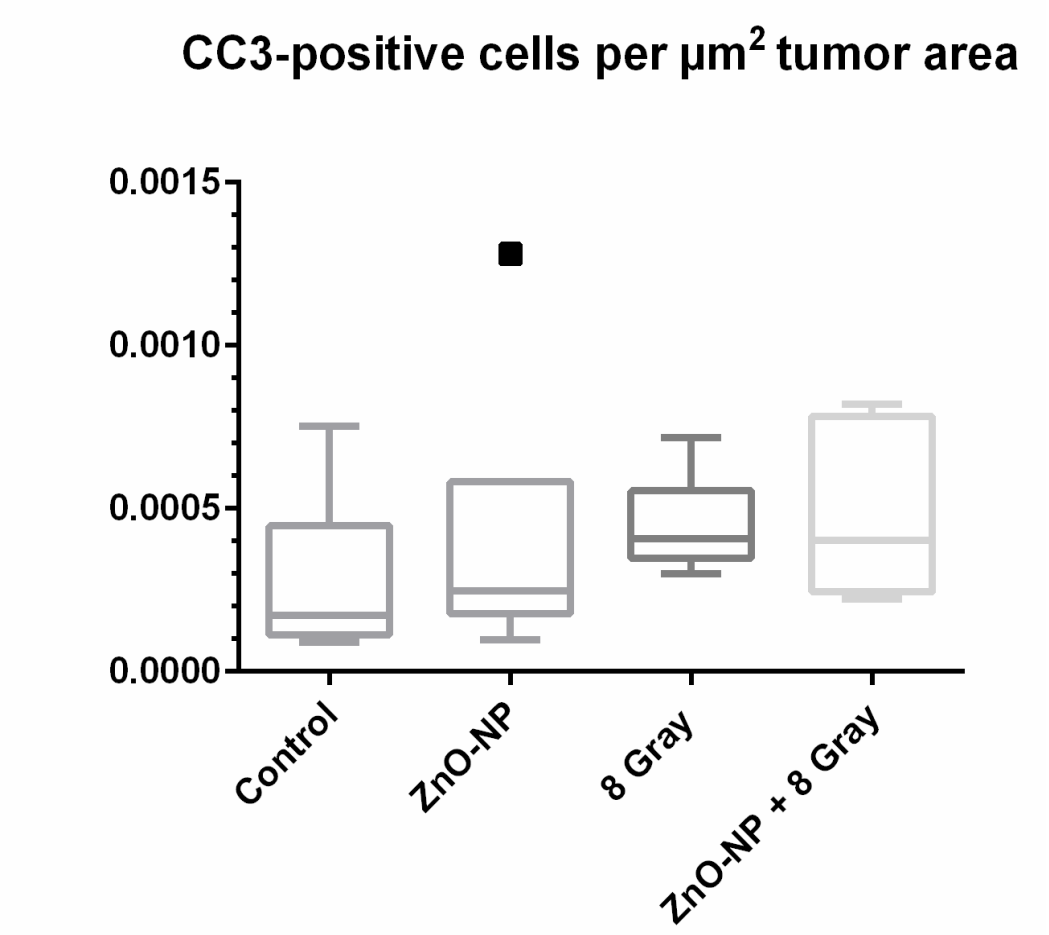

Figure 14: This graph shows the number of CC3-positive cells marking apoptoses in relation to the size e.g. the area of the tumor (in µm²) in form of a Boxplot diagram with whiskers showcasing the upper and lower border of a 95% confidence interval and the median marked as a bar. The square shows a value which is part of the group with application of ZnO-NP and marks a value which is *outside of the confidence interval. Group 1 as control (n=17), group 2 with only ZnO-NP application (n=22), group 3 with 8 Gy radiation treatment (n=22) and group 4 as combined ZnO-NP and radiation intervention (n=22) are shown, originating from six experimental rounds. A one-way analysis of variance (ANOVA) by performing Tukey's multiple comparisons test was used to check for statistical significance (p-value <0,05) which proved no statistical significance.*

As shown by Figure 14, it could be observed that the median and overall amount of apoptotic cells measured by determination of CC3-positive cells was lowest in group 1 (control group) and highest in group 3 (only radiation) and 4. Group 4 (combined intervention) shows the highest maximum value when considering the data point (marked by a square) of group 2 (only ZnO-NP) as a strongly deviating value because it was inconsistent with the other values within this group. The median of group 1 with a value of 0,00017 cells/μm^2 compared to groups 3 and 4 with values of 0,00040 cells/μm^2 showed an increase of approximately 135%.

Likewise, the mean value of group 1 with a value of 0,00028 cells/μm^2 was lowest while the mean of group 4 was determined at 0,00048 cells/μm^2. The mean of group 2 was at 0,00040 cells/μm^2 and the mean of group 3 at 0,00045 cells/μm^2. The standard deviation of the mean value of group 1 was 0,00025, for group 2 it was 0,00044, for group 3 it was 0,00015 and lastly for group 4 it was 0,00026. This causes an overlap in all cases, leading to a low statistical significance when the level of significance of 5% was applied.

It was nevertheless evident that in the control group 1 and group 2 with application of ZnO-NP, fewer apoptotic cells per tumor area occurred than compared to group 3 with 8 Gray and combined intervention of group 4.

6.5 Ki-67 staining

Ki-67 was used to depict proliferating cells within the tumorous tissue where Ki-67-positive cells were depicted in a brown color. An overview is shown below as well as a two more detailed areas (red and black box) within the chosen representative specimen CAM 68_20.

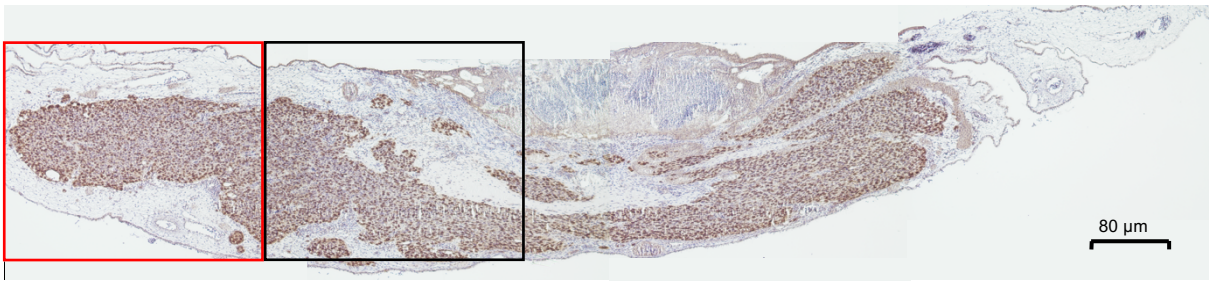

Figure 15: This figure illustrates the Ki-67 staining of the CAM 68_20 as a representative specimen (pictures with 100-times magnification fused into one picture as mentioned in the Guidelines for data analysis of the Methodology section) with marked focus on area (red border) shown in detail below.

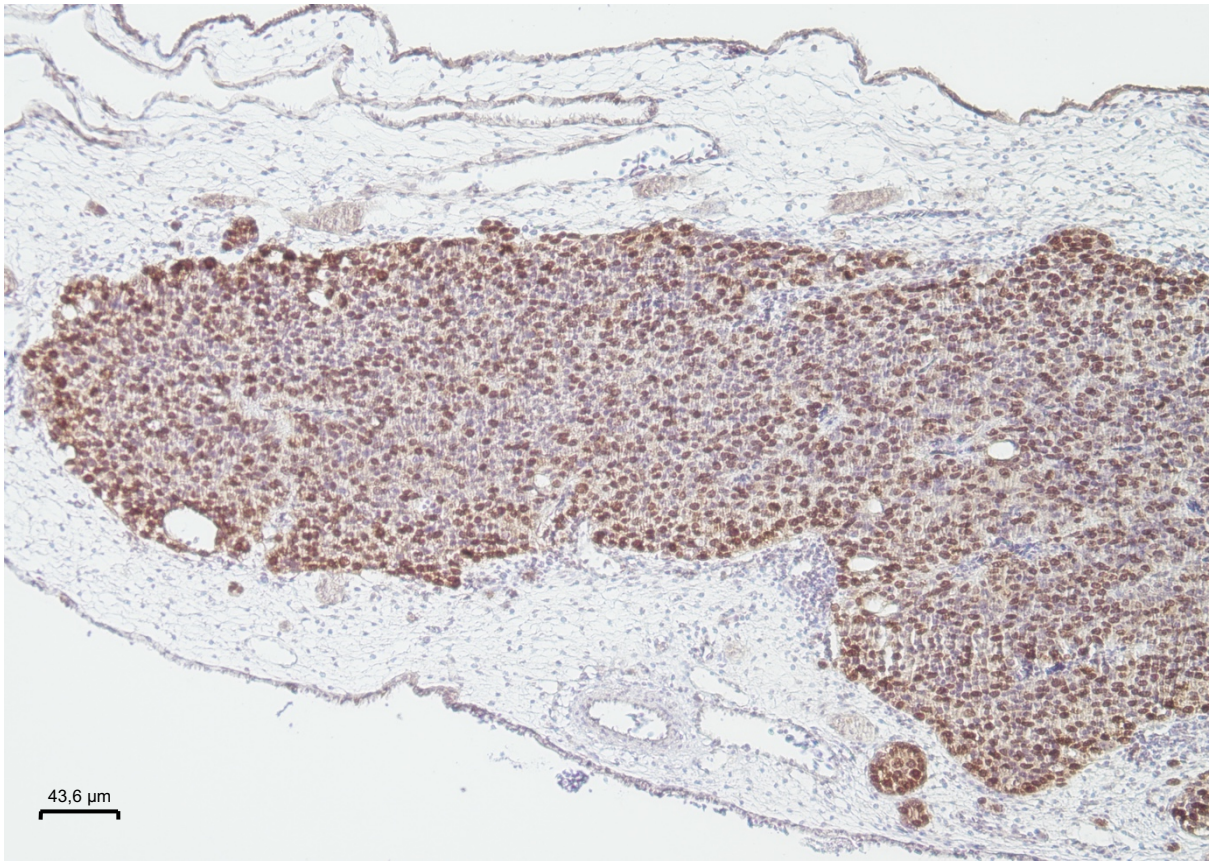

Figure 16: Detailed picture of CAM 68_20 as a representative specimen showing Ki-67-positive cells with brown color in 100-times magnification.

To further evaluate the proliferation rate, Ki-67-positive and Ki-67-negative cells within set regions of interest were identified. The ROIs were chosen in the PK staining as stated above to ensure that the region was of tumorous origin. Moreover, it was

therefore possible to choose the ROIs without bias of already being able to see the patterns of the Ki-67 staining. In total, 10 ROIs were set in each tumor whenever possible.

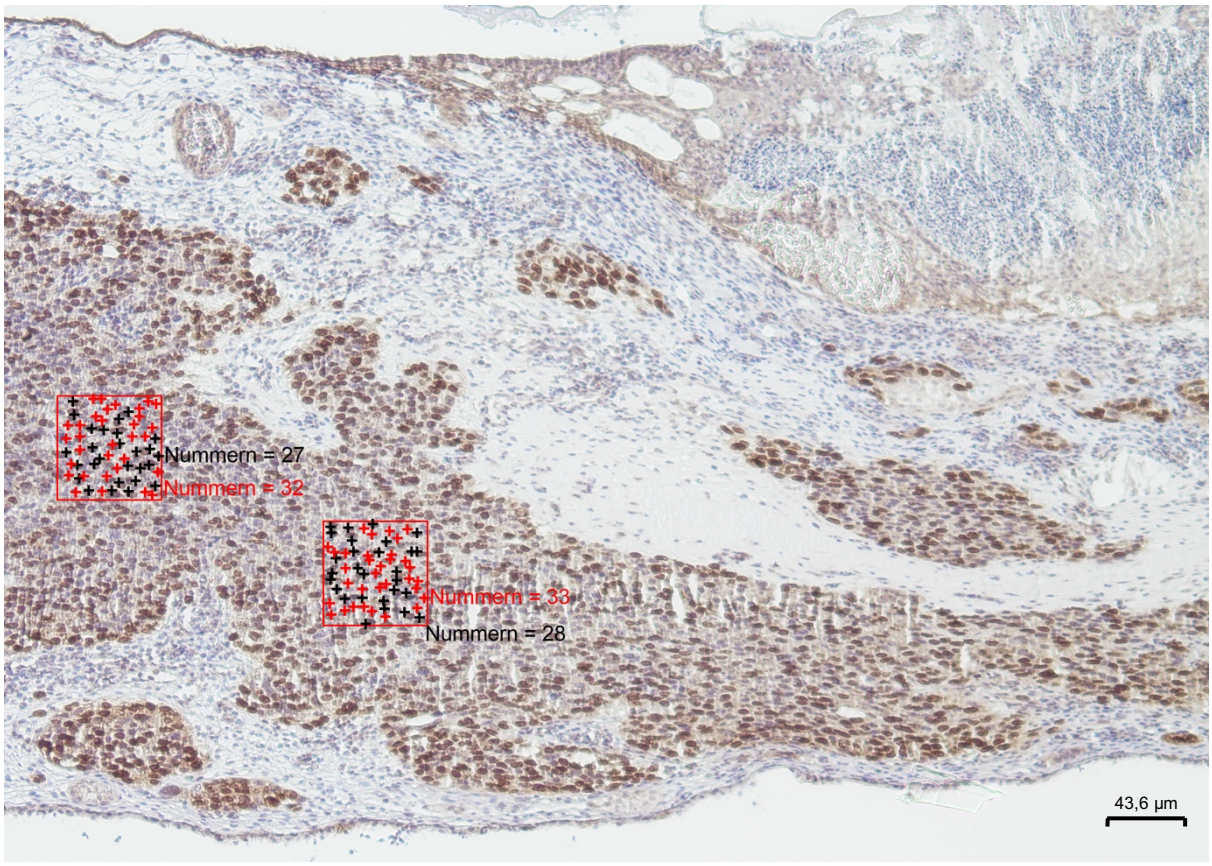

Figure 17: The above-mentioned area within the black margins in Figure 15 is shown here in detail. ROIs (size of 250 pixels and 250 pixels) were set within PK staining and afterwards in Ki-67 staining of the same sample, here CAM 68_20 is shown as a representative specimen. Black marks (+) identify Ki-67-positive cells and red marks (+) identify Ki-67-negative cells in 100-times magnification.

These counts of each Ki-67-positive and Ki-67-negative cells within the ROIs were noted for each specimen and it was calculated which share Ki-67-positive cells held of all cells, further portrayed as a percentage.

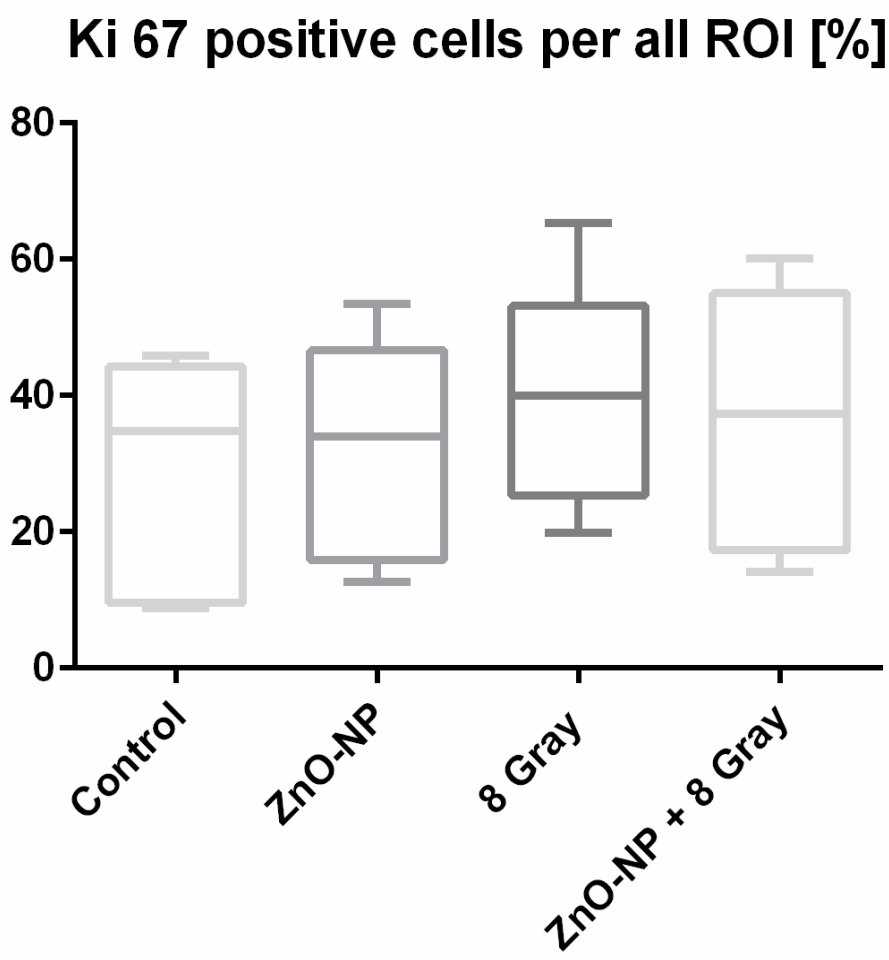

Figure 18: This graph illustrates the number of Ki-67-positive cells marking proliferating cells in relation to the Ki-67 negative cells within the 10 counted ROIs of each tumor in form of a Boxplot diagram with whiskers showcasing the upper and lower border of a 95% confidence interval and the median marked by a bar. Group 1 as control (n=17), group 2 with only ZnO-NP application (n=22), group 3 with 8 Gy radiation treatment (n=22) and group 4 as combined ZnO-NP and radiation intervention (n=22) are shown, originating from six experimental rounds. A one-way analysis of variance (ANOVA) by performing Tukey's multiple comparisons test was used to check for statistical significance (p-value <0,05) which proved no statistical significance.

As is portrayed in Figure 18, the highest relative amount of Ki-67-positive cells was present in group 3 with a median of 39,97%, which received a dose of 8 Gy as the only intervention. It was seen that both group 2 with exclusive ZnO-NP application (median of 33,99%) and group 4 (median of 37,31%) with a combined intervention also showed

higher ratios of Ki-67-positive cells compared to the control group 1 (median of 34,83%).

Likewise, the mean value of group 3 with a value of 40,25% was highest while the mean of group 1 was determined at 29,67% as the lowest value. The mean of group 2 was at 32,58% and the mean of group 4 at 36,76%. The standard deviation of the mean value of group 1 was 16,66, for group 2 it was 15,87, for group 3 it was 16,4 and lastly for group 4 it was 18,77. This causes an overlap in all cases when comparing the groups, leading to a low statistical significance when the level of significance of 5% was applied.

It was nevertheless evident that in the control group 1, the ratio of Ki-67 positive cells was lower than compared to group 3 with 8 Gray. Group 4 with combined intervention and group 2 with application of ZnO-NP also showed lower ratios of Ki-67 positive cells when compared to group 3 while it was noted that group 4 had an overall trend of higher values than group 2.

6.6 Alpha-SMA staining

The alpha-SMA staining method allowed for selective portrayal of structures with high amount of alpha-smooth muscle actin (α-SMA) such as smooth muscle cells and myofibroblasts present in blood vessels. This was of special interest within the tumor tissue to perform an analysis of the vascularization by showcasing the amount of vascular structures within the specified tumor area.

The following figures show an overview as well as a more detailed excerpt of the CAM 68_20 with positive alpha SMA structures.

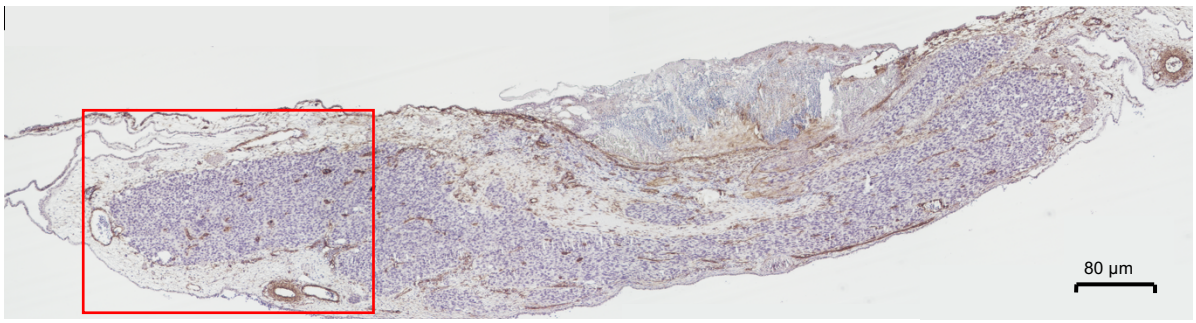

Figure 19: Alpha-SMA staining of CAM 68_20 as a representative specimen (100-times magnification fused into one picture as mentioned in the Guidelines for data analysis of the Methodology section)

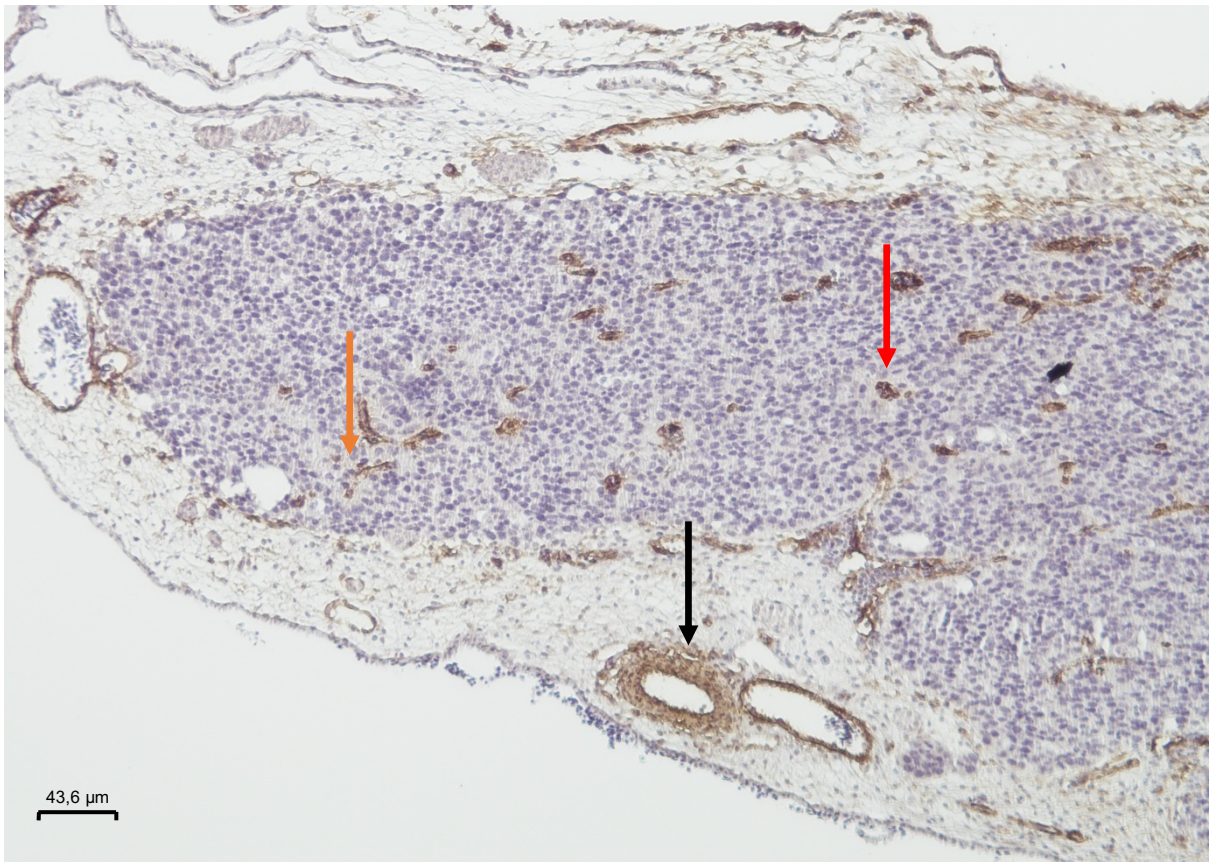

Figure 20: Detailed unfused picture of CAM 68_20 as a representative specimen showing alpha-SMA-positive structures with brown color (an exemplary structure within the central tumor tissue marked by red arrow, in the peripheral part by an orange arrow, while an alpha-SMA-positive structure in the CAM is marked by a black arrow) and cell nuclei in purple color in 100-times magnification.

In general, alpha-SMA-positive structures were found in all tumors which were not ruled out due to criteria as described in chapter 6.3. They were first manually categorized by the morphological distribution pattern of the vascular structures, as is showcased in Figure 21.

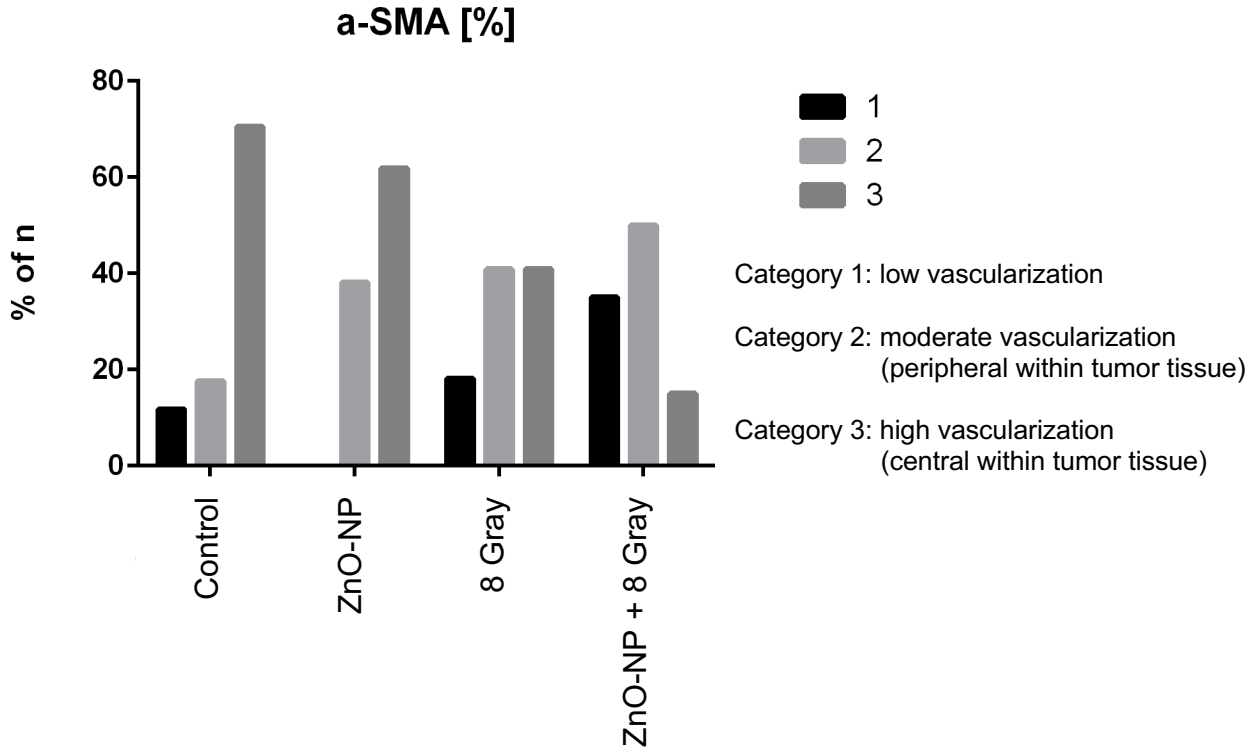

Figure 21: This multiple bar diagram shows the distribution of CAM specimens within the interventional groups (as shown on the x-axis) after categorization of the vascular patterns of each CAM specimen. Categories were assigned as either low vascularization (category 1), moderate vascularization with mostly peripheral vessels (category 2), and high vascularization with alpha-SMA-positive structures reaching the central part of the tumorous tissue (category 3). Group 1 as control (n=17), group 2 with only ZnO-NP application (n=22), group 3 with 8 Gy radiation treatment (n=22) and group 4 as combined ZnO-NP and radiation intervention (n=22) are shown, originating from six experimental rounds.

The multiple bar diagram of Figure 21 shows the percentage share of specimens within the groups of intervention after each CAM specimen was categorized by its level of vascularization (categories 1-3). In the control group, the highest amount of highly vascularized specimens (category 3) could be determined. The ZnO-NP group 2 shows a reduction of highly vascularized specimens while the value of category 2 with moderate vascularization rises to almost 40%. In group 3, where only radiation was applied, category 2 and 3 both have values of approximately 40%, while category 1 (low vascularization) is also present. Lastly, the group of combined intervention shows a further decrease of highly vascularized specimens (category 3) and rise of low and moderately vascularized CAMs, with an emphasis on category 1 as low vascularization levels reaching 37%.

Most notably, the trend of category 3 with high vascularization levels (where the central part of the tumorous tissue was also reached by vessels) was highest in the control group 1 and lowest in the group 4 when both interventions took place.

After counting positive alpha-SMA structures within the measured tumor size (determined by PK staining), data could be collected and resulted in the following graph.

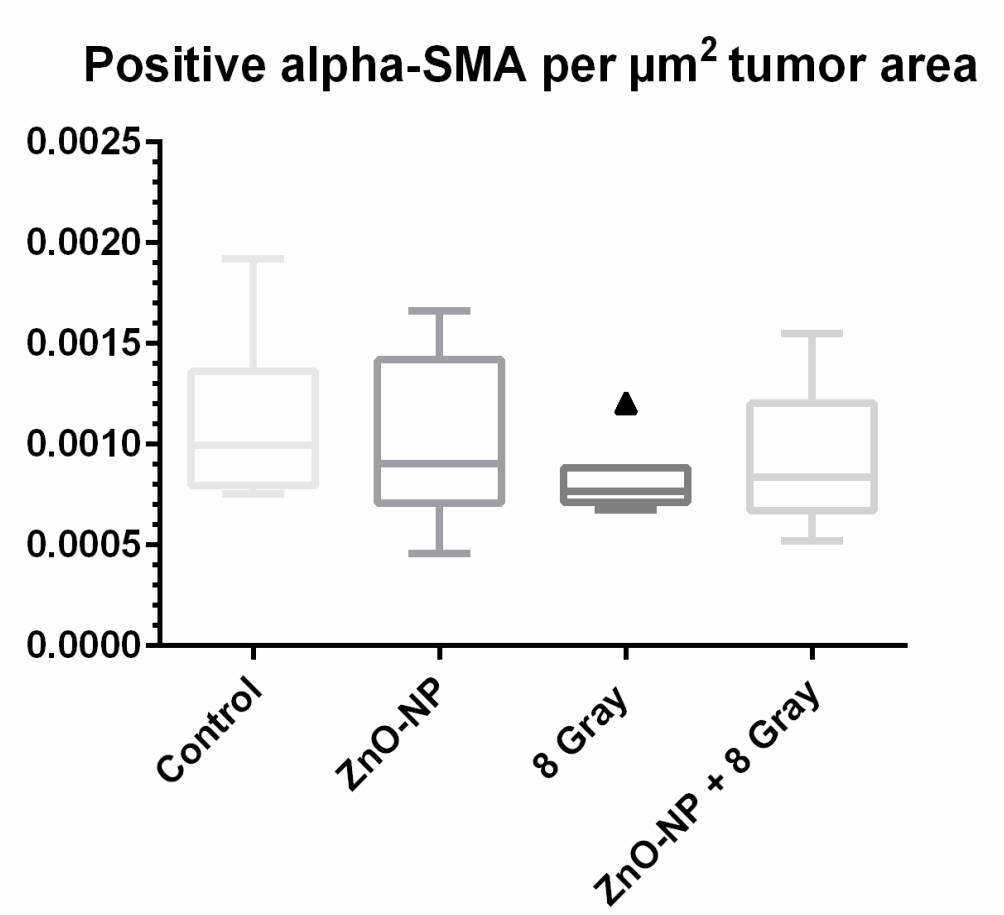

Figure 22: This diagram demonstrates the number of alpha-SMA-positive structures marking vessels in relation to the size e.g. the area of the tumor (in µm²) in form of a Boxplot diagram with whiskers showcasing the upper and lower border of a 95% confidence interval and the median marked as a bar. The triangle shows a value which is part of the group with application of 8 Gray *and marks a value which is outside of the confidence interval. Group 1 as control (n=17), group 2 with only ZnO-NP application (n=22), group 3 with 8 Gy radiation treatment (n=22) and group 4 as combined ZnO-NP and radiation intervention (n=22) are shown, originating from six experimental rounds. A one-way analysis of variance (ANOVA) by performing Tukey's multiple comparisons test was used to check for statistical significance (p-value <0,05) which proved no statistical significance.*

When examining Figure 22, the lowest amount of a-SMA-positive structures could be determined in group 3 after solitary radiation had taken place. The median was at 0,00077 n/µm^2. Likewise, a lower amount could be evaluated for both group 2 (only ZnO-NP) with solitary ZnO-NP application and group 4 with combined intervention. The median in group 2 was 0,00091 n/µm^2 and in group 4 a lower median was calculated at 0,00084 n/µm^2. It was evident that in the control group and ZnO-NP group, a higher amount of alpha-SMA-positive structures compared to the 8 Gy and combined intervention group was observed.

It could be observed that the median and overall amount of vascular structures was highest in group 1 (control group) and lowest in group 3 (only radiation).

Likewise, the mean value of group 1 with a value of 0,00111 n/µm^2 was highest while the mean of group 3 was determined at 0,00082 n/µm^2. The mean of group 2 was at 0,00101 n/µm^2 and the mean of group 4 at 0,00093 n/µm^2. The standard deviation of the mean value of group 1 and group 2 was 0,00043, for group 3 it was 0,00019 and lastly for group 4 it was 0,00036. This causes an overlap in all cases, leading to a low statistical significance when the level of significance of 5% was applied.

Nevertheless, it was evident that in the control group 1 and group 2 with application of ZnO-NP, more vascular structures were to be found within the tumorous tissue than compared to group 3 with 8 Gray and after combined intervention in group 4.

7 Discussion

The aim of this explorative study was to investigate the effects of radiation and intravascular ZnO-NP application on solid tumors using the HET-CAM-Assay. According to current literature, this type of experiment has not yet been conducted. In order to comprehend the results of this scientific work, a comparison and juxtaposition to distinctive sources from literature will be made in this section. All newly obtained scientific findings which were deduced from the Results (see chapter 6) will be presented explicitly.

Overall, the absence of statistical significance of differences between the experimental groups remains an important hurdle in the discussion and interpretation of the performed experiments. It could of course be due to the fact that no relevant effects were measured and indeed, all differences were within the normal range of fluctuation.

Then again, it has to be noted that the number of specimens may simply be too low. Whilst six experimental rounds were conducted, 83 specimens were eligible for data analysis. Following this, a Gaussian distribution of obtained values could not be determined. Small sample sizes may prevent universal statistical analyses, even though the effect size may nevertheless be biologically meaningful and relevant for interpretation. Therefore, it would therefore be of interest to include more specimens in each study group as well as to repeat the experiments in order to potentially observe a consistent effect. Moreover, the eggs are not uniform and may therefore show diverse reactions to interventions. It was further observed that in some cases, tumors failed to invade the surrounding CAM tissue or establish vascular connections with the host system. As no specific accumulation of CAMs unsuitable for data acquisition was observed within any particular experimental group, it may be attributable to a general dropout rate (see Table 7 and Table 8).

In order to clarify and discuss this further, results from other studies will be presented. First, the subject of both radiation (chapter 7.1) and ZnO-NP (chapter 7.2) with individual consequences on biological tissues will be presented. Afterward, the effects of combined treatment with radiation and ZnO-NP (chapters 7.3 and 7.4) will be demonstrated by portraying known facts and incorporating novel insights from this experimental study. Furthermore, the experimental setting of the HET-CAM-Assay will be evaluated and an outlook on the future will be given in chapter 7.5.

7.1 The consequences of radiation

Firstly, the effects of radiation on cells will be portrayed in this chapter with special emphasis on cell death and proliferation. In order to investigate the impact of ionizing radiation as an established cancer therapy, the HET-CAM-Assay was previously chosen in numerous studies (33). Most notably, it was used to develop different schedules for a combined radiochemotherapy as well as drug reduction options to optimize the therapeutic results (248).

Likewise, the question of whether application of ZnO-NP or radiation should take place in a different order and which effects this might have is a scope for future experiments. Similar to clinical treatment strategies, a repetitive application of radiation could be evaluated. This could very well be established in the proposed experimental setup of the HET-CAM-Assay, although it may change the exact points of time when application of ZnO-NP or radiation would take place. The time frame of 24 hours between radiation and termination on day 14 was chosen due to several literature sources which showed a maximum of effects of radiation *in vivo* up until this point of time (33, 249-251). Nevertheless, it may easily be possible to repeat this process during this period or to begin a repeated application on an earlier day of development. If this were to be done by already starting on day 12, the application of ZnO-NP has to be taken into account, which takes place 48 hours before termination of the experiment. In this context, an application before the transport to the radiation device may cause more losses of study organisms since they are at risk of bleeding after intravascular application of ZnO-NP.

In general, collecting results 24 and 48 hours after an intervention has taken place are durations which are commonly employed in biological and chemical research. They strike a balance between enabling the emergence of measurable cellular responses and maintaining practical feasibility within experimental laboratory conditions. While these are also organizational considerations, the results obtained from the performed experiments with the given study protocol are of high interest and shall be further discussed.

7.1.1 Cell death after radiation

Further going into detail to discuss the consequences of radiation, it is clear that it causes cell death, as is desirable in an antineoplastic use. When examining the CAM itself, cell death was analyzed by microscopic observation after immunohistochemical staining and DNA fragmentation analysis with a maximum until 6 hours post-intervention in an experimental setting (249). Similar observations were made when radiation has been applied to cell cultures of Huh-7 cells. This was investigated by flow cytometry and clonogenic cell assay after *in vitro* studies (252, 253). As is to be expected of the established antineoplastic treatment, cell survival and cell viability was decreased with accompanying cell-cycle arrest and cell death via apoptosis as well as necrosis (253-256).

Correspondingly, in this experimental setup, a noteworthy number of CC3-positive cells could be detected after ionizing radiation of 8 Gray was applied to solid tumors on the CAM 24 hours before immunohistochemical analyses took place (Figure 14). This can be portrayed by the mean values: 0,00045 cells/μm^2 ($\pm$0,00015) versus 0,00028 cells/μm^2 ($\pm$0,00025) in the control group.

A deviation from the values of the control group is noteworthy, although due to overlapping areas of standard deviation it was not proven to be statistically significant. Nevertheless, it indicates cells undergoing an apoptotic process. It may be noted that within all tissues cell death occurs continuously, especially within tumors (6). It is therefore not surprising that within the control group, apoptotic processes could also be detected. Since the tumors were originally all of the same cell culture origin but put into different experimental organisms, e.g. the eggs, a wide variance of results is certainly to be expected. Then again, the results may reflect true heterogeneity of organisms in response to interventions, which is important to report, especially for future translational or personalized uses.

Furthermore, it is crucial to recap that cell death encompasses apoptosis, necrosis and autophagy, as was explained in chapter 4.2.4. Moreover, many tumors lose the capacity to undergo apoptotic cell death. Instead, the primary antineoplastic effects of radiation are mediated through mitotic catastrophe or a senescence-like state of irreversible growth arrest (257). Therefore, the chosen CC3 staining method, which

portrays mostly apoptosis, cannot represent all of the cells which undergo different forms of cell death. It may be more successful to use cell viability assays to depict the sum of these processes.

Overall, this might explain the lack of significance in the difference of values obtained for CC3-positive cells within the tumorous tissue in between study groups, since the known biological mechanisms after radiation clearly lead to increased cell death compared to no intervention.

7.1.2 Cell proliferation after radiation

As another consequence of radiation, the proliferative activity of cells within the biological tissue changes. This will be further discussed in detail in this chapter. Depicting this, it was shown that the ratio of Ki-67-positive cells may also partially increase after application of ionizing radiation (Figure 18). A trend may be seen since the maximum values in group 3 where radiation had taken place exceed 60%, whereas the control group does not exceed 50%. Also, after taking into account the standard deviations, the mean of group 3 after sole intervention of radiation at 32,58% (±16,4) describes higher values than can be seen in the control group 1 with a mean of 29,67% (±16,66). It has to be noted though that these values did not withstand a test for statistical significance since the standard deviation nevertheless caused an extensive overlap. Therefore, it has to be considered that these differences in values may in fact be due to normal variance of proliferative activity and do not describe a trend in reality.

Still, if this were to be described as a trend, the following considerations can be made. Since Ki-67 staining displays cells in a cellular phase of proliferative action, several things may be taken into account. Firstly, it is obvious that radiation does not eliminate all metabolically active cells. This is a common occurrence during the treatment of tumorous diseases which is why repetitive treatment plans have been developed (see chapter 4.2). This way, the cells which remain after a single treatment of radiation has taken place may be damaged during a following application of radiation. In turn, this may lead to more extensive cell death and therefore reduction of tumor mass. As has been discussed in the previous section, a repetitive application of radiation may be realized using the HET-CAM-Assay.

Secondly, it is fathomable that remaining cells may become even more active, e.g. show proliferative action due to molecular signaling of neighboring cell death. Furthermore, cell signaling may even lead to recruitment of senescent cells, meaning cells which have been in a metabolically inactive state (1). Moreover, so-called cancer stem cells may remain after cytotoxic treatments have taken place, which has been studied in Huh-7 sphere cultures after radiation before (258). Following this thought, it may indicate a process of the solid tumor to evade radiation treatment, meaning radioresistance. This is driven by mechanisms such as evasion of cell death, DNA repair, and tumor heterogeneity (259).

Hepatocellular carcinoma is known to acquire radioresistance, which is clinically correlated with treatment failure (252). Many studies have been conducted in order to elucidate the effectiveness of radiotherapy in tumorous diseases and have come to the conclusion that p53 plays an integral role (257). It is known that mutation or inactivation of p53 causes genetic instability, initially resulting in the development of tumors and further the ineffectiveness of radiotherapy, as was described in chapter 4.2.2. The latter was shown via Western-blotting to measure p53 expression after radiation of Huh-7 cells *in vitro* (253). A normal and functional form of p53 in other hepatocellular carcinoma cell line leads to higher radiosensitivity, whereas absence of p53 showed opposite effects. Cell lines with a higher radiosensitivity showed a higher expression of functional p53, which may lead to induction of apoptotic cell death (252). Since the Huh-7 cells used in these experiments have an alteration in the gene sequence of p53 which is associated with a high expression of the dysfunctional protein, the effectiveness of radiation in the sense of reduction of cell viability within the tumor mass may be changed (259, 260).

Kasai et al. conducted genomic analysis to unravel the intricate karyotype of Huh-7 cells. The findings unveiled a loss of heterozygosity and other chromosomal alterations in more than 50% of the genome of the analyzed cells, proposing a heterogenous cell population (261). This may indeed lead to believe that the Huh7-cells which were used for the experiments in this study have similar characteristics. This would mean that effects of radiation on both cell death and cell proliferation may be higher on other cells than what could be studied using the Huh-7 cells of this study. Therefore, the results of cell death within group 4 with combined treatment may be lower and cell proliferation higher than expected from the knowledge gained from other experimental studies

applying radiation. In order to clarify this fact, a quantitative and qualitative analysis of p53 and the cellular DNA may be of interest in the future.

7.2 The consequences of intravascular application of ZnO-NP

As the second treatment, it was of interest to expand our knowledge of antineoplastic properties of ZnO-NP *in vivo*. This shall be further analyzed in this chapter. During the experimental setup, the ZnO-NP were injected into the vascular system of the chick embryo on day 12 which has been successfully implemented by the AG in past studies. Up until now, it was mostly used to evaluate toxicity mechanisms and dosages of ZnO-NP (262).

So far, in order to investigate toxicity of ZnO-NP on malignant cells, extensive *in vitro* studies have been performed with application of ZnO-NP on various cell lines. Notably, this was also done using human hepatocellular carcinoma cells (263), all of which showed a reduction of cell viability (3). Furthermore, the cytotoxic properties of ZnO-NP on the rat liver and its anti-neoplastic effects on human liver cancer cell lines was also investigated both *in vitro* and *in vivo* (264). A high proliferative activity of tumor cells and an overall increased ROS production of iron-accumulating tumor cells compared to normal cells may lead to an amplified damaging effect of ZnO-NP towards malignant cells (265). A cytotoxic effect to Huh-7 cells comparable to the established chemotherapeutic drug doxorubicin was explored to be at 40 µg/ml (266). The dose of 13,5 µg ZnO-NP, which was used in this study, is derived from data researching toxicity on the chick embryo (92) to ensure an adequate survival rate and at the same time a dosage high enough to elicit effects on the tumor cells. It is of tremendous interest to take this investigation of cytotoxic effects of nanoparticles from *in vitro* cell cultures to complex study organisms, as was performed in this experimental study.

7.2.1 Cell death after application of ZnO-NP

Similarly to the effects of radiation, the potential of ZnO-NP to elicit cell death in tumors *in ovo* was of interest and will be analyzed in this chapter. In order to interpret the results generated from the experimental setup, the immunohistochemical staining method of CC3 established by Yang et al. and showed that an increase of CC3 and

p53 are adequate markers to show triggered cell death after application of ZnO-NP on Huh-7 cells *in vitro* (267). In other studies, this rise in cell death was seen 48 hours post-intervention at a maximum after examining cell viability via MTT assay (148). This influenced the decision to apply a dose of 13,5 µg ZnO-NP intravascularly on day 12, which is in fact 48 hours before termination of the experiment.

As immunohistochemical analyses followed, the induction of cell death via apoptosis via ZnO-NP within the tumor area was documented when looking at different study groups (Figure 14). However, it has to be discussed whether these results are result of the intervention, as they did not withhold a statistical test to prove significance. Compared to before-mentioned radiation treatment with a mean of 0,00045 cells/µm^2, it seems to have a minimally lower effect since the mean was 0,00040 cells/µm^2 while when compared to the control group, the mean proves to be higher (0,00040 cells/µm^2 versus 0,00028 cells/µm^2). In group 2, when only ZnO-NP were applied, the standard deviation is quite high with a value of 0,00044. This signalizes a high scattering of values, while in the other groups, it was remarkably lower. It leads to believe that after ZnO-NP application, a manifold of cellular reactions takes place, while not leading to cell death every time. The occurring cellular reactions are on the one hand highly dependent on intracellular redox status while on the other hand, variations in nanoparticle characteristics - such as size, surface charge, aggregation behavior and dissolution rate - may further impact cellular uptake and generation of ROS.

Furthermore, it has to be noted that cell death following application of ZnO-NP does not only include the form of caspase-dependent apoptosis. In studies with endothelial cells *in vitro* and in mice models *in vivo,* this was clearly shown (57, 268). It is a matter of fact though, that CC3 was the only marker which was used for the acquisition of data portraying cell death in this experimental study. It is therefore highly likely that different forms of cell death such as ferroptosis, necrosis and other forms of autophagy have taken place as well. Likewise, it may be remarked that a senescence of tumor cells could have been induced, similar to the effects of radiation. Overall, the actual consequences of ZnO-NP on tumor cells may have a higher extent than those which are presented in the results section.

7.2.2 Cell proliferation after application of ZnO-NP

When looking at results of Ki-67 positive cells in the tumor area after application of ZnO-NP, a similar dynamic to the aforementioned effects post-radiation can be noted and will be discussed in this section. The ratio of Ki-67-positive cells after ZnO-NP application (mean of 32,58% ±16,66) was higher compared to the control group with no intervention whilst radiation treatment showed notably even higher counts, as their results were already described (see 7.1.2 and Figure 18). This may lead to interpretation that whilst similar results were obtained and alike effects may stand behind this, ZnO-NP have a lower effect size. Nevertheless, it has to be considered with caution whether the rise in Ki-67 compared to the control group is a trend since those may also lie within the usual range of fluctuation of values. Furthermore, the comparison to the radiation treatment has to be critically viewed as well since the distribution of values is very similar (see Figure 18). It is to question whether there really is a difference meaning less cell proliferation after ZnO-NP application (group 2) than after radiation (group 3), or in reality no difference.

As the effects of ZnO-NP are hitherto not fully known yet, the proliferative capabilities of remaining cells also have not been fully evaluated after application of ZnO-NP. It is clear that a rise in cell death leads to less cells which remain and are able to proliferate. Likewise, as the theory of cell death encompassing more than only apoptosis after application of ZnO-NP has already been established, it may be used to explain the proliferative action. Remaining cells are proliferating and it is also fathomable that dormant cells may in turn be activated. This is especially of relevance when comparing values to the control group and should be further evaluated including other tests, such as clonogenic assay methods or flow cytometry using BrdU staining as well as generational analyses via fluorescent staining.

A furthermore important question is whether the dose of ZnO-NP fully reached the tumor - and therefore were able to have an effect on the entirety of the tumor. As a simple yet feasible approach it may be said that the solution containing ZnO-NP escaped the vasculatory system upon application. Moreover, ZnO-NP may have reached the chick embryo and were metabolized, never fully reaching the solid tumor on the CAM. Then again, the tumor might not have been fully connected to the chick’s vasculatory system at the time of application of ZnO-NP.

7.3 Effects of a combined application on cell viability

The effects of a combined treatment will be further evaluated in this chapter. Up until now, the effects of ZnO-NP and radiation on tumor cells have been examined in studies *in vitro*, both as separate interventions and as a combination treatment. This research revealed ZnO-NP to induce cell death in tumor cells after the intervention of radiation had taken place by several methods (1). However, ZnO-NP have also been researched *in vivo* as a combination with other anti-neoplastic treatment methods: It should be noted that photocatalytic reactions leading to cell death were enhanced by ZnO-NP in *in vivo* studies (269). Furthermore, photo-stimulated ZnO-NP have been shown to enhance cytotoxic effects of established chemotherapeutic agents such as paclitaxel, cisplatin, and daunorubicin/doxorubicin in cancer cells, as was already mentioned (210, 214-219). As no *in vivo* studies have yet been performed exploring the effects of radiation and ZnO-NP, the experiments with a setting as described in this thesis provide new insights.

In the performed studies of this research project, the combined application of radiation and ZnO-NP shows the highest overall values of CC3-positive cells with a mean of 0,00048 cells/$\mu m^2 \pm$0,00026 (Figure 14). It is notable that the values of the combined treatment group resemble those after the radiation treatment, while the distribution of values is wider. Taking this into account as a real effect and not to attributing it to general fluctuation of values, it is well in line with the dynamics of the solitary treatments as described in chapter 7.1.1 and 7.2.1.: Radiation lead to high amounts of cell death while ZnO-NP lead to a wide distribution of amounts of cell death.

In order to clarify the effects on cell viability, the results of cell proliferation may be taken into consideration. After cell damage and following initiation of cell death within tissue as described above, the relations may shift in favor of proliferating cells. The proliferatively active cells remain and may further exhibit increased proliferation as a compensatory response. Likewise, a higher ratio of Ki-67 positive cells in the combined treatment group exists with a mean of group 4 at 36,76% ($\pm$18,77) when compared to the control group (29,67%$\pm$16,66), as is shown in Figure 18. It has to be noted though that the ratio of Ki-67-positive cells in group 3 and 4 do not show a remarkable

difference. Therefore, it is not derivable that the ZnO-NP add to the effects of radiation treatment in terms of cell proliferation - at least when looking at the parameter of Ki-67-positivity in this study.

As was already discussed in the previous chapters, it is to be questioned whether the obtained data are sustainable trends since they evade statistical significance. However, since previous studies and known biological mechanisms align with above-mentioned trends of ZnO-NP and radiation, they can be scientifically feasible and may lead to the hypothesis that a combined application exceeds the cytotoxic effect of solitary interventions. This shall be explained further in the following paragraphs.

Expected synergistic effects may be mostly attributed to the common mechanism of action of RONS release and damage to the cellular metabolism. It is clearly described how radiation influences DNA structure and changes within the cellular equilibrium mostly due to rise of ROS (see chapter 4.2). A ZnO-NP induced cytotoxicity is also presumed to be due to ROS generation and was shown to be potentiated by diverse types of radiation (47). It is therefore reasonable that the generation of RONS is potentiated when a combined treatment takes place and eventually exceeds the antioxidative capacity of cells, as was the presumed mechanism of action which proposed by the *in vitro* findings (1). It could match the results obtained from this study since a high number in CC3-positive cells was seen in group 4.

These processes have been extensively researched on whilst maintaining a focus on the use of ferroptosis-inducing nanomedicines to enhance standard antineoplastic treatments. As therapy resistance remains a key challenge in cancer treatment, recent *in vivo* studies on mice have highlighted the potential of several nanoparticles inducing ferroptosis as a therapeutic target, with offering promising strategies to overcome resistance and enhance treatment efficacy (265). Although ZnO-NPs have not received substantial attention in the aforementioned experiments, their known biological effects suggest that they may exert similar mechanisms of action. Therefore it has to be considered that the actual effects on cell death may be more extensive than by measuring only caspase-dependent apoptosis, as was done in this study.

Overall, the presented immunohistochemical staining methods do not encompass the entirety of changes in cell viability. Instead, this may be measured by a cell viability-assay or a clonogenic assay. This is also reasonable in order to portray the remaining

capacity of tumorous cells to proliferate as it offers a method to reach conclusions of the success of the proclaimed therapeutic method.

Nevertheless, this may lead to overall reduction of tumor cells and reduction in survival of aberrant cells, with possible inactivation of cancer stem cells or senescent cells, as i*n vitro* studies have clearly shown (1). They have clearly demonstrated senescent cells to be susceptible to ZnO-NP after radiation had taken place (40, 41, 270, 271). Although these studies applied a different order of interventions than what was performed in the experiments presented of this thesis. Therefore, to compare the effects and possibly obtain similar results, it would make sense to apply radiation before application of ZnO-NP. Likewise, it may be of interest to apply the before-mentioned repetitive radiotherapeutic approach. Then again, the ZnO-NP may have reached and altered the tumor but may not have been present in the tumorous tissue during the time of the second intervention. Whether this is a question of timing may in turn be clarified by possibly reducing the timespan between application of ZnO-NP and radiation. The vitality of the tumorous tissue may therefore be lowered.

In summary, as the synergistic effects of radiation and ZnO-NP have been proven *in vitro*, a next step towards *in vivo* experiments has been made by this study. It has to be born in mind that a translational threshold is present when comparing *in vitro* and *in vivo* findings. *In vitro* findings often show clear cytotoxic effects while similar trends *in vivo*, though subtle, may still contribute meaningfully since they were obtained in a complex biological environment. Likewise, variations in the tumor microenvironment or experimental models may mask or dilute statistically significant responses without negating their presence. If proposed trends were to be further confirmed by statistically significant results, the combined intervention could prove itself in line with the requirements for an anti-neoplastic treatment.

7.4 Effects on the quantity of vascular structures

In addition to the direct influence of radiation and ZnO-NP on cell viability of tumor cells, an influence on the tumor-associated vascular network offers new possibilities for the combined use in tumor therapy. Due to its central role in the progression of solid

tumors, the investigation of tumor vascularization and neo-angiogenesis is of great interest and will be elucidated in this section.

Vascular structures from the CAM have connected to the solid tumor during incubation after day 7 in the experimental setup, which has been well described in literature sources, also specifically in hepatocellular carcinoma xenografts (272). In this experimental study, this process was analyzed after termination on day 14, resulting in a static presentation of developments which took place in the days before. It has to be noted that the quantification of vascular structures by immunohistochemical staining poses an overview, but does not exhaust the many possibilities which are offered by the CAM assay in angiogenesis-related studies (273). In recent studies, the evaluation of vascular development in the CAM assay with solid tumors has been strategically advanced by proposing several investigation methods ranging from *in vivo* fluorescence or light microscopy to luminescence assays. Furthermore, clinical standard imaging techniques such as computed tomography, magnetic resonance imaging, and ultrasonography offer investigation of vascular structures on the CAM, the xenograft, and the embryo on a macroscopic level (98, 273).

By analyzing the number and distribution of alpha-SMA-positive structures within the tumor area, an influence on tumor-associated blood vessels of both radiation and ZnO-NP could be observed (Figure 21 and Figure 22). A low quantity of alpha-SMA-positive structures within the tumor area was detected after radiation. This can be seen by comparing the mean value of group 1 at 0,00111 n/µm^2 (±0,00043) while the mean of group 3 was determined at 0,00082 n/µm^2 (±0,00019). It has to be noted that due to the standard deviation, a high overlap was created, leading to a low statistical significance when the level of significance of 5% was applied. Nevertheless, a trend can be expressed, especially when taking into account known biological mechanisms of radiation.

Similarly, the intervention of ZnO-NP may also show a decline in vascular structures with a mean value of 0,00101 n/µm^2 (±0,00043) when compared to the control group. This difference in values certainly is much smaller and therefore it has to be taken into account that these values do not show a trend. This in turn may support the thesis that ZnO-NP do not have a direct anti-angiogenic effect themselves. Furthermore, it may

be discussed that ZnO-NP did not reach the tumor, as was already stated above, and therefore did not exert an effect.

However, the combined treatment lies in the middle of either values after solitary intervention as the mean of group 4 is at 0,00093 n/µm^2 (±0,00036). Whilst this does show a pronounced effect of reduction in vascular structures, it is questionable why the combined treatment does not reach the same levels as the solitary radiation treatment. It could of course be due to coincidental distribution of values and in reality lie much closer together than what is shown by the values obtained in these experiments. This would align well with known effects of radiation and the logic that addition of ZnO-NP may indeed add to but do not impede the effects of radiation.

The above-mentioned known biological consequences of radiation will now be explained in more detail. When radiation as an established anti-cancer treatment was applied to tumors on the CAM, the effects on vascular remodeling and angiogenesis could be evaluated (33). Furthermore, the extracellular matrix was modulated after application of 10 Gray. Especially proteins regulating angiogenesis were seen to be decreased in quantity via Western blot, while their mRNA expression was also reduced. Following this, angiogenesis was inhibited at a maximum of 24 hours post-radiation. All vascular structures and neo-angiogenesis were affected as well when tumor cells were added, which was examined via microscopic inspection (249, 274, 275). This is most probably due to reduced proliferative action of cells and induction of anti-angiogenic substances such as nitric oxide (NO^-) (276, 277). NO^- is part of RONS and proven to inhibit vascular growth, therefore offering a new therapeutic approach for targeted suppression of angiogenesis in tumorigenesis (250, 278). As generation of ROS is also a presumed mechanism of action of ZnO-NP, it is to be presumed that the combined application supports these effects.

It may therefore also be of interest to also analyze the distribution of vasculature within the tumor. The group of combined intervention shows in comparison to the other groups a notable decrease of highly vascularized specimens and rise of low and moderately vascularized CAMs (Figure 21). This may play an important role since the center of a solid tumor is most vulnerable to hypoxia, absence of nutrients and therefore cell death when no adequate vascular structures supply the cells (99). Overall, it may indicate a dynamic similar to above mentioned results concerning cell

viability and underscores the potential of a combined application for reduction of tumor growth due to effects on vascular structures within the solid tumor and those of the CAM.

However, it is to be noted that the quantity of vascular structures as well as their distribution within the solid tumor do not describe the quality of tumor-associated vessels, which may also play an important role. While alpha-SMA staining methods can identify mature vessels, it is not adequate to reveal newly formed microcapillaries, even though these may play an important role for the interpretation of tumor angiogenesis. Furthermore, the permeability and overall blood flow within vessels are important dynamics when considering the effects of possible anti-cancer treatments. A method to further evaluate the quality of vascular structures such as intravital fluorescence microscopy could be implemented in the experimental setup to monitor above mentioned criteria.

Correspondingly, it is known that application of ionizing radiation on tumorous tissue can both increase the permeability of the vessels and reduce blood flow due to increased apoptotic cell death of endothelial cells and vascular smooth muscle cells (279). As tumor-associated vascular structures already show an altered vascular architecture characterized by an irregular wall structure and vessel diameter, uneven blood flow and higher permeability of the vessel wall (67, 68, 140), this may be further influenced and deteriorated by the effects of radiation. Complex molecular processes take place, whilst the overall lack of oxygen and nutrients eventually lead to their demise. In general, RONS play an important role in vasodilation or -constriction with both effects taking place depending on which kind of molecules are present. While hyperoxides such as O_2^- can trigger vasoconstriction, NO causes vasodilation via the activation of cytosolic guanylate cyclase (280, 281). Relatedly, the above shown results of lower count of vascular structures could be caused by damage to microvessels by increased RONS due to radiation and ZnO-NP.

The therapeutic influence of interventions as described above could make tumor-associated blood vessels more susceptible to damage caused by high oxidative stress (34). This is not portrayed by the chosen method of data acquisition and therefore remains a hypothesis to be further evaluated. Furthermore, the cell signaling, growth factors and dynamic processes of vascular remodeling and neo-angiogenesis are of

interest as well as was mentioned in the references to literature. Other quantitative methods of mRNA and protein analysis shall be included in future experiments.

It is moreover to be discussed whether a drastically reduced amount of vascular structures within the tumor is the single desired effect during the anti-tumor treatment. Intravascularly applied drugs can only reach the tumor if vascularization is present, similar to intravascular antibiotics not reaching an encapsulated abscess. A reduction of blood supply to the tumor tissue could prevent sufficient accumulation of tumor therapeutics such as nanoparticulate drugs or chemotherapeutics. Similarly, and notably also due to higher vascular permeability, a rise in already high interstitial pressure within the tumor tissue is generated. This has been proven to be true after radiation treatment (281). This phenomenon can hinder the diffusion of substances, including chemotherapeutic agents, into the tumor tissue, potentially also accelerating their removal from the site (69-71). This was a reason for the application of ZnO-NP to take place before radiation, so that the effect of the nanoparticles may develop unimpeded. On the other hand, if cellular damages due to radiation were already present, the ZnO-NP may advance these if applied after the radiation.

Furthermore, a lower blood flow and higher permeability cause a longer amount of time which the drugs spend within the tumorous tissue, thus possibly leading to a higher effect locally and not systemic. A locally increased concentration of systemic active substances can potentially diminish side effects and adverse reactions of the organism. In the best-case scenario, a constant or higher efficacy of nanoparticulate drugs or chemotherapeutics in the tumor tissue could be achieved despite the use of a lower dose (45, 137, 282).

This further demands for a targeting strategy which ensures that ZnO-NP which are injected into the bloodstream primarily target the tumor and release their toxic load only at the tumor site, as is currently being investigated by using iRGD-mediated nano-carrier systems (283). An uncontrolled dissolution and release of ZnO NP in the organism should be avoided. For example, ZnO-NP could be protected by a coating to safely travel through the bloodstream and to protect the sensitive endothelial layer by e.g. silicone in nanoparticulate structure (2, 284, 285).

7.5 Outlook and future scientific use of the HET-CAM-Assay

This chapter will analyze specific characteristics and give an outlook into the future possibilities of the experimental setup to expand the knowledge on antineoplastic effects of ZnO-NP in combination with radiation.

Whilst in this experimental study only Huh-7 cells were present in the initial xenograft, it has to be noted that especially in the regions bordering on the CAM tissue, a recruitment of other cell types might have taken place (95). These may be endothelial cells, macrophages and fibroblasts, all of which create the multi-faceted constitution of a tumor and its microenvironment (73). How exactly this takes place and further influences the results of this study in order to establish new treatment options needs to be evaluated in detail. Likewise, initially forming complex solid tumors including other cell types such as fibroblasts rather than exclusively tumor cells may pose an important step towards more realistic experimental setups eventually leading to enhanced transferability of results (286).

As the understanding of tumor biology and radioresistance is of heightened interest, the CAM-Assay was also used to investigate this in the treatment of head and neck cancer when patient-derived tissue samples were set on the CAM directly (287). This may offer new insights since host-specific characteristics of the tumor were transferred as well, meaning the microenvironment. As the tumor microenvironment itself is a presumed player in the mechanisms of radioresistance, it is of increased relevance in the study of anti-neoplastic treatments. For instance, it may investigated by transcript analyses (288) or cellular analyses with emphasis on the angiogenic potential (289) within the tumor stroma, by using above-mentioned methods to measure the vasculatory system.

Furthermore, during the experimental setup, the timespan in which observation of the tumor on the CAM is possible and after interventions have taken place is limited. It is marked by start of the CAM development from day 6 of incubation, the development of the nervous system with perception of pain by the embryo starting on day 14 and the occurrence of immunological reactions. When following the timeline of the HET-CAM-Assay, a comparatively short observation period of the tumor on the CAM counting seven days in total was possible in this experimental setting which is a

common set-up (273). This may pose a certain disadvantage for examination of tumors as their long-term reactions cannot be investigated. On the other hand, rapid data acquisition is possible and especially immediate effects can be investigated optimally. Moreover, metabolism of Huh-7 cells has to be considered in order to receive information about cell death and even more importantly, proliferative activity. Since this revolves around a doubling time of 1,5 to 2 days, a reasonable timespan has to be added to let effects of interventions take place before terminating the experiment (107).

As the tumors can be harvested directly, immunohistochemical analyses of the tumor tissue and the surrounding CAM may follow. It has to be noted though that the microscopic evaluation is in reality two-dimensional and not the entire specimen can be examined. It should be considered to use more analytical methods in order to submit the entire specimen to data analysis. These may be flow cytometry (for cell and organelle characteristics), qRT-PCR (for DNA and RNA analysis) or Western blotting (for protein analysis) with parts of the excised tumor samples. Moreover, it would be of interest to measure parameters connected with oxidative stress, such as reduced intracellular glutathione expression or the mitochondrial membrane potential.

In general, it can be said that the results obtained from the presented experiments have an exploratory approach and show interesting trends. The directional hypothesis can be made that a combined application of ZnO-NP and radiation has indeed effects on solid tumors *in ovo*. The groundwork for further research is laid and justifies more targeted experiments as well as new approaches to evaluate the effects of ZnO-NP and radiation in the field of anti-neoplastic therapeutic systems.

8 Conclusion

This experimental study assessed the antineoplastic potential of ZnO-NP *in ovo*, both as a monotherapy and in combination with ionizing radiation using the CAM-Assay with xenografted human hepatocellular carcinoma (Huh-7) cells.

Histological and immunohistochemical analysis revealed that ionizing radiation alone (8 Gy) induced an expected pattern of increased apoptosis, evidenced by elevated CC3 staining, alongside enhanced proliferative activity (Ki-67 positivity) and a reduction in vascular structures within the tumor tissue. This dual increase in apoptosis and proliferation may reflect a compensatory mechanism, potentially involving the reactivation of dormant tumor cells or stress-induced mitogenic responses, as are known mechanisms of radioresistance.

As was the objective of this experimental study, ZnO-NP monotherapy (13.5 µg, intravascular administration) could be evaluated in the same manner and produced similar, although less pronounced effects, therefore suggesting inherent cytotoxic and anti-angiogenic properties of the nanoparticles *in ovo*.

On the other hand, in the study group of combined application, tumor sections demonstrated markedly increased levels of apoptosis (CC3) and a concurrent reduction in proliferative markers (Ki-67) when compared to monotherapies. This suggests a synergistic interaction between ZnO-NP and radiation, meaning ZnO-NP may enhance radiation-induced cytotoxicity while suppressing the proliferative rebound. Moreover, angiogenesis within the tumor tissue appeared further diminished in the combined treatment group, as evidenced by reduced quantity of α-SMA-positive structures and therefore indicating an impairment of vascular support essential for tumor growth and survival.

These findings align with prior studies indicating that ZnO-NP possess toxicity toward proliferative and therapy-resistant tumor cells. Although definitive conclusions await validation in statistically powerful studies, this study provides preliminary evidence which may ultimately lead to inclusion of ZnO-NP in multimodal oncologic strategies. Future research should focus on optimizing nanoparticle dosage, timing relative to radiation, and surface functionalization to enhance tumor specificity.

9 Abstract

Introduction: Innovative cancer therapies aim to exert selective cytotoxic effects while preventing tumor proliferation. Zinc oxide nanoparticles (ZnO-NP) have emerged as promising antitumor agents due to their cytotoxicity in various human cancer cell lines and favorable biocompatibility. This study explored the antineoplastic potential of ZnO-NPs alone and in combination with radiotherapy — a common cancer treatment hindered by tumor radioresistance and other side effects.

Aims: We aimed to evaluate whether ZnO-NP enhance the efficacy of radiotherapy by reduction of cell viability and vascular structures within the tumor area using the Hen's Egg Test – Chorioallantoic Membrane Model (HET-CAM-Assay) which included a xenograft of human hepatocellular carcinoma (Huh-7) cell-derived tumors.

Methods: CAMs were divided into four groups: untreated, ZnO-NP only, radiation only (8 Gy), and combination treatment. Depending on the study group, ZnO-NP (13.5 µg) were injected intravascularly 120 hours after the xenografts were applied while radiation treatment was performed 24 hours later. After another 24 hours, tumors were excised and analyzed immunohistochemically for morphology (H&E, pan-keratin), apoptosis (Cleaved Caspase-3), proliferation (Ki-67), and angiogenesis (α-smooth muscle actin).

Results: Radiation alone increased apoptosis and proliferation while reducing angiogenesis. ZnO-NP monotherapy showed similar, though milder effects. Both treatments elevated CC3 and Ki-67 levels, suggesting cytotoxicity accompanied by compensatory proliferation. Notably, the combination therapy increased apoptosis, while proliferation was reduced, and decreased vascularization — indicating synergistic effects.

Conclusion: ZnO-NPs exhibit notable antineoplastic effects *in ovo*, particularly in combination with radiation treatment. The findings suggest that ZnO-NPs may enhance radiotherapeutic outcomes by promoting apoptosis, suppressing proliferation, and inhibiting angiogenesis. Their potential as radiosensitizers in future cancer therapies is to be evaluated further.

10 References

1. Wiesmann N, Gieringer R, Viel M, Eckrich J, Tremel W, Brieger J. Zinc Oxide Nanoparticles Can Intervene in Radiation-Induced Senescence and Eradicate Residual Tumor Cells. Cancers (Basel). 2021;13(12).

2. Wiesmann N, Tremel W, Brieger J. Zinc oxide nanoparticles for therapeutic purposes in cancer medicine. J Mater Chem B. 2020;8(23):4973-89.

3. Wiesmann N, Kluenker M, Demuth P, Brenner W, Tremel W, Brieger J. Zinc overload mediated by zinc oxide nanoparticles as innovative anti-tumor agent. J Trace Elem Med Biol. 2019;51:226-34.

4. Ribatti D. The chick embryo chorioallantoic membrane (CAM). A multifaceted experimental model. Mech Dev. 2016;141:70-7.

5. Organization WH. https://www.who.int/news-room/fact-sheets/detail/cancer. last accessed on 13. December 2023.

6. Weinberg RA, Weinberg RA. The Biology of Cancer: W.W. Norton; 2013.

7. Kastan MB, Bartek J. Cell-cycle checkpoints and cancer. Nature. 2004;432(7015):316-23.

8. Gimeno-Valiente F, López-Rodas G, Castillo J, Franco L. The Many Roads from Alternative Splicing to Cancer: Molecular Mechanisms Involving Driver Genes. Cancers (Basel). 2024;16(11).

9. Ozaki T, Nakagawara A. Role of p53 in Cell Death and Human Cancers. Cancers (Basel). 2011;3(1):994-1013.

10. Mellman I, Coukos G, Dranoff G. Cancer immunotherapy comes of age. Nature. 2011;480(7378):480-9.

11. Kirkby M, Popatia AM, Lavoie JR, Wang L. The Potential of Hormonal Therapies for Treatment of Triple-Negative Breast Cancer. Cancers (Basel). 2023;15(19).

12. Peters C, Locatelli F, Bader P. Acute Lymphoblastic Leukaemia in Children and Adolescents. In: Sureda A, Corbacioglu S, Greco R, Kröger N, Carreras E, editors. The EBMT Handbook: Hematopoietic Cell Transplantation and Cellular Therapies. Cham (CH): Springer

Copyright 2024, The Author(s). 2024. p. 659-67.

13. Sharma A, Cressman E, Attaluri A, Kraitchman DL, Ivkov R. Current Challenges in Image-Guided Magnetic Hyperthermia Therapy for Liver Cancer. Nanomaterials (Basel). 2022;12(16).

14. Hong G, Chang JE. Enhancing Cancer Treatment Through Combined Approaches: Photodynamic Therapy in Concert with Other Modalities. Pharmaceutics. 2024;16(11).

15. National Institute of Health NCI. https://www.cancer.gov/about-cancer/treatment/types. last accessed on 13. December 2023.

16. Baskar R, Lee KA, Yeo R, Yeoh KW. Cancer and radiation therapy: current advances and future directions. Int J Med Sci. 2012;9(3):193-9.

17. Maier P, Hartmann L, Wenz F, Herskind C. Cellular Pathways in Response to Ionizing Radiation and Their Targetability for Tumor Radiosensitization. Int J Mol Sci. 2016;17(1).

18. McMillan TJ, Tobi S, Mateos S, Lemon C. The use of DNA double-strand break quantification in radiotherapy. Int J Radiat Oncol Biol Phys. 2001;49(2):373-7.

19. Kwatra D, Venugopal A, Anant S. Nanoparticles in radiation therapy: A summary of various approaches to enhance radiosensitization in cancer. Translational Cancer Research. 2013;2:330-42.

20. Nakashima J, Duong H. Radiation Physics. StatPearls. Treasure Island (FL) ineligible companies. Disclosure: Hieu Duong declares no relevant financial relationships with ineligible companies.: StatPearls Publishing

21. Liang X, Mohammadi H, Moreno KC, Beltran CJ, Holtzman AL. Heavy Ion Particle Therapy in Modern Day Radiation Oncology. Hematol Oncol Clin North Am. 2024.

22. Viswanathan AN, Erickson BA, Ibbott GS, Small W, Jr., Eifel PJ. The American College of Radiology and the American Brachytherapy Society practice parameter for the performance of low-dose-rate brachytherapy. Brachytherapy. 2017;16(1):68-74.

23. Mitchell AL, Gandhi A, Scott-Coombes D, Perros P. Management of thyroid cancer: United Kingdom National Multidisciplinary Guidelines. J Laryngol Otol. 2016;130(S2):S150-s60.

24. Kunz-Schughart LA, Dubrovska A, Peitzsch C, Ewe A, Aigner A, Schellenburg S, et al. Nanoparticles for radiooncology: Mission, vision, challenges. Biomaterials. 2017;120:155-84.

25. Rasmussen J, Martinez E, Louka P, Wingett D. Zinc Oxide Nanoparticles for Selective Destruction of Tumor Cells and Potential for Drug Delivery Applications. Expert opinion on drug delivery. 2010;7:1063-77.

26. Alcorn S, Cortés Á A, Bradfield L, Brennan M, Dennis K, Diaz DA, et al. External Beam Radiation Therapy for Palliation of Symptomatic Bone Metastases: An ASTRO Clinical Practice Guideline. Pract Radiat Oncol. 2024;14(5):377-97.

27. Barillot I, Azria D, Lisbona A, Mahé MA. External irradiation treatment process. Cancer Radiother. 2022;26(1-2):20-8.

28. Bourhis J, Sozzi WJ, Jorge PG, Gaide O, Bailat C, Duclos F, et al. Treatment of a first patient with FLASH-radiotherapy. Radiotherapy and oncology. 2019;139:18-22.

29. Deeg H. Seattle Marrow Transplant Team, Acute and delayed toxicities of total body irradiation. Int J Radiat Oncol Biol Phys. 1983;9(12):1933-9.

30. Chandra RA, Keane FK, Voncken FEM, Thomas CR, Jr. Contemporary radiotherapy: present and future. The Lancet. 2021;398(10295):171-84.

31. McMillan MT, Lawrence TS, Morgan MA. Targeting the DNA damage response for radiosensitization. Molecular Targeted Radiosensitizers: Opportunities and Challenges. 2020:191-218.

32. Vaupel P, Harrison L. Tumor Hypoxia: Causative Factors, Compensatory Mechanisms, and Cellular Response. The Oncologist. 2004;9(S5):4-9.

33. Dünker N, Jendrossek V. Implementation of the Chick Chorioallantoic Membrane (CAM) Model in Radiation Biology and Experimental Radiation Oncology Research. Cancers (Basel). 2019;11(10).

34. Jo M, Nishikawa T, Nakajima T, Okada Y, Yamaguchi K, Mitsuyoshi H, et al. Oxidative stress is closely associated with tumor angiogenesis of hepatocellular carcinoma. Journal of Gastroenterology. 2011;46(6):809-21.

35. Dong D, Fu Y, Chen F, Zhang J, Jia H, Li J, et al. Hyperoxia sensitizes hypoxic HeLa cells to ionizing radiation by downregulating HIF-1α and VEGF expression. Mol Med Rep. 2021;23(1).

36. Tsolou A, Lamprou I, Fortosi AO, Liousia M, Giatromanolaki A, Koukourakis MI. 'Stemness' and 'senescence' related escape pathways are dose dependent in lung cancer cells surviving post irradiation. Life Sci. 2019;232:116562.

37. Krause M, Dubrovska A, Linge A, Baumann M. Cancer stem cells: Radioresistance, prediction of radiotherapy outcome and specific targets for combined treatments. Advanced drug delivery reviews. 2017;109:63-73.

38. Peitzsch C, Kurth I, Kunz-Schughart L, Baumann M, Dubrovska A. Discovery of the cancer stem cell related determinants of radioresistance. Radiotherapy and Oncology. 2013;108(3):378-87.

39. Hanley R, Pagliari F, Garcia-Calderón D, Fernandes Guerreiro J, Genard G, Jansen J, et al. Radio-resistance of hypoxic tumors: exploring the effects of oxygen and x-ray radiation on non-small lung cancer cell lines. Radiat Oncol. 2023;18(1):81.

40. Kuwahara Y, Tomita K, Urushihara Y, Sato T, Kurimasa A, Fukumoto M. Association between radiation-induced cell death and clinically relevant radioresistance. Histochem Cell Biol. 2018;150(6):649-59.

41. Deorukhkar A, Krishnan S. Targeting inflammatory pathways for tumor radiosensitization. Biochem Pharmacol. 2010;80(12):1904-14.

42. Ancona A, Dumontel B, Garino N, Demarco B, Chatzitheodoridou D, Fazzini W, et al. Lipid-Coated Zinc Oxide Nanoparticles as Innovative ROS-Generators for Photodynamic Therapy in Cancer Cells. Nanomaterials (Basel). 2018;8(3).

43. Dolmans DE, Fukumura D, Jain RK. Photodynamic therapy for cancer. Nature reviews cancer. 2003;3(5):380-7.

44. Wang GD, Nguyen HT, Chen H, Cox PB, Wang L, Nagata K, et al. X-ray induced photodynamic therapy: A combination of radiotherapy and photodynamic therapy. Theranostics. 2016;6(13):2295.

45. Sharma H, Mishra PK, Talegaonkar S, Vaidya B. Metal nanoparticles: a theranostic nanotool against cancer. Drug Discovery Today. 2015;20(9):1143-51.

46. Azzam EI, Jay-Gerin JP, Pain D. Ionizing radiation-induced metabolic oxidative stress and prolonged cell injury. Cancer Lett. 2012;327(1-2):48-60.

47. Yang Q, Ma Y. Irradiation-Enhanced Cytotoxicity of Zinc Oxide Nanoparticles. International Journal of Toxicology. 2014;33(3):187-203.

48. Turrens JF. Mitochondrial formation of reactive oxygen species. The Journal of physiology. 2003;552(Pt 2):335-44.

49. Brown AM, Kristal BS, Effron MS, Shestopalov AI, Ullucci PA, Sheu K-FR, et al. Zn2+ inhibits α-ketoglutarate-stimulated mitochondrial respiration and the isolated α-ketoglutarate dehydrogenase complex. Journal of Biological Chemistry. 2000;275(18):13441-7.

50. Devasagayam TP, Tilak JC, Boloor KK, Sane KS, Ghaskadbi SS, Lele RD. Free radicals and antioxidants in human health: current status and future prospects. J Assoc Physicians India. 2004;52:794-804.

51. Hackenberg S, Scherzed A, Zapp A, Radeloff K, Ginzkey C, Gehrke T, et al. Genotoxic effects of zinc oxide nanoparticles in nasal mucosa cells are antagonized by titanium dioxide nanoparticles. Mutat Res Genet Toxicol Environ Mutagen. 2017;816-817:32-7.

52. Loft S, Høgh Danielsen P, Mikkelsen L, Risom L, Forchhammer L, Møller P. Biomarkers of oxidative damage to DNA and repair. Portland Press Ltd.; 2008.

53. Papadopoulos MC, Saadoun S. Key roles of aquaporins in tumor biology. Biochim Biophys Acta. 2015;1848(10 Pt B):2576-83.

54. Akhtar MJ, Ahamed M, Kumar S, Khan MM, Ahmad J, Alrokayan SA. Zinc oxide nanoparticles selectively induce apoptosis in human cancer cells through reactive oxygen species. Int J Nanomedicine. 2012;7:845-57.

55. Tait SW, Green DR. Mitochondria and cell death: outer membrane permeabilization and beyond. Nat Rev Mol Cell Biol. 2010;11(9):621-32.

56. Hotchkiss RS, Strasser A, McDunn JE, Swanson PE. Cell death. N Engl J Med. 2009;361(16):1570-83.

57. Qin X, Zhang J, Wang B, Xu G, Yang X, Zou Z, et al. Ferritinophagy is involved in the zinc oxide nanoparticles-induced ferroptosis of vascular endothelial cells. Autophagy. 2021;17(12):4266-85.

58. Elmore S. Apoptosis: a review of programmed cell death. Toxicol Pathol. 2007;35(4):495-516.

59. Mak IW, Evaniew N, Ghert M. Lost in translation: animal models and clinical trials in cancer treatment. Am J Transl Res. 2014;6(2):114-8.

60. Lucey BP, Nelson-Rees WA, Hutchins GM. Henrietta Lacks, HeLa cells, and cell culture contamination. Arch Pathol Lab Med. 2009;133(9):1463-7.

61. Hutchinson L, Kirk R. High drug attrition rates--where are we going wrong? Nat Rev Clin Oncol. 2011;8(4):189-90.

62. Kleinman HK, Martin GR. Matrigel: basement membrane matrix with biological activity. Semin Cancer Biol. 2005;15(5):378-86.

63. Breslin S, O'Driscoll L. Three-dimensional cell culture: the missing link in drug discovery. Drug Discov Today. 2013;18(5-6):240-9.

64. Sant S, Johnston PA. The production of 3D tumor spheroids for cancer drug discovery. Drug Discov Today Technol. 2017;23:27-36.

65. Langhans SA. Three-Dimensional in Vitro Cell Culture Models in Drug Discovery and Drug Repositioning. Front Pharmacol. 2018;9:6.

66. Olive PL, Vikse C, Trotter MJ. Measurement of oxygen diffusion distance in tumor cubes using a fluorescent hypoxia probe. Int J Radiat Oncol Biol Phys. 1992;22(3):397-402.

67. Konerding MA, Malkusch W, Klapthor B, van Ackern C, Fait E, Hill SA, et al. Evidence for characteristic vascular patterns in solid tumours: quantitative studies using corrosion casts. Br J Cancer. 1999;80(5-6):724-32.

68. Mangir N, Raza A, Haycock JW, Chapple C, Macneil S. An Improved In Vivo Methodology to Visualise Tumour Induced Changes in Vasculature Using the Chick Chorionic Allantoic Membrane Assay. In Vivo. 2018;32(3):461-72.

69. Minchinton AI, Tannock IF. Drug penetration in solid tumours. Nat Rev Cancer. 2006;6(8):583-92.

70. Heldin CH, Rubin K, Pietras K, Ostman A. High interstitial fluid pressure - an obstacle in cancer therapy. Nat Rev Cancer. 2004;4(10):806-13.

71. Baronzio G, Parmar G, Baronzio M. Overview of Methods for Overcoming Hindrance to Drug Delivery to Tumors, with Special Attention to Tumor Interstitial Fluid. Front Oncol. 2015;5:165.

72. Augustin HG, Christian S. Angiogenese. Die Onkologie. 2010:291-307.

73. Horsman MR, Vaupel P. Pathophysiological Basis for the Formation of the Tumor Microenvironment. Front Oncol. 2016;6:66.

74. Liberti MV, Locasale JW. The Warburg Effect: How Does it Benefit Cancer Cells? Trends Biochem Sci. 2016;41(3):211-8.

75. Russell WMS, Burch RL. The principles of humane experimental technique: Methuen; 1959.

76. Union E. „Richtlinie 2010/63/EU des Europäischen Parlaments und des Rates vom 22. September 2010 zum Schutz der für wissenschaftliche Zwecke verwendeten Tiere “. Amtsblatt der Europäischen Union. 2010:33-79.

77. Bundesrepublik Deutschland BfJ. Tierschutzgesetz, https://www.gesetze-im-internet.de/tierschg/BJNR012770972.html. 2013.

78. Gerlach L. Über neue Methoden auf dem Gebiet der experimentellen Embryologie. Anatomischer Anzeiger Centralblatt für die gesamte wissenschaftliche Anatomie Amtliches Organ der Anatomischen Gesellschaft. 1887:583-609.

79. Goerttler K. The" teratological basic experiment" on the incubated chick embryo, its possibilities and limitations. Klinische Wochenschrift. 1962;40:809-12.

80. Luepke NP. Hen's egg chorioallantoic membrane test for irritation potential. Food Chem Toxicol. 1985;23(2):287-91.

81. Ribatti D. The chick embryo chorioallantoic membrane (CAM) assay. Reprod Toxicol. 2017;70:97-101.

82. Fasenko G. Egg storage and the embryo. Poultry science. 2007;86(5):1020-4.

83. Bellairs R, Osmond M. Atlas of chick development: Elsevier; 2005.

84. Burton FG, Tullett S. Respiration of avian embryos. Comparative Biochemistry and Physiology Part A: Physiology. 1985;82(4):735-44.

85. Leeson T, Leeson C. The chorio-allantois of the chick. Light and electron microscopic observations at various times of incubation. Journal of Anatomy. 1963;97(Pt 4):585.

86. Makanya AN, Dimova I, Koller T, Styp-Rekowska B, Djonov V. Dynamics of the Developing Chick Chorioallantoic Membrane Assessed by Stereology, Allometry, Immunohistochemistry and Molecular Analysis. PLoS One. 2016;11(4):e0152821.

87. Eugenín J, Eyzaguirre C. Electrophysiological properties of rat nodose ganglion neurons co-transplanted with carotid bodies into the chick chorioallantoic membrane. Biol Res. 2005;38(4):329-34.

88. Dohle DS, Pasa SD, Gustmann S, Laub M, Wissler JH, Jennissen HP, et al. Chick ex ovo culture and ex ovo CAM assay: how it really works. J Vis Exp. 2009(33).

89. Mohan S, Foley PL. Everything You Need to Know About Satisfying IACUC Protocol Requirements. Ilar j. 2019;60(1):50-7.

90. Ribatti D. The chick embryo chorioallantoic membrane as a model for tumor biology. Exp Cell Res. 2014;328(2):314-24.

91. Wiesmann N, Brieger J, Eckrich J. Toxicological Analysis by Assessment of Vascularization and Cell Viability Using the Chicken's Chorioallantoic Membrane (CAM Assay). Methods Mol Biol. 2023;2644:403-21.

92. Buhr CR, Eckrich J, Kluenker M, Bruns K, Wiesmann N, Tremel W, et al. Determination of the LD(50) with the chick embryo chorioallantoic membrane (CAM) assay as a promising alternative in nanotoxicological evaluation. Nanotoxicology. 2021;15(5):690-705.

93. Murphy JB, Rous P. The behavior of chicken sarcoma implanted in the developing embryo. The Journal of experimental medicine. 1912;15(2):119-32.

94. Murphy JB. TRANSPLANTABILITY OF TISSUES TO THE EMBRYO OF FOREIGN SPECIES : ITS BEARING ON QUESTIONS OF TISSUE SPECIFICITY AND TUMOR IMMUNITY. J Exp Med. 1913;17(4):482-93.

95. Ribatti D. The chick embryo chorioallantoic membrane in the study of tumor angiogenesis. Rom J Morphol Embryol. 2008;49(2):131-5.

96. Janković B, Isaković K, Lukić M, Vujanović N, Petrović S, Marković B. Immunological capacity of the chicken embryo. I. Relationship between the maturation of lymphoid tissues and the occurrence of cell-mediated immunity in the developing chicken embryo. Immunology. 1975;29(3):497.

97. Janse EM, Jeurissen SH. Ontogeny and function of two non-lymphoid cell populations in the chicken embryo. Immunobiology. 1991;182(5):472-81.

98. Eckrich J, Kugler P, Buhr CR, Ernst BP, Mendler S, Baumgart J, et al. Monitoring of tumor growth and vascularization with repetitive ultrasonography in the chicken chorioallantoic-membrane-assay. Scientific reports. 2020;10(1):18585.

99. Hagedorn M, Javerzat S, Gilges D, Meyre A, de Lafarge B, Eichmann A, et al. Accessing key steps of human tumor progression in vivo by using an avian embryo model. Proceedings of the National Academy of Sciences. 2005;102(5):1643-8.

100. Knighton D, Ausprunk D, Tapper D, Folkman J. Avascular and vascular phases of tumour growth in the chick embryo. Br J Cancer. 1977;35(3):347-56.

101. Lugassy C, Barnhill RL. Angiotropic melanoma and extravascular migratory metastasis: a review. Advances in anatomic pathology. 2007;14(3):195-201.

102. Shioda T, Munn LL, Fenner MH, Jain RK, Isselbacher KJ. Early events of metastasis in the microcirculation involve changes in gene expression of cancer cells. Tracking mRNA levels of metastasizing cancer cells in the chick embryo chorioallantoic membrane. The American journal of pathology. 1997;150(6):2099.

103. Deryugina EI, Quigley JP. Chick embryo chorioallantoic membrane model systems to study and visualize human tumor cell metastasis. Histochemistry and cell biology. 2008;130:1119-30.

104. De Magalhães N, Liaw LH, Berns M, Cristini V, Chen Z, Stupack D, et al. Applications of a new In vivo tumor spheroid based shell-less chorioallantoic membrane 3-D model in bioengineering research. J Biomed Sci Eng. 2010;3(1):20-6.

105. Bearer EL, Lowengrub JS, Frieboes HB, Chuang YL, Jin F, Wise SM, et al. Multiparameter computational modeling of tumor invasion. Cancer Res. 2009;69(10):4493-501.

106. Frieboes HB, Lowengrub JS, Wise S, Zheng X, Macklin P, Bearer EL, et al. Computer simulation of glioma growth and morphology. Neuroimage. 2007;37 Suppl 1(Suppl 1):S59-70.

107. Nakabayashi H, Taketa K, Miyano K, Yamane T, Sato J. Growth of human hepatoma cells lines with differentiated functions in chemically defined medium. Cancer Res. 1982;42(9):3858-63.

108. Li M, Pathak RR, Lopez-Rivera E, Friedman SL, Aguirre-Ghiso JA, Sikora AG. The In Ovo Chick Chorioallantoic Membrane (CAM) Assay as an Efficient Xenograft Model of Hepatocellular Carcinoma. J Vis Exp. 2015(104).

109. Al-Fartusie F, Mohssan S. Essential Trace Elements and Their Vital Roles in Human Body. Indian Journal of Advances in Chemical Science. 2017;5:127-36.

110. Sandstead HH. Understanding zinc: recent observations and interpretations. J Lab Clin Med. 1994;124(3):322-7.

111. Andreini C, Banci L, Bertini I, Rosato A. Zinc through the three domains of life. J Proteome Res. 2006;5(11):3173-8.

112. Cassandri M, Smirnov A, Novelli F, Pitolli C, Agostini M, Malewicz M, et al. Zinc-finger proteins in health and disease. Cell Death Discov. 2017;3:17071.

113. Klug A. The discovery of zinc fingers and their applications in gene regulation and genome manipulation. Annu Rev Biochem. 2010;79:213-31.

114. Stiles LI, Ferrao K, Mehta KJ. Role of zinc in health and disease. Clin Exp Med. 2024;24(1):38.

115. Kloubert V, Rink L. Zinc as a micronutrient and its preventive role of oxidative damage in cells. Food Funct. 2015;6(10):3195-204.

116. Maret W. Zinc in Cellular Regulation: The Nature and Significance of "Zinc Signals". Int J Mol Sci. 2017;18(11).

117. Maret W, Krezel A. Cellular zinc and redox buffering capacity of metallothionein/thionein in health and disease. Mol Med. 2007;13(7-8):371-5.

118. Colvin RA, Holmes WR, Fontaine CP, Maret W. Cytosolic zinc buffering and muffling: their role in intracellular zinc homeostasis. Metallomics. 2010;2(5):306-17.

119. Ahamed M, Akhtar MJ, Raja M, Ahmad I, Siddiqui MKJ, AlSalhi MS, et al. ZnO nanorod-induced apoptosis in human alveolar adenocarcinoma cells via p53, survivin

and bax/bcl-2 pathways: role of oxidative stress. Nanomedicine: Nanotechnology, Biology and Medicine. 2011;7(6):904-13.

120. A R, Jagadeesan S, Cho YJ, Lim JH, Choi KH. Synthesis and evaluation of the cytotoxic and anti-proliferative properties of ZnO quantum dots against MCF-7 and MDA-MB-231 human breast cancer cells. Mater Sci Eng C Mater Biol Appl. 2017;81:551-60.

121. Marreiro DD, Cruz KJ, Morais JB, Beserra JB, Severo JS, de Oliveira AR. Zinc and Oxidative Stress: Current Mechanisms. Antioxidants (Basel). 2017;6(2).

122. Jarosz M, Olbert M, Wyszogrodzka G, Młyniec K, Librowski T. Antioxidant and anti-inflammatory effects of zinc. Zinc-dependent NF-κB signaling. Inflammopharmacology. 2017;25(1):11-24.

123. Plum LM, Rink L, Haase H. The essential toxin: impact of zinc on human health. Int J Environ Res Public Health. 2010;7(4):1342-65.

124. Hanley C, Thurber A, Hanna C, Punnoose A, Zhang J, Wingett DG. The Influences of Cell Type and ZnO Nanoparticle Size on Immune Cell Cytotoxicity and Cytokine Induction. Nanoscale Res Lett. 2009;4(12):1409-20.

125. Yamasaki S, Hasegawa A, Hojyo S, Ohashi W, Fukada T, Nishida K, et al. A novel role of the L-type calcium channel α1D subunit as a gatekeeper for intracellular zinc signaling: zinc wave. PLoS One. 2012;7(6):e39654.

126. Hambidge M. Human zinc deficiency. J Nutr. 2000;130(5S Suppl):1344s-9s.

127. Prasad AS. Zinc: mechanisms of host defense. J Nutr. 2007;137(5):1345-9.

128. Boverhof DR, Bramante CM, Butala JH, Clancy SF, Lafranconi M, West J, et al. Comparative assessment of nanomaterial definitions and safety evaluation considerations. Regul Toxicol Pharmacol. 2015;73(1):137-50.

129. Heiligtag FJ, Niederberger M. The fascinating world of nanoparticle research. Materials Today. 2013;16(7):262-71.

130. Bayda S, Adeel M, Tuccinardi T, Cordani M, Rizzolio F. The History of Nanoscience and Nanotechnology: From Chemical-Physical Applications to Nanomedicine. Molecules. 2019;25(1).

131. Heinzerling P, Oetken M. Nanochemistry—A Split between 18th Century and Modern Times. World J Chem Educ. 2018;6(1):1-7.

132. Kołodziejczak-Radzimska A, Jesionowski T. Zinc Oxide-From Synthesis to Application: A Review. Materials (Basel). 2014;7(4):2833-81.

133. Wang ZL. Nanostructures of zinc oxide. Materials Today. 2004;7(6):26-33.

134. Grassian V. When Size Really Matters: Size-Dependent Properties and Surface Chemistry of Metal and Metal Oxide Nanoparticles in Gas and Liquid Phase Environments†. Journal of Physical Chemistry C - J PHYS CHEM C. 2008;0.

135. Ventola CL. Progress in Nanomedicine: Approved and Investigational Nanodrugs. P t. 2017;42(12):742-55.

136. Punnoose A, Dodge K, Rasmussen JW, Chess J, Wingett D, Anders C. Cytotoxicity of ZnO Nanoparticles Can Be Tailored by Modifying Their Surface Structure: A Green Chemistry Approach for Safer Nanomaterials. ACS Sustain Chem Eng. 2014;2(7):1666-73.

137. Wicki A, Witzigmann D, Balasubramanian V, Huwyler J. Nanomedicine in cancer therapy: challenges, opportunities, and clinical applications. J Control Release. 2015;200:138-57.

138. Tran S, DeGiovanni PJ, Piel B, Rai P. Cancer nanomedicine: a review of recent success in drug delivery. Clin Transl Med. 2017;6(1):44.

139. Bai C, Liu M. From chemistry to nanoscience: not just a matter of size. Angewandte Chemie International Edition. 2013;52(10).

140. Hashizume H, Baluk P, Morikawa S, McLean JW, Thurston G, Roberge S, et al. Openings between defective endothelial cells explain tumor vessel leakiness. Am J Pathol. 2000;156(4):1363-80.

141. Nakamura Y, Mochida A, Choyke PL, Kobayashi H. Nanodrug Delivery: Is the Enhanced Permeability and Retention Effect Sufficient for Curing Cancer? Bioconjug Chem. 2016;27(10):2225-38.

142. Bar-Zeev M, Livney YD, Assaraf YG. Targeted nanomedicine for cancer therapeutics: Towards precision medicine overcoming drug resistance. Drug Resistance Updates. 2017;31:15-30.

143. Grassian VH. Nanoscience and nanotechnology: environmental and health impacts: John Wiley & Sons; 2008.

144. Sivakumar P, Lee M, Kim YS, Shim MS. Photo-triggered antibacterial and anticancer activities of zinc oxide nanoparticles. J Mater Chem B. 2018;6(30):4852-71.

145. Hsu JC, Tang Z, Eremina OE, Sofias AM, Lammers T, Lovell JF, et al. Nanomaterial-based contrast agents. Nature Reviews Methods Primers. 2023;3(1):30.

146. Canfield SE, George AK, Jue JS, Lewis SC, Davenport MS, Tammisetti VS, et al. A Multi-Institutional Study of Magnetic Resonance/Ultrasound Fusion-Guided Nanoparticle-Directed Focal Therapy for Prostate Ablation: Erratum. J Urol. 2025;213(4):541.

147. Zheng X, Wu Y, Zuo H, Chen W, Wang K. Metal Nanoparticles as Novel Agents for Lung Cancer Diagnosis and Therapy. Small. 2023;19(18):e2206624.

148. Ashoub MH, Amiri M, Fatemi A, Farsinejad A. Evaluation of ferroptosis-based anti-leukemic activities of ZnO nanoparticles synthesized by a green route against Pre-B acute lymphoblastic leukemia cells (Nalm-6 and REH). Heliyon. 2024;10(17):e36608.

149. Racca L, Canta M, Dumontel B, Ancona A, Limongi T, Garino N, et al. 12 - Zinc Oxide Nanostructures in Biomedicine. In: Ciofani G, editor. Smart Nanoparticles for Biomedicine: Elsevier; 2018. p. 171-87.

150. Padmavathy N, Vijayaraghavan R. Enhanced bioactivity of ZnO nanoparticles-an antimicrobial study. Sci Technol Adv Mater. 2008;9(3):035004.

151. Abdelhakim HK, El-Sayed ER, Rashidi FB. Biosynthesis of zinc oxide nanoparticles with antimicrobial, anticancer, antioxidant and photocatalytic activities by the endophytic Alternaria tenuissima. J Appl Microbiol. 2020;128(6):1634-46.

152. Lakshmi Prasanna V, Vijayaraghavan R. Insight into the Mechanism of Antibacterial Activity of ZnO: Surface Defects Mediated Reactive Oxygen Species Even in the Dark. Langmuir. 2015;31(33):9155-62.

153. Clogston JD, Patri AK. Zeta potential measurement. Characterization of nanoparticles intended for drug delivery. 2011:63-70.

154. Schubert J, Chanana M. Coating Matters: Review on Colloidal Stability of Nanoparticles with Biocompatible Coatings in Biological Media, Living Cells and Organisms. Curr Med Chem. 2018;25(35):4553-86.

155. Abdelmonem AM, Pelaz B, Kantner K, Bigall NC, Del Pino P, Parak WJ. Charge and agglomeration dependent in vitro uptake and cytotoxicity of zinc oxide nanoparticles. J Inorg Biochem. 2015;153:334-8.

156. Condello M, De Berardis B, Ammendolia MG, Barone F, Condello G, Degan P, et al. ZnO nanoparticle tracking from uptake to genotoxic damage in human colon carcinoma cells. Toxicol In Vitro. 2016;35:169-79.

157. Taccola L, Raffa V, Riggio C, Vittorio O, Iorio MC, Vanacore R, et al. Zinc oxide nanoparticles as selective killers of proliferating cells. Int J Nanomedicine. 2011;6:1129-40.

158. Brenner BE, Keyes D. Metal Fume Fever. StatPearls. Treasure Island (FL) ineligible companies. Disclosure: Daniel Keyes declares no relevant financial relationships with ineligible companies.: StatPearls Publishing

159. Hadrup N, Rahmani F, Jacobsen NR, Saber AT, Jackson P, Bengtson S, et al. Acute phase response and inflammation following pulmonary exposure to low doses of zinc oxide nanoparticles in mice. Nanotoxicology. 2019;13(9):1275-92.

160. Osmond MJ, Mccall MJ. Zinc oxide nanoparticles in modern sunscreens: an analysis of potential exposure and hazard. Nanotoxicology. 2010;4(1):15-41.

161. Sharma V, Singh SK, Anderson D, Tobin DJ, Dhawan A. Zinc oxide nanoparticle induced genotoxicity in primary human epidermal keratinocytes. J Nanosci Nanotechnol. 2011;11(5):3782-8.

162. Manke A, Wang L, Rojanasakul Y. Mechanisms of nanoparticle-induced oxidative stress and toxicity. Biomed Res Int. 2013;2013:942916.

163. Song W, Zhang J, Guo J, Zhang J, Ding F, Li L, et al. Role of the dissolved zinc ion and reactive oxygen species in cytotoxicity of ZnO nanoparticles. Toxicology Letters. 2010;199(3):389-97.

164. Xia T, Kovochich M, Liong M, Mädler L, Gilbert B, Shi H, et al. Comparison of the Mechanism of Toxicity of Zinc Oxide and Cerium Oxide Nanoparticles Based on Dissolution and Oxidative Stress Properties. ACS Nano. 2008;2(10):2121-34.

165. Žūkienė R, Snitka V. Zinc oxide nanoparticle and bovine serum albumin interaction and nanoparticles influence on cytotoxicity in vitro. Colloids Surf B Biointerfaces. 2015;135:316-23.

166. Yin H, Chen R, Casey PS, Ke PC, Davis TP, Chen C. Reducing the cytotoxicity of ZnO nanoparticles by a pre-formed protein corona in a supplemented cell culture medium. RSC Advances. 2015;5(90):73963-73.

167. Moos PJ, Chung K, Woessner D, Honeggar M, Cutler NS, Veranth JM. ZnO Particulate Matter Requires Cell Contact for Toxicity in Human Colon Cancer Cells. Chemical Research in Toxicology. 2010;23(4):733-9.

168. Churchman AH, Wallace R, Milne SJ, Brown AP, Brydson R, Beales PA. Serum albumin enhances the membrane activity of ZnO nanoparticles. Chemical Communications. 2013;49(39):4172-4.

169. Mu Q, David CA, Galceran J, Rey-Castro C, Krzemiński L, Wallace R, et al. Systematic investigation of the physicochemical factors that contribute to the toxicity of ZnO nanoparticles. Chem Res Toxicol. 2014;27(4):558-67.

170. Shen C, James SA, de Jonge MD, Turney TW, Wright PF, Feltis BN. Relating cytotoxicity, zinc ions, and reactive oxygen in ZnO nanoparticle-exposed human immune cells. Toxicol Sci. 2013;136(1):120-30.

171. Gilbert B, Fakra S, Xia T, Pokhrel S, Mädler L, Nel A. The Fate of ZnO Nanoparticles Administered to Human Bronchial Epithelial Cells. ACS nano. 2012;6:4921-30.

172. Zhang C, Liu Z, Zhang Y, Ma L, Song E, Song Y. "Iron free" zinc oxide nanoparticles with ion-leaking properties disrupt intracellular ROS and iron homeostasis to induce ferroptosis. Cell Death Dis. 2020;11(3):183.

173. Gojova A, Guo B, Kota RS, Rutledge JC, Kennedy IM, Barakat AI. Induction of Inflammation in Vascular Endothelial Cells by Metal Oxide Nanoparticles: Effect of Particle Composition. Environmental Health Perspectives. 2007;115(3):403-9.

174. Wahab R, Dwivedi S, Umar A, Singh S, Hwang IH, Shin HS, et al. ZnO nanoparticles induce oxidative stress in Cloudman S91 melanoma cancer cells. J Biomed Nanotechnol. 2013;9(3):441-9.

175. Prasanth R, Gopinath D. Effect of ZnO nanoparticles on nasopharyngeal cancer cells viability and respiration. Applied Physics Letters. 2013;102.

176. Sensi S, Ton-That D, Sullivan P, Jonas E, Gee K, Kaczmarek L, et al. Modulation of mitochondrial function by endogenous Zn2+ pools. Proceedings of the National Academy of Sciences of the United States of America. 2003;100:6157-62.

177. Premanathan M, Karthikeyan K, Jeyasubramanian K, Manivannan G. Selective toxicity of ZnO nanoparticles toward Gram-positive bacteria and cancer cells by apoptosis through lipid peroxidation. Nanomedicine. 2011;7(2):184-92.

178. Martínez-Balbás MA, Jiménez-García E, Azorín F. Zinc(II) ions selectively interact with DNA sequences present at the TFIIIA binding site of the Xenopus 5S-RNA gene. Nucleic Acids Res. 1995;23(13):2464-71.

179. Lu S. Zn2+ blocks annealing of complementary single-stranded DNA in a sequence-selective manner. Sci Rep. 2014;4:5464.

180. Lee JS, Latimer LJ, Reid RS. A cooperative conformational change in duplex DNA induced by Zn2+ and other divalent metal ions. Biochem Cell Biol. 1993;71(3-4):162-8.

181. Wahab R, Kim Y-S, Hwang IH, Shin H-S. A non-aqueous synthesis, characterization of zinc oxide nanoparticles and their interaction with DNA. Synthetic Metals. 2009;159(23):2443-52.

182. Babu E, Ariraman S, Suyavaran A, Rao P, Kumar M, Jeevaratnam K, et al. Extracellularly synthesized ZnO nanoparticles interact with DNA and augment gamma radiation induced DNA damage through reactive oxygen species. RSC Advances. 2015;5:62067-77.

183. Fujihara J, Tongu M, Hashimoto H, Yamada T, Kimura-Kataoka K, Yasuda T, et al. Distribution and toxicity evaluation of ZnO dispersion nanoparticles in single intravenously exposed mice. J Med Invest. 2015;62(1-2):45-50.

184. Zijno A, De Angelis I, De Berardis B, Andreoli C, Russo MT, Pietraforte D, et al. Different mechanisms are involved in oxidative DNA damage and genotoxicity induction by ZnO and TiO2 nanoparticles in human colon carcinoma cells. Toxicol In Vitro. 2015;29(7):1503-12.

185. Gao F, Ma N, Zhou H, Wang Q, Zhang H, Wang P, et al. Zinc oxide nanoparticles-induced epigenetic change and G2/M arrest are associated with apoptosis in human epidermal keratinocytes. Int J Nanomedicine. 2016;11:3859-74.

186. El Yamani N, Collins AR, Rundén-Pran E, Fjellsbø LM, Shaposhnikov S, Zienolddiny S, et al. In vitro genotoxicity testing of four reference metal nanomaterials, titanium dioxide, zinc oxide, cerium oxide and silver: towards reliable hazard assessment. Mutagenesis. 2017;32(1):117-26.

187. Chakraborti S, Chakraborty S, Saha S, Manna A, Banerjee S, Adhikary A, et al. PEG-functionalized zinc oxide nanoparticles induce apoptosis in breast cancer cells

through reactive oxygen species-dependent impairment of DNA damage repair enzyme NEIL2. Free Radic Biol Med. 2017;103:35-47.

188. De Berardis B, Civitelli G, Condello M, Lista P, Pozzi R, Arancia G, et al. Exposure to ZnO nanoparticles induces oxidative stress and cytotoxicity in human colon carcinoma cells. Toxicology and Applied Pharmacology. 2010;246(3):116-27.

189. Zhang H, Ji Z, Xia T, Meng H, Low-Kam C, Liu R, et al. Use of metal oxide nanoparticle band gap to develop a predictive paradigm for oxidative stress and acute pulmonary inflammation. ACS nano. 2012;6(5):4349-68.

190. Choudhury SR, Ordaz J, Lo C-L, Damayanti NP, Zhou F, Irudayaraj J. From the cover: zinc oxide nanoparticles-induced reactive oxygen species promotes multimodal cyto-and epigenetic toxicity. Toxicological Sciences. 2017;156(1):261-74.

191. Pati R, Das I, Mehta RK, Sahu R, Sonawane A. Zinc-Oxide Nanoparticles Exhibit Genotoxic, Clastogenic, Cytotoxic and Actin Depolymerization Effects by Inducing Oxidative Stress Responses in Macrophages and Adult Mice. Toxicol Sci. 2016;150(2):454-72.

192. Bai DP, Zhang XF, Zhang GL, Huang YF, Gurunathan S. Zinc oxide nanoparticles induce apoptosis and autophagy in human ovarian cancer cells. Int J Nanomedicine. 2017;12:6521-35.

193. Moratin H, Scherzad A, Gehrke T, Ickrath P, Radeloff K, Kleinsasser N, et al. Toxicological characterization of ZnO nanoparticles in malignant and non-malignant cells. Environ Mol Mutagen. 2018;59(3):247-59.

194. Wilhelmi V, Fischer U, Weighardt H, Schulze-Osthoff K, Nickel C, Stahlmecke B, et al. Zinc oxide nanoparticles induce necrosis and apoptosis in macrophages in a p47phox- and Nrf2-independent manner. PLoS One. 2013;8(6):e65704.

195. Bisht G, Rayamajhi S. ZnO Nanoparticles: A Promising Anticancer Agent. Nanobiomedicine. 2016;3:9.

196. Hanley C, Layne J, Punnoose A, Reddy KM, Coombs I, Coombs A, et al. Preferential killing of cancer cells and activated human T cells using ZnO nanoparticles. Nanotechnology. 2008;19(29):295103.

197. Wahab R, Kaushik N, Khan F, Kaushik NK, Choi EH, Musarrat J, et al. Self-Styled ZnO Nanostructures Promotes the Cancer Cell Damage and Supresses the Epithelial Phenotype of Glioblastoma. Scientific Reports. 2016;6(1):19950.

198. Kc B, Paudel SN, Rayamajhi S, Karna D, Adhikari S, Shrestha BG, et al. Enhanced preferential cytotoxicity through surface modification: synthesis, characterization and comparative in vitro evaluation of TritonX-100 modified and unmodified zinc oxide nanoparticles in human breast cancer cell (MDA-MB-231). Chemistry Central Journal. 2016;10(1):16.

199. Sasidharan A, Chandran P, Menon D, Raman S, Nair S, Koyakutty M. Rapid dissolution of ZnO nanocrystals in acidic cancer microenvironment leading to preferential apoptosis. Nanoscale. 2011;3(9):3657-69.

200. Gatenby RA, Gillies RJ. Why do cancers have high aerobic glycolysis? Nat Rev Cancer. 2004;4(11):891-9.

201. Avramescu ML, Rasmussen PE, Chénier M, Gardner HD. Influence of pH, particle size and crystal form on dissolution behaviour of engineered nanomaterials. Environmental Science and Pollution Research. 2017;24(2):1553-64.

202. Odzak N, Kistler D, Sigg L. Influence of daylight on the fate of silver and zinc oxide nanoparticles in natural aquatic environments. Environmental Pollution. 2017;226:1-11.

203. Wingett D, Louka P, Anders CB, Zhang J, Punnoose A. A role of ZnO nanoparticle electrostatic properties in cancer cell cytotoxicity. Nanotechnol Sci Appl. 2016;9:29-45.

204. Wang H, Wingett D, Engelhard MH, Feris K, Reddy KM, Turner P, et al. Fluorescent dye encapsulated ZnO particles with cell-specific toxicity for potential use in biomedical applications. Journal of Materials Science: Materials in Medicine. 2009;20(1):11-22.

205. Ran S, Downes A, Thorpe PE. Increased exposure of anionic phospholipids on the surface of tumor blood vessels. Cancer Res. 2002;62(21):6132-40.

206. Shi D. Cancer Cell Surface Negative Charges: A Bio-Physical Manifestation of the Warburg Effect. Nano LIFE. 2017;07:1771001.

207. Hassan A, Elebeedy D, Matar ER, Fahmy Mohamed Elsayed A, Abd El Maksoud AI. Investigation of Angiogenesis and Wound Healing Potential Mechanisms of Zinc Oxide Nanorods. Front Pharmacol. 2021;12:661217.

208. Sanaeimehr Z, Javadi I, Namvar F. Antiangiogenic and antiapoptotic effects of green-synthesized zinc oxide nanoparticles using Sargassum muticum algae extraction. Cancer Nanotechnol. 2018;9(1):3.

209. Divya M, Vaseeharan B, Abinaya M, Vijayakumar S, Govindarajan M, Alharbi NS, et al. Biopolymer gelatin-coated zinc oxide nanoparticles showed high antibacterial, antibiofilm and anti-angiogenic activity. J Photochem Photobiol B. 2018;178:211-8.

210. Guo D, Wu C, Jiang H, Li Q, Wang X, Chen B. Synergistic cytotoxic effect of different sized ZnO nanoparticles and daunorubicin against leukemia cancer cells under UV irradiation. J Photochem Photobiol B. 2008;93(3):119-26.

211. Anjum S, Hashim M, Malik SA, Khan M, Lorenzo JM, Abbasi BH, et al. Recent Advances in Zinc Oxide Nanoparticles (ZnO NPs) for Cancer Diagnosis, Target Drug Delivery, and Treatment. Cancers (Basel). 2021;13(18).

212. Bai Aswathanarayan J, Rai Vittal R, Muddegowda U. Anticancer activity of metal nanoparticles and their peptide conjugates against human colon adenorectal carcinoma cells. Artif Cells Nanomed Biotechnol. 2018;46(7):1444-51.

213. Mishra P, Mishra H, Ekielski A, Talegaonkar S, Vaidya B. Zinc oxide nanoparticles: A promising nanomaterial for biomedical applications. Drug Discovery Today. 2017;22.

214. Deng Y, Zhang H. The synergistic effect and mechanism of doxorubicin-ZnO nanocomplexes as a multimodal agent integrating diverse anticancer therapeutics. Int J Nanomedicine. 2013;8:1835-41.

215. Sharma H, Kumar K, Choudhary C, Mishra PK, Vaidya B. Development and characterization of metal oxide nanoparticles for the delivery of anticancer drug. Artif Cells Nanomed Biotechnol. 2016;44(2):672-9.

216. Hackenberg S, Scherzed A, Harnisch W, Froelich K, Ginzkey C, Koehler C, et al. Antitumor activity of photo-stimulated zinc oxide nanoparticles combined with paclitaxel or cisplatin in HNSCC cell lines. Journal of Photochemistry and Photobiology B: Biology. 2012;114:87-93.

217. Zhang Y, Chen W, Wang S, Liu Y, Pope C. Phototoxicity of Zinc Oxide Nanoparticle Conjugatesin Human Ovarian Cancer NIH: OVCAR-3 Cells. Journal of Biomedical Nanotechnology. 2008;4:432-8.

218. Li J, Guo D, Wang X, Wang H, Jiang H, Chen B. The Photodynamic Effect of Different Size ZnO Nanoparticles on Cancer Cell Proliferation In Vitro. Nanoscale Res Lett. 2010;5(6):1063-71.

219. Wang C-C, Wang S, Xia Q, He W, Yin J-J, Fu PP, et al. Phototoxicity of zinc oxide nanoparticles in HaCaT keratinocytes-generation of oxidative DNA damage during UVA and visible light irradiation. Journal of nanoscience and nanotechnology. 2013;13(6):3880-8.

220. Hosny AEM, Kashef MT, Taher HA, El-Bazza ZE. The use of unirradiated and γ-irradiated zinc oxide nanoparticles as a preservative in cosmetic preparations. Int J Nanomedicine. 2017;12:6799-811.

221. Kumaraswamy S, Sheikh S, Chandrashekar K, H M S. Antibacterial Studies of Gamma Irradiated Zinc Oxide Nanoparticles on Klebsiella pneumoniae and Pseudomonas aeruginosa. IOSR Journal of Applied Physics. 2015;7:58-63.

222. Generalov R, Kuan WB, Chen W, Kristensen S, Juzenas P. Radiosensitizing effect of zinc oxide and silica nanocomposites on cancer cells. Colloids Surf B Biointerfaces. 2015;129:79-86.

223. Sainz B, Jr., TenCate V, Uprichard SL. Three-dimensional Huh7 cell culture system for the study of Hepatitis C virus infection. Virol J. 2009;6:103.

224. Freymuth F, Vabret A, Rozenberg F, Dina J, Petitjean J, Gouarin S, et al. Replication of respiratory viruses, particularly influenza virus, rhinovirus, and coronavirus in HuH7 hepatocarcinoma cell line. J Med Virol. 2005;77(2):295-301.

225. Cheng B, Shi W, Russell-Tanner JM, Zhang L, Samulski ET. Synthesis of variable-aspect-ratio, single-crystalline ZnO nanostructures. Inorg Chem. 2006;45(3):1208-14.

226. Pradhan S, Hedberg J, Blomberg E, Wold S, Odnevall Wallinder I. Effect of sonication on particle dispersion, administered dose and metal release of non-functionalized, non-inert metal nanoparticles. J Nanopart Res. 2016;18(9):285.

227. Pan-Keratin (C11) Mouse mAb (#4545) Datasheet Without Images: Cell Signaling Technology; last accessed on 13. December 2023 [Available from: https://www.cellsignal.com/datasheet.jsp?productId=4545&images=0.

228. Cleaved Caspase-3 (Asp175) Antibody (#9661) Datasheet with Images: Cell Signaling Technology; last accessed on 13. December 2023 [Available from: https://www.cellsignal.com/datasheet.jsp?productId=9661&images=1.

229. Ki-67 Antigen Antibody (Concentrate) Data Sheet: Agilent/Dako Glostrup Denmark; last accessed on 13. December 2023 [Available from: https://www.agilent.com/cs/library/packageinsert/public/SSM7240CEEFG_03.pdf.

230. Monoclonal Mouse antibody alpha - Smooth Muscle Actin (alpha-SMA) Clone 1A4 Data Sheet: Sigma Aldrich; last accessed on 13. December 2023 [Available from: https://www.sigmaaldrich.com/deepweb/assets/sigmaaldrich/product/documents/114/759/a2547dat.pdf.

231. Titford M. The long history of hematoxylin. Biotechnic & Histochemistry. 2005;80(2):73-8.

232. Wittekind D. Traditional staining for routine diagnostic pathology including the role of tannic acid. 1. Value and limitations of the hematoxylin-eosin stain. Biotech Histochem. 2003;78(5):261-70.

233. Schweizer Jr, Bowden PE, Coulombe PA, Langbein L, Lane EB, Magin TM, et al. New consensus nomenclature for mammalian keratins. The Journal of cell biology. 2006;174(2):169-74.

234. Makin C, Bobrow L, Bodmer W. Monoclonal antibody to cytokeratin for use in routine histopathology. Journal of Clinical Pathology. 1984;37(9):975-83.

235. Miettinen M. Keratin immunohistochemistry: update of applications and pitfalls. Pathol Annu. 1993;28:113-43.

236. Rekhtman N, Bishop JA. Quick reference handbook for surgical pathologists: Springer; 2011.

237. Dabbs DJ. Diagnostic immunohistochemistry: theranostic and genomic applications: Elsevier Health Sciences; 2021.

238. Asadi M, Taghizadeh S, Kaviani E, Vakili O, Taheri-Anganeh M, Tahamtan M, et al. Caspase-3: Structure, function, and biotechnological aspects. Biotechnol Appl Biochem. 2022;69(4):1633-45.

239. Nicholson DW. Caspase structure, proteolytic substrates, and function during apoptotic cell death. Cell Death Differ. 1999;6(11):1028-42.

240. Juríková M, Danihel Ľ, Polák Š, Varga I. Ki67, PCNA, and MCM proteins: Markers of proliferation in the diagnosis of breast cancer. Acta Histochem. 2016;118(5):544-52.

241. Gerdes J, Li L, Schlueter C, Duchrow M, Wohlenberg C, Gerlach C, et al. Immunobiochemical and molecular biologic characterization of the cell proliferation-associated nuclear antigen that is defined by monoclonal antibody Ki-67. The American journal of pathology. 1991;138(4):867.

242. Inwald EC, Klinkhammer-Schalke M, Hofstädter F, Zeman F, Koller M, Gerstenhauer M, et al. Ki-67 is a prognostic parameter in breast cancer patients: results of a large population-based cohort of a cancer registry. Breast Cancer Research and Treatment. 2013;139(2):539-52.

243. Remes SM, Tuominen VJ, Helin H, Isola J, Arola J. Grading of neuroendocrine tumors with Ki-67 requires high-quality assessment practices. Am J Surg Pathol. 2012;36(9):1359-63.

244. Cherng S, Young J, Ma H. Alpha-smooth muscle actin (α-SMA). J Am Sci. 2008;4.

245. Younesi FS, Son DO, Firmino J, Hinz B. Myofibroblast Markers and Microscopy Detection Methods in Cell Culture and Histology. Methods Mol Biol. 2021;2299:17-47.

246. Brey EM, McIntire LV, Johnston CM, Reece GP, Patrick CW, Jr. Three-dimensional, quantitative analysis of desmin and smooth muscle alpha actin expression during angiogenesis. Ann Biomed Eng. 2004;32(8):1100-7.

247. Preibisch S, Saalfeld S, Tomancak P. Globally optimal stitching of tiled 3D microscopic image acquisitions. Bioinformatics. 2009;25(11):1463-5.

248. Kleibeuker EA, Ten Hooven MA, Castricum KC, Honeywell R, Griffioen AW, Verheul HM, et al. Optimal treatment scheduling of ionizing radiation and sunitinib improves the antitumor activity and allows dose reduction. Cancer Med. 2015;4(7):1003-15.

249. Giannopoulou E, Katsoris P, Hatziapostolou M, Kardamakis D, Kotsaki E, Polytarchou C, et al. X-rays modulate extracellular matrix in vivo. Int J Cancer. 2001;94(5):690-8.

250. Hadjimichael C, Kardamakis D, Papaioannou S. Irradiation dose-response effects on angiogenesis and involvement of nitric oxide. Anticancer Res. 2005;25(2a):1059-65.

251. Kardamakis D, Hadjimichael C, Ginopoulos P, Papaioannou S. Effects of paclitaxel in combination with ionizing radiation on angiogenesis in the chick embryo chorioallantoic membrane. A radiobiological study. Strahlenther Onkol. 2004;180(3):152-6.

252. Lee YR, Park SY. P53 expression in hepatocellular carcinoma: influence on the radiotherapeutic response of the hepatocellular carcinoma. Clin Mol Hepatol. 2015;21(3):230-1.

253. Gomes AR, Abrantes AM, Brito AF, Laranjo M, Casalta-Lopes JE, Gonçalves AC, et al. Influence of P53 on the radiotherapy response of hepatocellular carcinoma. Clin Mol Hepatol. 2015;21(3):257-67.

254. Koom WS, Park SY, Kim W, Kim M, Kim JS, Kim H, et al. Combination of radiotherapy and adenovirus-mediated p53 gene therapy for MDM2-overexpressing hepatocellular carcinoma. J Radiat Res. 2012;53(2):202-10.

255. Huang CY, Lin CS, Tai WT, Hsieh CY, Shiau CW, Cheng AL, et al. Sorafenib enhances radiation-induced apoptosis in hepatocellular carcinoma by inhibiting STAT3. Int J Radiat Oncol Biol Phys. 2013;86(3):456-62.

256. Jang WI, Kim MS, Jeong JH, Kim W, Kim JS. Enhancement of Radiation Response Associated With Metformin in Hepatocellular Carcinoma: Preclinical Animal and Clinical Cohort Study. Anticancer Res. 2022;42(2):867-76.

257. Gudkov AV, Komarova EA. The role of p53 in determining sensitivity to radiotherapy. Nat Rev Cancer. 2003;3(2):117-29.

258. Pradella M. Tumorstammzellen und Strahlenresistenz des hepatozellulären Karzinoms. München2016.

259. Bressac B, Galvin KM, Liang TJ, Isselbacher KJ, Wands JR, Ozturk M. Abnormal structure and expression of p53 gene in human hepatocellular carcinoma. Proc Natl Acad Sci U S A. 1990;87(5):1973-7.

260. Kaino M. Alterations in the tumor suppressor genes p53, RB, p16/MTS1, and p15/MTS2 in human pancreatic cancer and hepatoma cell lines. J Gastroenterol. 1997;32(1):40-6.

261. Kasai F, Hirayama N, Ozawa M, Satoh M, Kohara A. HuH-7 reference genome profile: complex karyotype composed of massive loss of heterozygosity. Hum Cell. 2018;31(3):261-7.

262. Buhr CR, Wiesmann N, Tanner RC, Brieger J, Eckrich J. The Chorioallantoic Membrane Assay in Nanotoxicological Research-An Alternative for In Vivo Experimentation. Nanomaterials (Basel). 2020;10(12).

263. Ezhuthupurakkal PB, Ariraman S, Arumugam S, Subramaniyan N, Muthuvel SK, Kumpati P, et al. Anticancer potential of ZnO nanoparticle-ferulic acid conjugate on Huh-7 and HepG2 cells and diethyl nitrosamine induced hepatocellular cancer on Wistar albino rat. Nanomedicine: Nanotechnology, Biology and Medicine. 2018;14(2):415-28.

264. Rahimi Kalateh Shah Mohammad G, Seyedi SMR, Karimi E, Homayouni-Tabrizi M. The cytotoxic properties of zinc oxide nanoparticles on the rat liver and spleen, and its anticancer impacts on human liver cancer cell lines. J Biochem Mol Toxicol. 2019;33(7):e22324.

265. Cai J, Xu X, Saw PE. Nanomedicine targeting ferroptosis to overcome anticancer therapeutic resistance. Science China Life Sciences. 2024;67(1):19-40.

266. Ananthalakshmi R, Rathinam SRXR, Sadiq AM. Apoptotic Signalling of Huh7 Cancer Cells by Biofabricated Zinc Oxide Nanoparticles. Journal of Inorganic and Organometallic Polymers and Materials. 2021;31(4):1764-73.

267. Yang R, Wu R, Mei J, Hu FR, Lei CJ. Zinc oxide nanoparticles promotes liver cancer cell apoptosis through inducing autophagy and promoting p53. Eur Rev Med Pharmacol Sci. 2021;25(3):1557-63.

268. Qin X, Tang Q, Jiang X, Zhang J, Wang B, Liu X, et al. Zinc Oxide Nanoparticles Induce Ferroptotic Neuronal Cell Death in vitro and in vivo. Int J Nanomedicine. 2020;15:5299-315.

269. Hackenberg S, Scherzed A, Kessler M, Froelich K, Ginzkey C, Koehler C, et al. Zinc oxide nanoparticles induce photocatalytic cell death in human head and neck squamous cell carcinoma cell lines in vitro. Int J Oncol. 2010;37(6):1583-90.

270. Affolter A, Drigotas M, Fruth K, Schmidtmann I, Brochhausen C, Mann WJ, et al. Increased radioresistance via G12S K-Ras by compensatory upregulation of MAPK and PI3K pathways in epithelial cancer. Head Neck. 2013;35(2):220-8.

271. Krisnawan VE, Stanley JA, Schwarz JK, DeNardo DG. Tumor Microenvironment as a Regulator of Radiation Therapy: New Insights into Stromal-Mediated Radioresistance. Cancers (Basel). 2020;12(10).

272. Marzullo A, Vacca A, Roncali L, Pollice L, Ribatti D. Angiogenesis in hepatocellular carcinoma: an experimental study in the chick embryo chorioallantoic membrane. Int J Oncol. 1998;13(1):17-21.

273. Richardson M, Singh G. Observations on the use of the avian chorioallantoic membrane (CAM) model in investigations into angiogenesis. Curr Drug Targets Cardiovasc Haematol Disord. 2003;3(2):155-85.

274. Giannopoulou E, Katsoris P, Parthymou A, Kardamakis D, Papadimitriou E. Amifostine protects blood vessels from the effects of ionizing radiation. Anticancer Res. 2002;22(5):2821-6.

275. Nowak-Sliwinska P, Segura T, Iruela-Arispe ML. The chicken chorioallantoic membrane model in biology, medicine and bioengineering. Angiogenesis. 2014;17(4):779-804.

276. Polytarchou C, Kardamakis D, Katsoris P, Papadimitriou E. Antioxidants modify the effect of X rays on blood vessels. Anticancer Res. 2006;26(4b):3043-7.

277. Brooks PC, Montgomery AM, Cheresh DA. Use of the 10-day-old chick embryo model for studying angiogenesis. Methods Mol Biol. 1999;129:257-69.

278. Hatjikondi O, Ravazoula P, Kardamakis D, Dimopoulos J, Papaioannou S. In vivo experimental evidence that the nitric oxide pathway is involved in the X-ray-induced antiangiogenicity. Br J Cancer. 1996;74(12):1916-23.

279. Jarosz-Biej M, Smolarczyk R, Cichoń T, Kułach N. Tumor Microenvironment as A "Game Changer" in Cancer Radiotherapy. Int J Mol Sci. 2019;20(13).

280. Krammer B. Vascular effects of photodynamic therapy. Anticancer Res. 2001;21(6b):4271-7.

281. Yamazaki T, Young KH. Effects of radiation on tumor vasculature. Mol Carcinog. 2022;61(2):165-72.

282. Pallares RM, Abergel RJ. Nanoparticles for targeted cancer radiotherapy. Nano Research. 2020;13(11):2887-97.

283. Kang S, Lee S, Park S. iRGD Peptide as a Tumor-Penetrating Enhancer for Tumor-Targeted Drug Delivery. Polymers (Basel). 2020;12(9).

284. Susewind M, Schilmann AM, Heim J, Henkel A, Link T, Fischer K, et al. Silica-coated Au@ZnO Janus particles and their stability in epithelial cells. J Mater Chem B. 2015;3(9):1813-22.

285. Król A, Pomastowski P, Rafińska K, Railean-Plugaru V, Buszewski B. Zinc oxide nanoparticles: Synthesis, antiseptic activity and toxicity mechanism. Adv Colloid Interface Sci. 2017;249:37-52.

286. Victorelli FD, Cardoso VMdO, Ferreira NN, Calixto GMF, Fontana CR, Baltazar F, et al. Chick embryo chorioallantoic membrane as a suitable in vivo model to evaluate drug delivery systems for cancer treatment: A review. European Journal of Pharmaceutics and Biopharmaceutics. 2020;153:273-84.

287. Kauffmann P, Troeltzsch M, Cordesmeyer R, Heidekrueger PI, Schliephake H, Canis M, et al. Presentation of a variation of the chorioallantoic membrane set up as a potential model for individual therapy for squamous cell carcinoma of the oropharynx. Clin Hemorheol Microcirc. 2017;67(3-4):453-7.

288. Fergelot P, Bernhard JC, Soulet F, Kilarski WW, Léon C, Courtois N, et al. The experimental renal cell carcinoma model in the chick embryo. Angiogenesis. 2013;16(1):181-94.

289. Pinto AT, Pinto ML, Velho S, Pinto MT, Cardoso AP, Figueira R, et al. Intricate Macrophage-Colorectal Cancer Cell Communication in Response to Radiation. PLoS One. 2016;11(8):e0160891.

11 Attachments

Table 7: List of all CAM specimens and description whether data acquisition was possible

Group 1 as control (n=17), group 2 with only ZnO-NP application (n=22), group 3 with 8 Gy radiation treatment (n=22) and group 4 as combined ZnO-NP and radiation intervention (n=22) are shown, originating from six experimental rounds.

Experimental round	CAM number	Group number	Use for data acquisition	Reason for exclusion
1	322_19	1	no	Low tumor size
1	323_19	1	yes	/
1	324_19	1	no	No PK-positive areas
1	325_19	1	yes	/
1	326_19	1	no	Tumor not grown into CAM
1	327_19	2	yes	/
1	328_19	2	yes	/
1	329_19	2	yes	/
1	330_19	2	no	Tumor not grown into CAM
1	331_19	3	no	Low tumor size
1	332_19	3	no	Tumor not grown into CAM
1	333_19	3	yes	/
1	334_19	3	yes	/
1	335_19	4	no	No PK-positive areas
1	336_19	4	yes	/
1	337_19	4	yes	/
1	338_19	4	no	Tumor not grown into CAM
1	339_19	4	yes	/
1	340_19	4	no	Low tumor size
1	341_19	4	yes	/
2	349_19	1	yes	/
2	350_19	1	yes	/
2	351_19	1	yes	/
2	352_19	1	yes	/
2	353_19	1	no	Tumor not grown into CAM
2	354_19	2	no	Low tumor size
2	355_19	2	yes	/
2	356_19	2	yes	/
2	357_19	2	no	Tumor not grown into CAM
2	358_19	2	yes	/
2	359_19	3	yes	/
2	360_19	3	yes	/
2	361_19	3	yes	/
2	362_19	3	yes	/

2	363_19	3	no	Tumor not grown into CAM
2	364_19	4	yes	/
2	365_19	4	yes	/
2	366_19	4	no	No PK-positive areas
2	367_19	4	yes	/
2	368_19	4	no	Tumor not grown into CAM
2	369_19	4	yes	/
3	378_19	1	yes	/
3	379_19	1	no	No PK-positive areas
3	380_19	1	yes	/
3	381_19	1	yes	/
3	382_19	1	yes	/
3	383_19	2	yes	/
3	384_19	2	no	No PK-positive areas
3	385_19	2	yes	/
3	386_19	2	yes	/
3	387_19	2	yes	/
3	388_19	3	yes	/
3	389_19	3	yes	/
3	390_19	3	no	Low tumor size
3	391_19	3	yes	/
3	392_19	3	yes	/
3	393_19	4	yes	/
3	394_19	4	no	Low tumor size
3	395_19	4	no	Tumor not grown into CAM
3	396_19	4	yes	/
3	397_19	4	yes	/
4	451_19	1	yes	/
4	452_19	1	yes	/
4	453_19	1	yes	/
4	454_19	1	yes	/
4	455_19	1	no	Tumor not grown into CAM
4	456_19	2	yes	/
4	457_19	2	yes	/
4	458_19	2	yes	/
4	459_19	2	yes	/
4	460_19	2	no	Low tumor size
4	461_19	3	yes	/
4	462_19	3	yes	/

4	463_19	3	yes	/
4	464_19	3	yes	/
4	465_19	3	no	Tumor not grown into CAM
4	466_19	4	yes	/
4	467_19	4	yes	/
4	468_19	4	yes	/
4	469_19	4	yes	/
4	470_19	4	no	Tumor not grown into CAM
5	55_20	1	yes	/
5	56_20	1	no	.
5	57_20	1	no	Low tumor size
5	58_20	1	yes	/
5	59_20	2	yes	/
5	60_20	2	yes	/
5	61_20	2	yes	/
5	62_20	2	yes	/
5	63_20	2	no	Tumor not grown into CAM
5	64_20	3	yes	/
5	65_20	3	yes	/
5	66_20	3	yes	/
5	67_20	3	yes	/
5	68_20	4	yes	/
5	69_20	4	yes	/
5	70_20	4	yes	/
5	71_20	4	yes	/
6	76_20	1	no	Tumor not grown into CAM
6	77_20	1	yes	/
6	78_20	1	yes	/
6	79_20	2	yes	/
6	80_20	2	yes	/
6	81_20	2	yes	/
6	82_20	2	no	No PK-positive areas
6	83_20	2	yes	/
6	84_20	3	yes	/
6	85_20	3	yes	/
6	86_20	3	yes	/
6	87_20	3	yes	/
6	88_20	4	no	Tumor not grown into CAM
6	89_20	4	yes	/

6	90_20	4	yes	/
6	91_20	4	yes	/
6	92_20	4	no	Low tumor size

Table 8: Number of CAM specimens not included in data acquisition by group number and experimental round

	Round 1 (CAM 322_19 – 341_19)	Round 2 (CAM 349_19 – 369_19)	Round 3 (CAM 378_19 – 397_19)	Round 4 (CAM 451_19 – 470_19)	Round 5 (CAM 55_20 – 71_20)	Round 6 (CAM 76_20 – 92_20)	**Sum**
Group 1	3	1	1	1	2	1	9
Group 2	1	2	1	1	1	1	7
Group 3	2	1	1	1	0	0	5
Group 4	3	2	2	1	0	2	10
Sum	9	6	5	4	3	4	**31**

Overall, 112 CAM specimens reached day 14 of the experimental run during six experimental rounds. 31 of these were not included in the data analysis, which equals 27,68%. It has to be noted that more eggs were used at the beginning of each experimental round, but difficulties in the technicalities of the breeding and after preparation of the eggs were present. This includes breakage, mold, and death of the embryo. A designation to each reason for exclusion and quantification of each share was not made.

Table 9: List of CAM specimens and values used for data analysis

Experimental round	**CAM**	**Group**	**Tumor area [µm²]**	**Values for CC3-positive cells per µm²**	**Values for Ki-67-positive cells per 10 ROIs each [%]**	**Category of vascularization in alpha-SMA staining (1=low, 2=moderate, 3=high)**	**Values for alpha-SMA-positive structures per µm²**
1	323_19	1	92015,19	0,0008150828		2	0,000934628
1	325_19	1	27498,17	0,0006909551	9,836065574	3	0,002909285
1	327_19	2	199631,84	0,0000601107		3	0,000616134
1	328_19	2	80817,06	0,0002103516	11,94029851	2	0,000606308
1	329_19	2	92346,54	0,0003573496	13,51351351	3	0,001158679
1	333_19	3	70265,27	0,0004981124	22,61072261	2	0,00088237
1	334_19	3	37856,45	0,0005018960	31,83856502	3	0,001532104
1	336_19	4	113685,42	0,0005101798	21,8503937	1	0,000774066
1	339_19	4	65760,48	0,0004562010	8,955223881	1	0,000790748
1	340_19	4			11,29707113		
1	341_19	4	86787,37	0,0003111052	14,5323741	1	0,000679822
2	349_19	1	95152,48	0,0003783401		3	0,001092983

2	350_19	1	102319,44	0,0008405050		2	0,000557079
2	351_19	1	81260,29	0,0000369184	9,760273973	3	0,001181389
2	352_19	1	106750,29	0,0001217795	7,889908257	3	0,000730677
2	355_19	2	32258,69	0,0002169958	20,40302267	2	0,000650987
2	356_19	2	35396,8	0,0005650228	12,35955056	2	0,001158297
2	358_19	2	64428,55	0,0002638582	18	2	0,000776053
2	359_19	3	103258,9	0,0003486382	16,17312073	2	0,000706961
2	360_19	3	76092,05	0,0003022655	21,36150235	1	0,000762235
2	361_19	3	62369,3	0,0006734082	21,88295165	1	0,000464972
2	362_19	3	55055,04	0,0002179637	20,2173913	2	0,000762873
2	364_19	4	47616,61	0,0003360172	17,12538226	1	0,000525027
2	365_19	4	90958,17	0,0003518101	17,27642276	1	0,000307834
2	367_19	4	151016,03	0,0001854108	20,18691589		
2	369_19	4	29619,47	0,0006414700	18,75	2	0,002430834
3	378_19	1	163356,63	0,0004040240	23,0994152	3	0,000924358
3	380_19	1	103125,69	0,0001066660	48,08126411	3	0,000727268
3	381_19	1	176575,84	0,0000792860	50,38363171	2	0,000690921
3	382_19	1	233810,45	0,0000427697	53,65296804	3	0,000893886
3	383_19	2	161930,53	0,0000988078	53,75586854	3	0,000994254
3	385_19	2	195700,68	0,0001277461	58,33333333	3	0,000786916
3	386_19	2	106012,54	0,0001509255	58,40909091	3	0,001301733
3	387_19	2	293899,14	0,0000136101	43,52941176	3	0,000711128
3	388_19	3	115583,25	0,0004412404	65,10416667	2	0,000821918
3	389_19	3	154386,68	0,0002526125	65,36312849	2	0,00049227
3	391_19	3	75007,76	0,0005732740	70,41284404	2	0,001213208
3	392_19	3	113133,54	0,0004419556	60,37296037	3	0,000583381
3	393_19	4	96551,73	0,0002382143	63,61655773	3	0,0010875
3	396_19	4	55489,2	0,0003063659	57,36040609	2	0,000883055
3	397_19	4	182232,14	0,0002085252	59,47368421	2	0,000812151
4	451_19	1	247230,6	0,0000970754	47,4137931	3	0,000946485
4	452_19	1	151232,71	0,0000727356	44,78021978	3	0,00093895
4	453_19	1	60903,85	0,0001641932	48,56321839	3	0,001477739
4	454_19	1	407826,19	0,0001471215	42,72151899	3	0,001042111
4	456_19	2	47793,12	0,0001673881	44,96314496	3	0,001527416
4	457_19	2	148974,62	0,0001611013	39,0776699	3	0,001194834
4	458_19	2	23096,53	0,0046760271	48,16901408	2	0,002770979
4	459_19	2	77594,73	0,0001159873	45,16129032	2	0,001159873
4	461_19	3	135149,94	0,0002293749	59,95085995	2	0,000776915
4	462_19	3	92123,31	0,0004667657	36,56716418	3	0,000857546
4	463_19	3	221157,21	0,0004431237	55,5	1	0,000479297
4	464_19	3	195706,38	0,0000562066	44,3902439	3	0,000955513
4	466_19	4	197614,85	0,0001163880	54,98839907	2	0,000460492

4	467_19	4	138602,82	0,0000144297	55,04807692	1	0,000476181
4	468_19	4	150819,07	0,0003182621	55,18018018	1	0,000596742
4	469_19	4	128799,25	0,0004425492	48,01864802	2	0,000543481
5	55_20	1	73.889	0,0002571434	37,79069767	1	0,000392482
5	58_20	1	50219,45	0,0001194756	46,24413146	1	0,001115106
5	59_20	2	89368,96	0,0002685496	37,41007194	2	0,000604237
5	60_20	2	185111,91	0,0001080428	35,67134269	3	0,000885951
5	61_20	2	21806,34	0,0003668658	40,40178571	2	0,002338769
5	62_20	2	103194,13	0,0000775238	40,26717557	3	0,001521404
5	64_20	3	117887,39	0,0003308242	44,24603175	2	0,000415651
5	65_20	3	126689,49	0,0003078393	39,44353519	3	0,000868265
5	66_20	3	82278,56	0,0017501522	39,84819734	3	0,000692769
5	67_20	3	117758,27	0,0004840424	57,36842105	3	0,000934117
5	68_20	4	123225,18	0,0008845595	47,13375796	2	0,000957596
5	69_20	4	31589,95	0,0011712586	58,6490939	3	0,003767021
5	70_20	4	175860,22	0,0005743198	34,69827586	3	0,000835891
5	71_20	4	72613,82	0,0006472597	35,55555556	2	0,000633488
6	77_20	1	89356,38	0,0000895291	30,14256619	3	0,00117507
6	79_20	2	117646,45	0,0001105006	26,07843137	3	0,000569503
6	80_20	2	235482,81	0,0000552057	35,75418994	2	9,76717E-05
6	81_20	2	141405,08	0,0008274102	32,32	3	0,000629397
6	83_20	2	126047,01	0,0001507374	24,04371585	3	0,000539481
6	84_20	3	43330,08	0,0005769664	32,6171875	2	0,001061618
6	85_20	3	136483,62	0,0004029788	40,47619048	1	0,000219807
6	86_20	3	58140,35	0,0003439952	21,44288577	3	0,001135184
6	87_20	3	210052,95	0,0001332997	44,23076923	3	0,000656977
6	89_20	4	147177,08	0,0007609881	36,34920635	2	0,000876495
6	90_20	4	103391,64	0,0008124448	28,65853659	2	0,000619006
6	91_20	4	182558,39	0,0007394894	26,82926829	2	0,000673757

The CAM specimens (see column 2) are listed continuously and distinguished by groups which describe the intervention which has taken place (see column 3). Group 1 as control (n=17), group 2 with only ZnO-NP application (n=22), group 3 with 8 Gy radiation treatment (n=22) and group 4 as combined ZnO-NP and radiation intervention (n=22) are shown, originating from six experimental rounds (see column 1).

The values gained from counting CC3-positive cells were collected for each group originating from all six experimental rounds and then the middle value was , culminating in 24 values which were portrayed in the results section 5.2.5.3 (see column 5).

The values gained from Ki-67-positive cells in each ROI were added to compute a sum and then it was calculated which share Ki-67-positive cells held of all cells within the ROIs, further portrayed as a percentage (see column 6).

The CAM specimens were manually categorized by the amount of vascularization in the alpha-SMA staining (see column 7). The values for alpha-SMA-positive structures were counted for each CAM specimen and then divided by the tumor area to portray the value per μm^2 (see column 8).

The fact that some values are missing is due to the fact that sometimes the immunohistochemical staining method was not successful.

12 Acknowledgements

Last but not least: Mein persönlicher Dank an die folgenden Kolleg*innen, Freund*innen und Begleiter*innen. Ohne diesen Hintergrund wäre diese Arbeit nicht möglich und abschließbar gewesen. Ich hoffe, ich konnte außer diesem ausdrücklichen Dank auch so allen Wertschätzung und gegebenenfalls etwas Unterstützung zurückgeben.

Ich danke allen voran allen Mitarbeitenden der AG, in welcher ich tätig sein durfte. Vielen Dank für die herzliche Aufnahme und uneingeschränkte Unterstützung die ich bei Euch erfahren durfte. Eine solche Zusammenarbeit in der wissenschaftlichen Tätigkeit muss seinesgleichen finden und ist für mich ein absolut positives Beispiel.

Dir danke ich für Deine Geduld, Deine ehrlichen Worte, Deine fachlichen und weiterführenden Ratschläge. Ich hätte mir keinen besseren „Doktorvater“ wünschen können. Ich habe durch diese Erfahrung und den persönlichen Austausch mit Dir enorm profitiert und werde in meiner weiteren Berufslaufbahn sicherlich davon beeinflusst bleiben.

Dir danke ich für die stetige (eigentlich ja irgendwie inoffizielle) Betreuung und den fachlichen Input, die vielen Gespräche auch abseits der fachlichen Fragen und das Korrekturlesen. Ohne Deine gute Seele, Dein Verständnis und die vielen Gespräche auch abseits der fachlichen Fragen wäre diese Arbeit so nicht zustande gekommen.

danke für Deine Herzlichkeit, die Gespräche, die Geduld, die Anleitung und die Unterstützung beim „Laufenlernen“ im Labor. Die immunhistochemischen Färbungen und damit Früchte der Arbeit sind durch Deinen Fleiß und Deine Gewissenhaftigkeit möglich gewesen.

danke für Deine fachlichen Ratschläge, Deine niedrigschwellige Ansprechbarkeit und dass Du eine erreichbare Vorbildfunktion darstellst.

vielen Dank für Eure unterstützende Tätigkeiten und den persönlichen Austausch im Labor.

Meinen damaligen Kommilitonen und Mitpromovenden bin ich dankbar für den fachlichen Austausch und die gemeinsame Zeit im Labor. Schön, dass wir im gleichen Boot saßen!

Für die weitere kollegiale Unterstützung über Institutsgrenzen hinaus möchte ich der Klinik und Poliklinik für Radioonkologie und Strahlentherapie der Universitätsmedizin Mainz sowie der AG von am Institut für Anorganische und Analytische Chemie der Johannes Gutenberg-Universität Mainz danken. Ohne das gemeinsame Interesse an diesem Forschungsthema und dem reibungslosen Kontakt hätte das Projekt so nicht stattfinden können.

Die Durststrecken, welche sicherlich für jeden normal sind, der ein solches Promotionsverfahren angeht und/oder in der Forschung tätig ist, haben mich zum ersten Mal ernsthaft an meine persönlichen Leistungsgrenzen gebracht. Ich bin dankbar für diese Erfahrung und verneige den Kopf vor allen Voll- und genauso Teilzeitforschenden.

Ebenfalls danke ich meinen Freund*innen und meiner Familie, besonders meinem Bruder und meiner Mutter. Ohne Eure Unterstützung, Eure offenen Ohren, Eure Toleranz und Eure Geduld wäre ich auch im weiteren Leben nicht da, wo ich jetzt bin.

Diese wertvolle Erfahrung ist ein persönlicher Meilenstein und hat mir eine persönliche sowie berufliche Entwicklung verschafft, die ohne alle oben genannten Menschen so nicht möglich gewesen wäre. Von ganzem Herzen danke ich dafür!

13 Curriculum vitae